STUDIES IN CONTACT MECHANICS WITH REFERENCE TO FRETTING FATIGUE OF GAS TURBINE BLADE/DISC ATTACHMENTS

Thesis submitted to the Department of Engineering Science of Oxford University in partial fulfilment of the requirements for the degree of Doctor in Engineering - Engineered Metals for High Performance Applications in Aerospace, and Related Technologies.

by

MATHEW DAVIES

LINCOLN COLLEGE

OXFORD

Trinity Term, 2011

Abstract

Explicit recipes have been derived for finding the contact law and contact pressure distribution for an asymmetric punch whose profile is defined in a piecewise quadratic sense, using uncoupled half-plane theory. An incremental formulation is provided for contact pressure, shear traction and relative strain between bodies brought into contact under the simultaneous proportional application of normal load, shear load and bulk tension and the condition for complete adhesion derived. When this condition is not satisfied, partial slip ensues.

A complete account of all possible states for two load phases with different distributions of normal load, shear load and moderate bulk tension is given, *viz*. (i) two phases of full adhesion, (ii) sliding followed by full adhesion and (iii) full adhesion followed by partial slip.

This approach is developed further to provide a solution for the complete stick-slip pattern and shearing traction distribution for periodic loading in $P-Q$ space, including both the transient and steady state problem.

A method for obtaining the steady state stick-slip zone evolution for a half-plane contact subject to a constant normal load and a periodically varying shear and bulk tension has been found. The solutions found include those for the 'two slip zone' regime, which implies 'lens like' loci in $Q-\sigma$ space. Advancing stick has been demonstrated to occur for a smooth loop in $Q-\sigma$ space.

The following publications or submissions for publication have been based on work in this thesis

1. M. Davies, D.A. Hills, Closed form solutions for a piecewise quadratic half-plane contact problem, *Journal of Strain analysis*, **45**, October 2010, 505-511.
2. D.A. Hills, M. Davies, J.R. Barber, An incremental formulation for half plane contact problem subject to varying normal load shear and tension, *Journal of Strain analysis*, **46**, August 2011, 436-443
3. J.R. Barber, M. Davies, D.A. Hills, Frictional elastic contact with periodic loading, *International Journal of Solids and Structures*, **48**, June 2011, 2041-2047.
4. M. Davies, D.A. Hills, J.R. Barber, Energy Dissipation in a Frictional Incomplete Contact with varying Normal Load, *International Journal of Mechanical Sciences*, **55**, February 2012,13–21

Acknowledgements

I would like to thank Rolls-Royce plc for funding this research, especially the staff at Elton Road, all of whom have been extremely supportive. Particular thanks to Dr. Nina Banerjee, Dr. Ivan Brunton, Mr. Adam Coles, Mr. Anthony Phipps and Dr. Tom Hyde. Thanks also to the Solid Mechanics group at Oxford University, especially Prof. David Nowell and Mr. Anothai Thaitirarot and to Prof. Jim Barber from the University of Michigan.

The completion of this work was inspired by the arrival of my son, Jamie. During the later stages of both this Thesis and her pregnancy, my Wife demonstrated the patience of a saint, and has my eternal gratitude. I would also like to thank my Mother and Father for nurturing, rather than suppressing, my inquisitive nature and my Mother and Father in law, who have kindly accepted me and my family into their own. I would also like to thank my brother and sisters, both natural and in law: Mr. Bryn Jones, Mrs. Sarah Jones and Miss. Briony Johnson.

My friends have contributed to this in more ways than they will ever know, thanks to Mr. Carl James, Mr. Stephen Pearson, Mr. Shaun Smith, Mr. Keith Crosse, Mr. Nick Tyson, Dr. Jon Blackburn, Mr. Ian Mitchell and Dr. Tom Watson. Also Dr. John Harris and Mr. Tunde Oyinloye have been both inspiring colleagues and personal friends.

Finally, I would like to offer special thanks to my academic supervisor Prof. David Hills for his patience, guidance and friendship, which has been instrumental in the completion of this thesis and led me to discover an affinity for solid mechanics research.

Dedicated to my Father

Contents

1. Gas turbines and Fretting Fatigue

Introduction

This thesis is concerned with furthering our understanding of problems arising in gas turbine ('jet') engines caused by fretting and fretting fatigue. 'Fretting' is the name given to the occurrence of minute amounts of slip arising between notionally clamped components, usually as a result of some vibrational or oscillatory element of external loading. Although the word (borrowed from common usage) suggests that it is deleterious, in fact the presence of some fretting is important in certain areas of the gas turbine, because it dissipates energy, and is useful in limiting the amplitude of motion of connecting components subject to vibrational forces. On the other hand, fretting does cause surface modification, erosion and damage, and it may accelerate the nucleation of fatigue cracks - this is the phenomenon of 'fretting fatigue'. Turning to the question of fatigue in slightly more detail, we see that the main difference between fretting and 'plain' fatigue is, indeed, in the nucleation phase. When cracks have a significant length their growth characteristics are governed entirely by the crack tip stress intensity factor, and there is no difference between the two forms of fatigue - it is simply that 'fretting' fatigue induced cracks have a contact loading contribution to the crack tip stress intensity factor, but the mechanics of crack extension are no different for the two cases. On the other hand, plain fatigue cracks are either 'freely initiated' at relatively smooth, flat surfaces (rare) or they start at geometric stress raising features, producing localisation of the remote stress field, whilst fretting fatigue cracks nucleate either at or very close to the edges of contacts; their location is therefore very well defined and, in many ways, the conditions are also clearer than in the case of plain fatigue, where the presence of randomly arising stress raising microscopic features - perhaps in the form of machining marks - will have an important but hard to quantify effect.

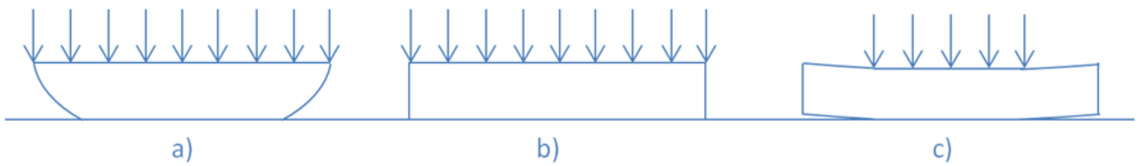

Figure 1-1 – Example of a) incomplete, b) complete and c) receding contacts

A full understanding of fretting fatigue under all conditions and all geometries is yet to be achieved, but there are well defined elements to the phenomenon which, by and large, can be studied independently: the first aspect is to understand the conditions along the contact, *viz*. the interfacial contact pressure distribution, the coefficient of friction, the shear traction distribution and, most importantly, the regions of contact which are stuck and those which slip - all as functions of time. This will enable, as a primary output, quantification of the energy absorbed per loading cycle, i.e. the 'damping coefficient'. Crack nucleation may be studied separately, as a second phase. As the mechanics of the nucleation process are imperfectly understood, this will normally demand a laboratory experiment, and hitherto these have often been performed on 'representative elements', designed to mimic the key aspects of the prototype within a simplified specimen. These *ad hoc* solutions are now being superceded by a more systematic approach in which the contact edge is encapsulated in a characteristic 'asymptotic form'[1], so that the precise conditions in the prototype contact may faithfully be reproduced in the laboratory experiment and where the results may, with equal accuracy, be applied to a range of other problems. The key idea behind this approach is that the factors controlling the process zone (state of stress and stress range) are funnelled through (usually) just two parameters - the multipliers on the asymptotic forms - and so there is a very much reduced dependence of fretting on the overall geometry of the problem.

In this thesis I make no assertion about the nature or details of the parameter controlling initiation. Such a set of variables is not properly fully understood in either plain fatigue or fretting fatigue. We know that initiation is associated with very localised irreversible deformation, which is probably associated with the presence of a microscopic defect (e.g. manufacturing imperfection), and is certainly influenced by grain-level heterogeneities. Further, the role of interfacial slip remains unclear, but clearly there is surface degradation caused by the slip, and this will have an effect. Various work towards the characterisation of fretting using localised plasticity have been made, such as C.-H. Goh et. al.[2] and the work of Zhang, Neu and McDowell [3]. In this thesis, I have a sought a very simple means of predicting where a crack might start, and the irreversible energy expended against friction, as explored by, Szolwinski and Farris[4], would seem to be one measure which fits this bill. Further, because nucleation is a phenomenon which occurs on a very small scale, I felt that the localisation of irreversible work would be a good measure.

In order to start the modelling process, we must first classify the types of contact which might arise, and list their characteristics. Figure 1-1 shows, in a idealized form, the basic types often found and demonstrates some of their properties. First, Figure

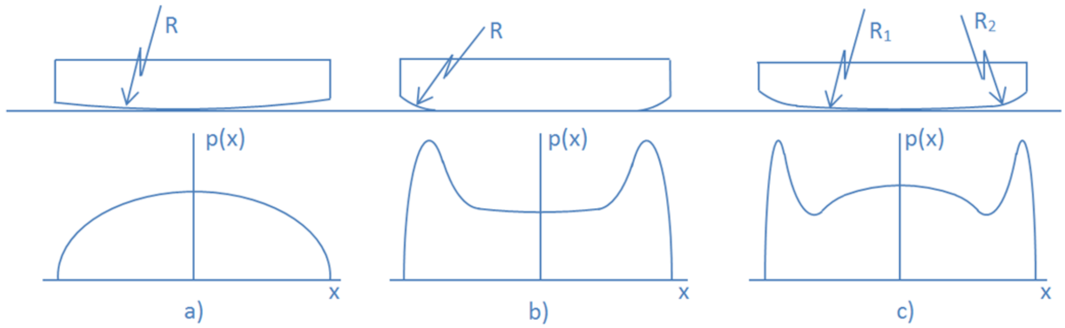

Figure 1-2 – Example of a) Hertz, b) 'Flat and Rounded' and c) 'Barrelled' incomplete contacts

1-1(a) shows a convex body pressed into a flat-faced block, which we will assume is made from the same material. This is an 'incomplete' contact. The profile and normal traction distribution for three example incomplete contact geometries is shown in Figure 1-2. The pressure falls smoothly to zero at the contact edges and, provided that the contact is small compared with the radius of curvature of the upper body front face, each may be idealised by a 'half-plane'. Further, if they are made from the same material the presence of contact pressure causes no relative tangential surface displacement, and the presence of interfacial shear induces no change in relative profile, and therefore of contact pressure: the contact is 'uncoupled'. The majority of contacts studied in this thesis are of this kind.

Figure 1-1(b) shows a square elastic block pressed into an elastically similar but much larger block of material, also having a flat face. Such a contact is said to be 'complete'. The main characteristics relevant to this discussion are that the contact defining body cannot be idealized as a half-plane and therefore the contact is highly coupled, as well as producing, under a wide range of conditions, apparently singular behaviour at the contact edges. Figure 1-1(c) shows a receding contact such as that exhibited

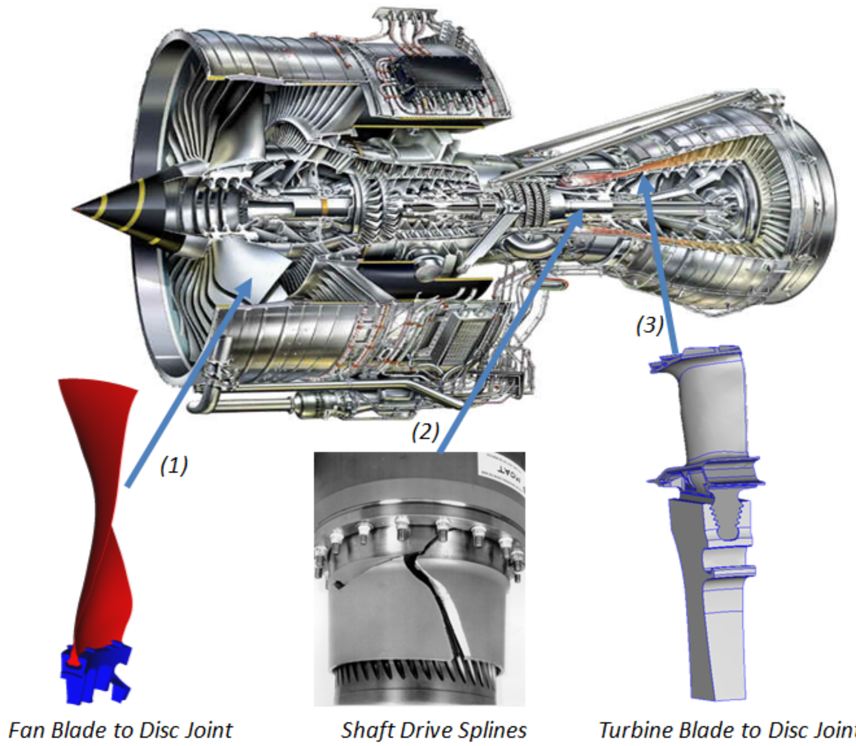

Figure 1-3 – Diagram of jet engine with relevant contacts magnified

by a bolted joint. Here, application of a normal load over a region smaller than the total width of the punch causes the contact to open at the edge, with the contact width being independent of increasing normal load.

We turn, now, to some typical stationary joints in the gas turbine, Figure 1-2, and classify them. Arrow (1) indicates the fan blade root, shown magnified at the side. It consists of a symmetrical, dovetail-shaped lug fitted into a conforming socket. The dovetail geometry normally has a flat central section and radii at each edge, and it therefore, formally, gives rise to an incomplete contact. However, there is some doubt about whether it may correctly be described by half-plane theory. Recent procedures adopted by Rolls-Royce have assumed that it may be idealised by the geometry shown in Figure 1-3, i.e. a flat-faced punch pressed onto an elastically

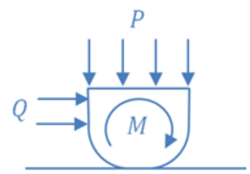

Figure 1-4 – Theoretical model used for dovetail approximation

similar block [5]. The idealization is a reasonably good one, but is compromised by two (geometrical) features; the first is that the edges of the contact faces in the female element (the 'disk') are very close to corners, and this may compromise its idealization by a true half-plane. Secondly, even within the idealised model itself (Figure 1-3) there is some doubt about whether the punch may properly be described by half-plane theory; this may seem counter-intuitive, because it may be thought that the flat section actually enhances the fidelity of the idealization, but preliminary investigations of the appropriateness of a half-plane model show that this is not so. This aspect will not be pursued in the thesis.

Arrow (2) shows the spline connexion used to couple the split shafts together, and this, too, is shown in more detail at the side. The sectional view of the tubular shafts shows that the inner one is fitted with a set of male involute 'lugs' like a coarse gear. But the outer shaft has female involutes formed which conform precisely with those on the inner shaft, so that the contact edges are abrupt, and hence the contact is complete.

Arrow (3) shows the location of blades fitted into the compressor and turbine disks. These are again shown magnified at the side, and it may be seen that so called 'fir trees' (multi-lobe connectors) fix these in place. The specification of the profiles of the male and female elements is such that they are formally, an incomplete-pair, but there is a relatively high degree of conformality between the contacting surfaces.

Thus, both incomplete and complete contacts arise at several points are found at several points within the engine. Bolted flange joints are also to be found at several points, such as the intermediate casing section. Usually, both complete and receding contacts must be handled by numerical methods, such as the finite element procedure, although progress in being made in characterizing the salient features of this class of problem analytically [6, 7]. Here, though, we shall restrict ourselves to a study of incomplete contacts and, furthermore, we shall look only at those pairs which may adequately be treated using uncoupled half-plane theory. Therefore, we shall be interested in contacts between elastically similar components, and where the degree of conformality is not high. This means that, in practice, most of the results found are relevant to the design of dovetail roots, although some of the ideas may be relevant also to firtree lugs.

Mechanics of Problem

The geometry of the problem to be studied here is shown in figure 1-4, which displays a general half-plane contact problem, with the contact defining body of arbitrary profile, and subject to three generic forms of external loading; a normal force, P, a shear force, Q, and remote tensions σ_1, σ_2. Our intention is to investigate the following effects;

First, we will look at the characteristics of a contact with a general, so-called ‘barrelled’ profile. This is a generalization of the Hertz problem in which the central section is

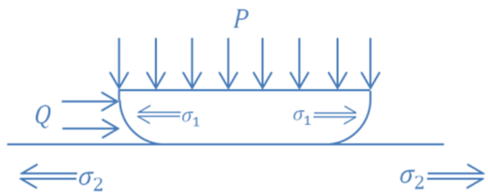

Figure 1-5 – Generic contact subject to three forms of external loading

circular and of a particular radius, whilst the outer parts are also circular, but generally of a different radius, and arranged so as to blend together smoothly at the transition point. Our object, here, is to investigate the possibility of modifying the profile of the contact so as to improve the fretting fatigue strength of the joint. This is not an easy thing to achieve, not least because we cannot say precisely what we need to optimise in order to improve the strength. So, we will, initially, simply derive a solution for the traction distribution for this problem, and the contact law.

Secondly, an important factor in assessing the fretting fatigue strength of all of these configurations is to determine the stick-slip regime present, as a function of time.

In this thesis we will examine *ab initio* the most general case of profile, loading sequence and simultaneous normal load, shear load and tension effects, and this will form a very large part of the work. This is of major importance to our understanding of the functioning of a dovetail root, for example, where, upon engine start-up, all loads develop approximately in proportional, and then, superimposed on these primary loads are a set of vibrational forces which will modify the stick-slip regime significantly.

Literature review

This thesis draws heavily on half-plane contact theory, which has its origins in the Hertz analysis [8] and which defines the contact load for a general second order body.

Since then the general principles have been used to develop a wide variety of contact solutions, and have now entered postgraduate texts such as those by Gladwell [9], Hills, Nowell and Sackfield [10] and Barber’s book on fundamentals of elasticity [11]. An excellent review is given by Deresiewicz [12] who also introduces and reviews the problem of partial slip. Historically, the first solution of this class is that defined by Carter [13] for a locomotive driving wheel, and the seminal contribution to stationary contacts is that by Cattaneo [14]. Cattaneo’s solution was re-discovered a decade or so later by Mindlin [15], who went on to treat other loading histories, in particular when the normal and shearing forces are proportional - another way of looking at this is to think of an oblique force of constant angle but increasing value [16]. Some time later Jäger [17] and Ciavarella [18] went on to extend the procedure to bodies having other forms (but still within uncoupled half-plane theory). In every case the contact was devoid of remote ‘bulk’ tensions. A separate strand of investigation examined the behaviour of a Hertzian contact when first the normal load was applied and held constant, and then a shearing force and differential bulk tension were subsequently exerted [19].

Summary

The thesis comprises an investigation of the contact stress problem for the ‘barrelled’ contact, already described, and an extensive treatment of the effects of loading history on the interfacial stress and slip. A basic premise is that the fretting fatigue nucleation process itself will normally be measured by laboratory experiment, and part of the ‘output’ from this work is to specify the contact-edge conditions required in the experiment in order to simulate reliably and with fidelity those occurring in, for example, a fan blade dovetail. A lack of prescription of the precise quantities quantifying nucleation precludes the use of a simple object function to determine an optimal geometry to support the service loads for the longest possible time. However, in order to give some guidance on what the optimal geometry might be, the density of frictional energy expenditure has been used as a possible controlling quantity, and as a means of beginning the optimisation process.

2. Piecewise quadratic Punch

Introduction

In chapter 1 it was stated that one of the aims of this piece of work was to explore the possibility of devising more enduring contact profiles, with application to the form of a fan blade dovetail root, and conceivably the multi-lobe firtree connexions, within the context of half-plane elasticity theory [10]. Constraining the problem to that of a half-plane is required to find a sufficiently simple analytical solution for numerical optimisation, which will require a number of contact geometries to be analysed for key operating conditions within an aircraft flight cycle. For example, a given form may need to be evaluated at the takeoff, climb, cruise and reverse thrust phases to assess properly its effectiveness. If interfacial shearing tractions are absent, either because the contact is lubricated or the bodies have the same elastic constants, an 'uncoupled' form of the solution is appropriate, which gives rise to a Cauchy singular integral equation of the first kind. The best known solution of this class is the celebrated Hertz contact problem in which one or both bodies have a cylindrical profile, but it is equally possible to treat, for example, shallow wedges by this method.

The problem we now consider is this; if we have a given load to carry, and a maximum permitted contact size, what is the optimal profile for the punch face to achieve this? The difficulty is that we cannot, easily, define what we mean by 'optimal', because we have no explicit object function to define the optimisation needed. Notwithstanding this obvious difficulty we shall, here, consider a quite general form of contact profile, parametrically defined, so that a number of different possible object functions might be accommodated. One simple geometry involves a central gently curved (or barrelled) profile with sharper 'dub off' edge radii, and this has already been examined[20], but it is possible to include further generality by representing the profile in a more extensive piecewise way, for example by letting the profile within each segment be quadratic in form, and requiring the profile itself and its slope to be continuous across each boundary. Ciavarella has already produced such a solution[21], and this will be further developed here. This has been made possible partly by the sustained development and widespread use of the algebraic manipulator, and the code developed is included in the thesis as Appendix A.

The problem to be solved is shown in figure 2-1. For simplicity, one of the contacting bodies is assumed to have a truly flat surface, whilst the front (contacting) face of the other has a profile defined over n segments. It is fully specified by R_i, the radius of curvature within each segment, and b_j the segment transition points, where ($1 \leq i \leq n$), ($1 \leq j \leq n+1$) and n is the number of segments.

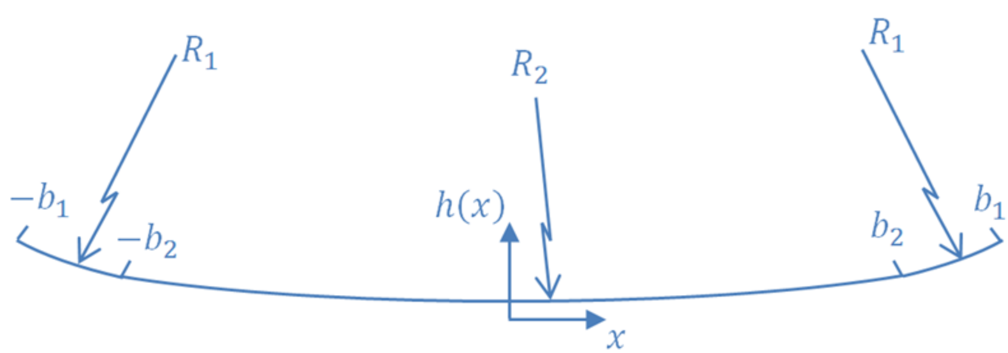

Figure 2-1 - Symmetric punch example

The constraints that apply to Hertz contacts also apply here, so that, in addition to the small strain/rotation restrictions, all segment lengths must be small in comparison with the local segment radius, partly so that a circular arc may be approximated by a parabola, and partly to ensure that surface slopes remain modest. Also, although the end segments defining the contact extent must be convex, there is no requirement for *all* internal elements to be so: one or more segments may have a negative curvature, implying concavity, with the restriction that the contact load must be sufficiently high to ensure that the contact is simply connected, and this will be looked at in some detail. In order to develop the solution in the simplest, most easily followed way, the case of a symmetric punch, will be treated first. The formulation will then be extended to the general case.

Symmetric Punch

Contact Pressure

Basic half-plane contact theory shows that the contact pressure, $p(x)$, beneath a punch making contact over the interval $[-a, a]$, is given by

$$p\left(x\right)=\frac{w\left(x\right)}{\pi}\frac{2\mu}{\kappa+1}\int_{-a}^{a}\frac{h'\left(t\right)}{\left(t-x\right)w\left(t\right)}dt, \tag{2-1}$$

provided that the punch profile, $h(x)$, is symmetric in x, where x and t are locations on the interface, measured from the centre of contact . Here $h'(x)$ is the slope of the punch, dh/dx, μ is the modulus of rigidity and κ is Kolosov's constant, giving the following relationship for two similar bodies under transverse plane strain

$$\frac{\kappa+1}{2\mu}=\frac{4\left(1-\nu^2\right)}{E} \tag{2-2}$$

where E is Young's modulus and ν Poisson's ratio, and, lastly, $w\left(x\right)=\sqrt{a^2-x^2}$. If we suppose that the punch profile is composed of a series of n discrete regions, in the i^{th} one of which the profile is given by $h_i'(t)$, we may write

$$p(x) = \frac{2\mu w(x)}{\pi(1+\kappa)} \sum_{i=1}^{n} \int_{b_i}^{b_{i+1}} \frac{h_i'(t)}{(t-x)\,w(t)} dt \qquad -a < x < a. \tag{2-3}$$

The profile gradient, $h_i'(x)$, is related to the radius of curvature in a general segment, i, by the relation

$$h_i'(x) = \frac{x}{R_i} - c_i \qquad b_i < t < b_{i+1} \tag{2-4}$$

where c_i is chosen to give continuity of slope, and hence a smooth pressure profile[1], and R_i refers to the local radius in the i^{th} segment, b_i and b_{i+1} give the bounding coordinates for the i^{th} segment. Note that although no algebraic restriction has been imposed, the profile specified must be symmetrical in x if the contact is to be symmetrical with respect to the origin.

Equation (2-5) gives the constant terms which ensure $h'(x)$ is continuous for a given array of bounding coordinates and local radii. The offset for each segment, c_i, is given by the following recursive formula

$$c_i = \begin{cases} 0 & i = 1 \\ b_i\left(\frac{1}{R_i} - \frac{1}{R_{i-1}}\right) + c_{i-1} & i = 2, 3 \ldots n \end{cases}. \tag{2-5}$$

The consistency condition demands that $c_i = 0$ for the segment(s) about which the punch is symmetric, which can be achieved by subtracting c_ι from the entire c array, where ι is the index of the central segment. Using these definitions, we arrive at the

[1] In general the slope of the profile gradient could have internal discontinuites, which would give rise to a local logarithmic singularity in the contact pressure, but here we are interested only in generating a smoothly varying contact pressure distribution.

following description of the contact pressure

$$p\left(x\right)\frac{\pi\left(\kappa+1\right)}{2\mu}=w\left(x\right)\sum_{i=1}^{n}\int_{b_i}^{b_{i+1}}\frac{R_i c_i-t}{R_i\left(x-t\right)w\left(t\right)}dt, \tag{2-6}$$

so that we may separate the integrals

$$p\left(x\right)\frac{\pi\left(\kappa+1\right)}{2\mu}=w\left(x\right)\sum_{i=1}^{n}\frac{1}{R_i}\left[\left(R_i c_i-x\right)\int_{b_i}^{b_{i+1}}\frac{dt}{\left(x-t\right)w\left(t\right)}-\int_{b_i}^{b_{i+1}}\frac{dt}{w\left(t\right)}\right]. \tag{2-7}$$

The first is always regular, with the (constant) result

$$\int_{b_i}^{b_{i+1}}\frac{dt}{w\left(t\right)}=\sin^{-1}\frac{b_{i+1}}{a}-\sin^{-1}\frac{b_i}{a}, \tag{2-8}$$

whilst the second may be either regular or Cauchy, depending on the location of the evaluation point, x, but in either case, it may be represented by the result

$$\int_{b_i}^{b_{i+1}}\frac{w\left(x\right)dt}{\left(x-t\right)w\left(t\right)} = F_1\left(x,b_{i+1}\right)-F_1\left(x,b_i\right) \tag{2-9}$$

$$F_1\left(x,b\right) = \begin{cases}\log\left(\frac{a^2-xb+\sqrt{(a^2-x^2)(a^2-b^2)}}{a(b-x)}\right) & |x|<a \\ 0 & x=\pm a\end{cases} \tag{2-10}$$

so that finally,

$$p\left(x\right)=\frac{2\mu}{\left(\kappa+1\right)\pi}\sum_{i=1}^{n}\left[\begin{array}{c}\frac{2\mu\sqrt{a^2-x^2}}{R_i\pi(\kappa+1)}\left(\sin^{-1}\frac{b_{i+1}}{a}-\sin^{-1}\frac{b_i}{a}\right)\\ -\frac{2\mu(x-R_i c_i)}{R_i\pi(\kappa+1)}\left(F_1\left(x,b_{i+1}\right)-F_1\left(x,b_i\right)\right)\end{array}\right]. \tag{2-11}$$

Contact Load

The contact load is found by ensuring overall normal equilibrium,

$$P=\int_{-a}^{a}p(x)dx, \tag{2-12}$$

which can be evaluated directly from

$$P = \int_{-a}^{a} \frac{2\mu t\, h'(t)}{(\kappa+1)\, w(t)} dt, \tag{2-13}$$

first published by Ciavarella [21], which, after some algebra, gives

$$P = \sum_{i=1}^{n} \left[\frac{\mu}{(\kappa+1) R_i} \begin{pmatrix} (b_i - 2R_i c_i)\sqrt{a^2 - b_i^2} \\ -(b_{i+1} - 2R_i c_i)\sqrt{a^2 - b_{i+1}^2} \\ +a^2 \left(\sin^{-1}\frac{b_{i+1}}{a} - \sin^{-1}\frac{b_i}{a} \right) \end{pmatrix} \right]. \tag{2-14}$$

The above formula can be used to calculate the extent of contact by evaluating over all defined regions.

Muskhelishvili Potential

The internal state of stress induced is readily found from the Muskhelishvili potential, and all the operations needed are easily performed using a manipulator. The basic recipe for the potential itself, $\phi(z)$, where z is a complex physical coordinate ($= x+iy$), is given by

$$\phi(z) = \frac{\mu\sqrt{(z^2 - a^2)}}{i\,\pi(\kappa+1)} \int_{-a}^{a} \frac{h'(t)}{w(t)(t-z)} dt \tag{2-15}$$

and, after several algebraic steps following the general strategy outlined above for the contact pressure, with the necessary changes having been made, we finally arrive at

$$\phi(z) = \frac{\mu}{i\,\pi(\kappa+1)} \sum_{i=1}^{n} \left[\frac{1}{R_i} \begin{pmatrix} (z - R_i c_i)(i\,F_2(z, b_{i+1}) - iF_2(z, b_i)) \\ -\sqrt{(z^2-a^2)}\left(\sin^{-1}\frac{b_{i+1}}{a} - \sin^{-1}\frac{b_i}{a} \right) \end{pmatrix} \right]. \qquad |b| < a \tag{2-16}$$

where

$$F_2(z, b) = \begin{cases} -i\pi & z = -a \\ \log\left(\dfrac{\sqrt{\frac{z-a}{z+a}} - \sqrt{\frac{b-a_i}{a+b}}}{\sqrt{\frac{z-a}{z+a}} + \sqrt{\frac{b-a_i}{a+b}}} \right) & |z| < a \\ 0 & z = a \end{cases}. \tag{2-17}$$

Asymmetric Punch

When the punch profile is not symmetric, as in figure 2-2, or if the profile remains symmetric but is tilted by an angle, θ, several extra complications arise which have been averted in the formulation described above.

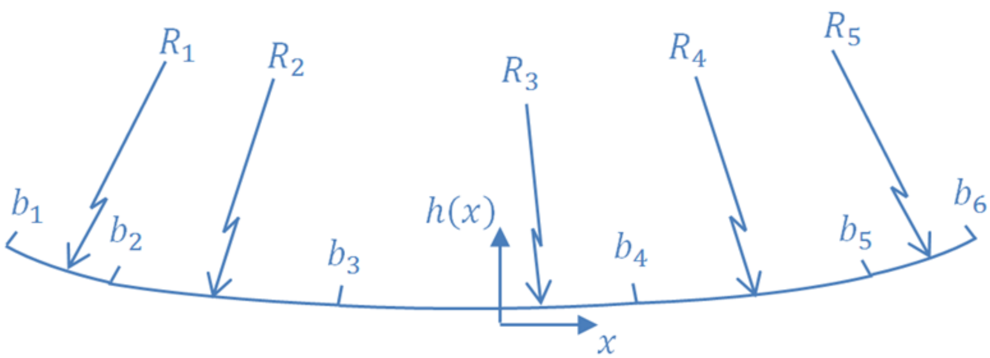

Figure 2-2 - Asymmetric punch example

First, in lieu of equation (2-1) we must now write the fundamental result for the contact pressure in the form

$$p\left(x\right) = \frac{w\left(x\right)}{\pi} \int_{a_1}^{a_2} \frac{2\mu h'\left(t\right) / \left(\kappa+1\right) - \theta}{\left(t-x\right) w\left(t\right)} dt, \tag{2-18}$$

where $a_1 \neq -a_2$, and we must find not only the *extent* of the contact patch, but also its *location* relative to the coordinate set. An immediate consequence is that the form of the fundamental function, $w(x)$, must be made a little more general by letting

$$w\left(t\right) = \sqrt{\left(a_1 - t\right)\left(t + a_2\right)}. \tag{2-19}$$

Equation 2-5 can also be used for an asymmetric punch, to find the array of intercepts, c_i. Again, the consistency condition demands that $c_i = 0$ for the segment containing the x-coordinate through which the load is applied.

The general form of the solution process follows the same pattern as before but, before we pursue this a further side-condition, identically satisfied in the case of a symmetric problem, must be imposed, and it is this which provides the extra condition needed. Geometrically, the side condition reduces the location of the two opposing sides of the contact to one degree of freedom (i.e. a contact half-width on one side of the contact has a one-to-one mapping with a contact half-width on the opposing side). Explicitly,

$$\int_{a_1}^{a_2} \frac{h'(t)}{w(t)} dt = 0. \tag{2-20}$$

As we are using a piecewise representation of $h'(t)$, we may represent the integral as the summation of a series of integrals over each segment, giving

$$\sum_{i=1}^{n} \left[\int_{b_i}^{b_{i+1}} \frac{t - R_i \left(c_i + \frac{\kappa+1}{2\mu}\theta \right)}{w(t)} dt \right] = 0 \tag{2-21}$$

so that

$$\sum_{i=1}^{n} \left[\int_{b_i}^{b_{i+1}} \frac{t\,dt}{w(t)} - R_i \left(c_i + \frac{\kappa+1}{2\mu}\theta \right) \int_{b_i}^{b_{i+1}} \frac{dt}{w(t)} \right] = 0. \tag{2-22}$$

We also define the following function,

$$N(b_i) = \frac{2b_i - a_1 - a_2}{a_2 - a_1}. \tag{2-23}$$

so that the integrals then provides the following outcome

$$\sum_{i=1}^{n} \left[\frac{1}{R_i} \left(\begin{array}{c} 2\sqrt{(a_1 - b_i)(b_i - a_2)} - 2\sqrt{(a_1 - b_{i+1})(b_{i+1} - a_2)} \\ +a_1 + a_2 + 2R_i \left(c_i + \frac{\kappa+1}{2\mu}\theta \right) \left(\sin^{-1} N(b_{i+1}) - \sin^{-1} N(b_i) \right) \end{array} \right) \right] = 0. \tag{2-24}$$

The solution to the integral for an asymmetric contact is given by

$$\int_{b_i}^{b_{i+1}} \frac{w(x)\,dt}{(x-t)\,w(t)} = F_3(x, b_{i+1}) - F_3(x, b_i) \qquad (2\text{-}25)$$

where

$$F_3(x,b) = \begin{cases} 0 & |x| < a \\ \log\left(\frac{2\sqrt{(x-a_1)(x-a_2)(a_1-b)(a_2-b)}+(a_1+a_2)(x+b)-2(xb+a_1a_2)}{(a_1-a_2)(x-b)}\right) & x = \pm a \end{cases} . \qquad (2\text{-}26)$$

The contact pressure is given by

$$p(x) = \frac{\mu}{(\kappa+1)\pi}\sum_{i=1}^{n}\left(\begin{array}{c} \frac{\sqrt{(x-a_1)(a_2-x)}}{R_i}\left(\sin^{-1}N(b_{i+1}) - \sin^{-1}N(b_i)\right) \\ -\left(F_2(x,b_{i+1}) - F_2(x,b_i)\right)\left(x/R_i - \frac{\kappa+1}{2\mu}\theta + c_i\right)\end{array}\right) \qquad (2\text{-}27)$$

and the contact law, defining the relationship between the load and contact size is

$$P = \sum_{i=1}^{n}\left[\frac{2\mu}{(\kappa+1)R_i}\left(\begin{array}{c} \frac{3a_1^2-3a_2^2-4R_i\left(c_i+\frac{\kappa+1}{2\mu}\theta\right)}{4}\left(\sqrt{\frac{(a_1-b_{i+1})(b_{i+1}-a_2)}{(a_1-a_2)^2}} - \sqrt{\frac{(a_1-b_i)(b_i-a_2)}{(a_1-a_2)^2}}\right) \\ +\frac{a_1-a_2}{2}\left(b_{i+1}\sqrt{\frac{(a_1-b_{i+1})(b_{i+1}-a_2)}{(a_1-a_2)^2}} - b_i\sqrt{\frac{(a_1-b_i)(b_i-a_2)}{(a_1-a_2)^2}}\right) \\ -\frac{3a_1^2+2a_1a_2+3a_2^2-4R_i(c_i+\frac{\kappa+1}{2\mu}\theta)(a_1+a_2)}{8}\left(\sin^{-1}N(b_i) - \sin^{-1}N(b_{i+1})\right)\end{array}\right)\right] . \qquad (2\text{-}28)$$

This, together with the side condition (equation 2-24), is needed to specify both the size and precise location of the contact once the contact load, P, and punch rotation, θ, have been defined. Note that, with this formulation, the following is also true:

$$\int_{a_1}^{a_2} p(x)x\,dx = 0, \qquad (2\text{-}29)$$

so that we know that the applied normal load passes through the origin of coordinates.

Lastly, the Muskhelishvili potential is given by

$$\phi(z) = \sum_{i=1}^{n}\left[\frac{-\mu}{(\kappa+1)\pi R_i}\left(\begin{array}{c} \left(z - R_i\left(c_i + \frac{\kappa+1}{2\mu}\theta\right)\right) i\left(F_4(z,b_{i+1}) - F_4(z,b_i)\right) \\ -i\left(\sin^{-1}N(b_{i+1}) - \sin^{-1}N(b_i)\right)\sqrt{z-a_1}\sqrt{z-a_2}\end{array}\right)\right] \qquad (2\text{-}30)$$

where

$$F_4\left(z,b\right)=\begin{cases} -i\pi & z=a_1 \\ \log\left[\frac{\log\left[\frac{b-a_2}{|a_2-b|}\right]\sqrt{\frac{z-a_2}{z-a_1}}-\log\left[\frac{a_1-b}{|a_1-b|}\right]\sqrt{\frac{a_2-b}{a_1-b}}}{\log\left[\frac{b-a_2}{|a_2-b|}\right]\sqrt{\frac{z-a_2}{z-a_1}}+\log\left[\frac{a_1-b}{|a_1-b|}\right]\sqrt{\frac{a_2-b}{a_1-b}}}\right] & a_1<z<a_2 \\ 0 & z=a_2 \end{cases} . \tag{2-31}$$

Results

As a partial check on the accuracy of the above results, it may easily be shown that they reduce, correctly, to the known results for both a Hertzian contact and a contact having a central flat face with equal radii on either side. The Mathematica code derived is given in Appendix A.

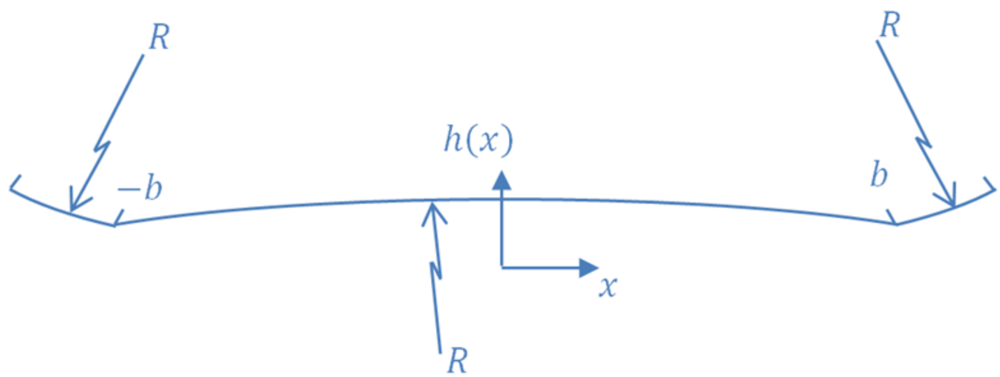

Figure 2-3 - Punch with concave central segment

As an example of the extent to which this process can be extended, although a slight deviation from the main consideration of the thesis, we consider the case of a punch comprising a central concave section bounded by two convex sections of equal radius, as shown in figure 2-3. The contact law reduces to

$$P = 2\mu \frac{a^2\left(\frac{\pi}{2} - 2\sin^{-1}\frac{b}{a}\right) - 2b\sqrt{a^2-b^2}}{(\kappa+1)\,R}, \tag{2-32}$$

and a minimum load must be imposed in order maintain the requirement that the contact be simply connected. This is given by

$$P \geq \frac{1.098\mu a^2}{(\kappa+1)\,R}. \tag{2-33}$$

Provided the load exceeds this value, the contact pressure will be everywhere positive within the contact. It is

$$p\,(x) = \frac{4\mu}{(\kappa+1)\,\pi R}\left(\sqrt{a^2-x^2}\left(\frac{\pi}{2} - 2\sin^{-1}\frac{b}{a}\right) - (b-x)F_5\,(-b) - (b+x)\,F_5\,(b)\right) \tag{2-34}$$

where

$$F_5\,(b) = \log\left(\frac{-bx + a^2 + \sqrt{(a^2-b^2)\,(a^2-x^2)}}{a(b+x)}\right). \tag{2-35}$$

A sample output, for the limiting case of incipient internal separation, is shown in figure 2-4.

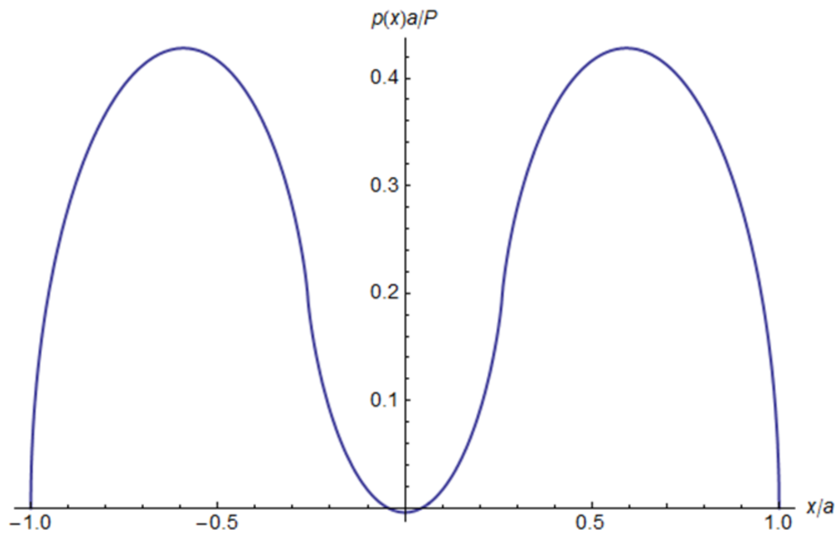

Figure 2-4 - Contact pressure distribution for limiting case of validity for a punch with a concave central segment

The assumption that the radii are equal is now relaxed, and the following parameter introduced relating the edge radius, R_1 to the central concave radius R_2.

$$k = \frac{R_1 + R_2}{R_2} \qquad R_2 > R_1 > 0 \text{ , } 1 < k < 2 \tag{2-36}$$

It is trivial to use the Mathematica code to treat this new, more general case. The result is identical to that found by Vazquez[20]. The minimum load to ensure the contact is simply connected can now be plotted as a function of k, which is shown in figure 2-5.

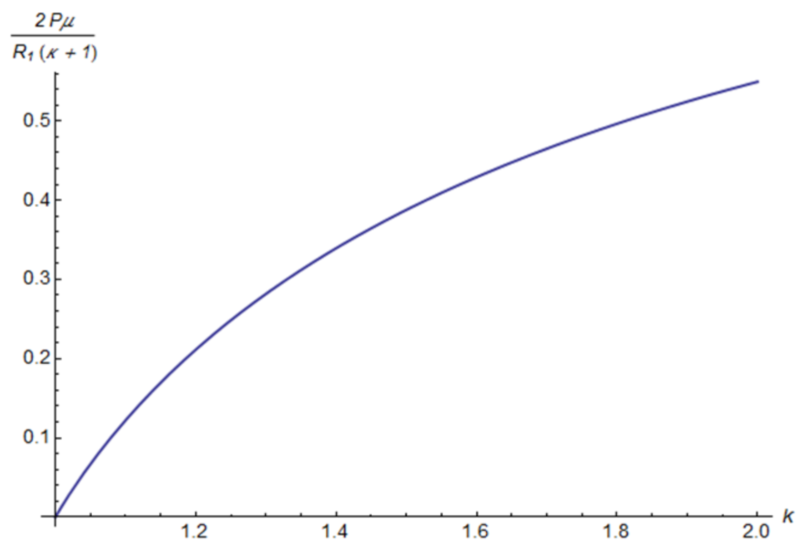

Figure 2-5 - Punch with convex centre radius not equal to outer radius: Minimum load required for single contact region.

Conclusion

An explicit recipe has been derived for finding the contact law and contact pressure distribution for a punch whose profile is defined in a piecewise quadratic sense, using uncoupled half-plane theory. The solution is derived in one of two forms; first for the case when the geometry of the punch is symmetrical, so that the contact pressure itself is even in x, and secondly, for the more general case of a punch with arbitrary profile. The latter is particularly important for partial slip contact problems, because it is needed for a symmetrical indenter which has been rotated, and this, in turn, is demanded as a corrective shear traction in partial slip contact problems, as will become clear later [18].

3. Formulation for Frictional Punch with General Loading Trajectory

Introduction

In Chapter 2 we developed a new contact pressure solution for a punch with arbitrary profile. The contact law and pressure distribution were found, but no thought was given to the effects of either a shearing force, or the presence of remote tensions in the contacting bodies. Both of these forms of external load have an important effect on the interfacial shearing traction distribution when friction is present. As discussed in Chapter one, stationary contacts subject to shear and tension have already been studied, but only when either (a) the normal load is held constant, or (b) for the special case when there is no bulk tension and the normal and shear loads are increased in proportion[23]. This is over-restrictive in the case of contacts found in gas turbines, as explained earlier. The intention in this chapter is to set out a general formulation for half-plane contact problems capable of handling almost any loading trajectory in ($P - Q - \Delta\sigma$) space under conditions of full adhesion. It also provides the basis for analysis of loading when there *is* partial slip, and this will be treated in the next chapter.

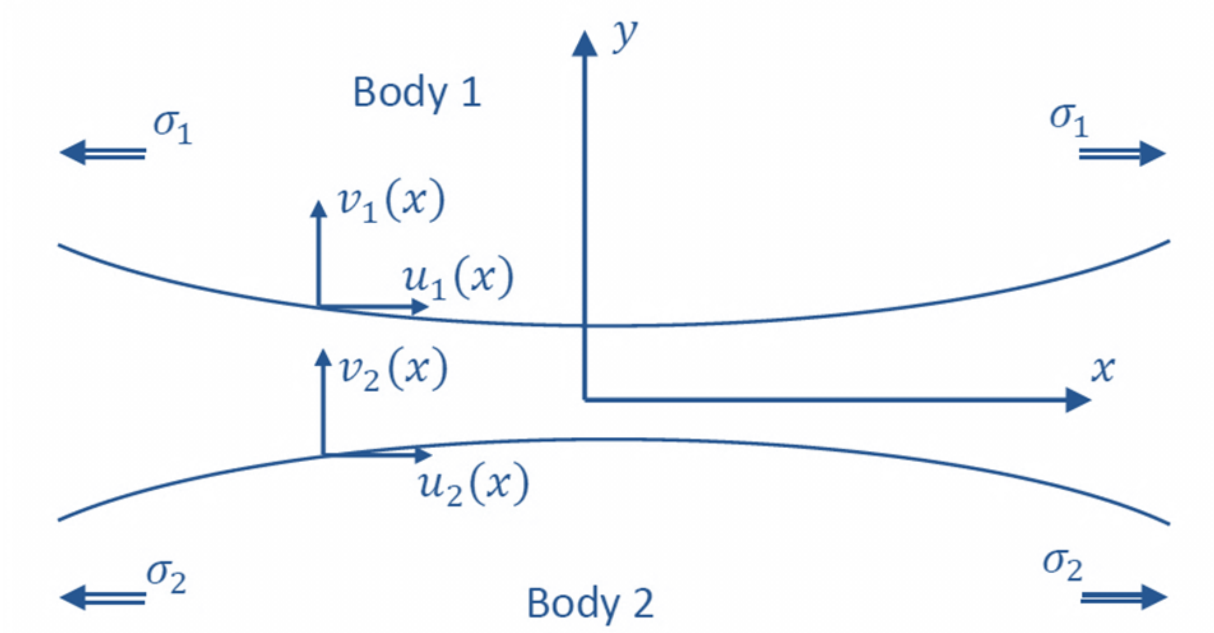

Figure 3-1(a) – Definition of the problem geometry.

The starting point for uncoupled half-plane analysis is to determine the state of stress induced by a line force, as described in [11]. From there the surface displacements due to normal and tangential line forces may be found, and superposition used to find the connexion between distributed tractions over the contact surface and the corresponding surface displacements. To avoid the unknown rigid body term, which arises when employing a half plane, we normally specify the derivatives of the surface displacements and, provided that the contacting bodies are elastically similar, arrive at the following pair of integral equations for the relative normal displacement, $v(x) = v_1(x) - v_2(x)$ (see Figure 3-1(a)), and relative surface tangential displacement, $u(x) = u_1(x) - u_2(x)$, in terms of the contact pressure, $p(x)$ and shear traction, $q(x)$

$$\frac{dv}{dx} = \frac{\kappa+1}{2\mu\pi} \int_{\text{contact}} \frac{p(\xi)\,d\xi}{x-\xi} \tag{3-1}$$

$$\frac{du}{dx} = \frac{\kappa+1}{2\mu\pi} \int_{\text{contact}} \frac{q(\xi)\,d\xi}{x-\xi} \tag{3-2}$$

where μ is the modulus of rigidity, κ Kolosov's constant ($= 3-4\nu$ in plane strain, where ν is Poisson's ratio). Indeed, it was the first of these two integrals which formed the basis of all the analysis described in chapter 2. These integrals take a different value if the observation point is within the the interval of integration (i.e. the contact) when they assume 'Cauchy principal values', from when the observation point is outside the range of integration (outside the contact), when they are 'regular'. The normal contact problem is usually solved first by setting the relative surface normal displacement gradient equal in magnitude to the slope of the gap between the bodies before they are pressed together, $g_o'(x)$,as was done in chapter 2 and, to obtain the contact law, we need to establish equilibrium between the contact pressure and the applied load, P, giving

$$P = \int_{\text{contact}} p(x)\, dx. \tag{3-3}$$

Once this has been done, the effect of tangential tractions may be found. Details of the application will dictate whether the tractions are known everywhere (if the contact is sliding) or if the displacements are known everywhere (if the contact is fully adhered) or if the interface has a mixture of slipping and adhered regions (so that a state of partial slip exists).

This method is satisfactory, and is particularly effective when first the normal load is applied and held constant, and then the shearing force is developed, but is not well suited to problems where both the normal and shearing force are varying functions of time. In these cases an alternative method, developed by Mossakovskii[24], Spence[25] and Jäger[17], which builds on the Cauchy integral equations already quoted, and uses them to form an alternative representation of the general contact problem is appropriate. The formulation, which has previously been employed without a remote tension difference between the bodies, leads to Abel type integral equations instead of the Cauchy ones, allowing a general method that is well suited to frictional problems considered incrementally in terms of normal and shear applied forces as well as bulk tension. Clearly the last two effects both excite shearing tractions.

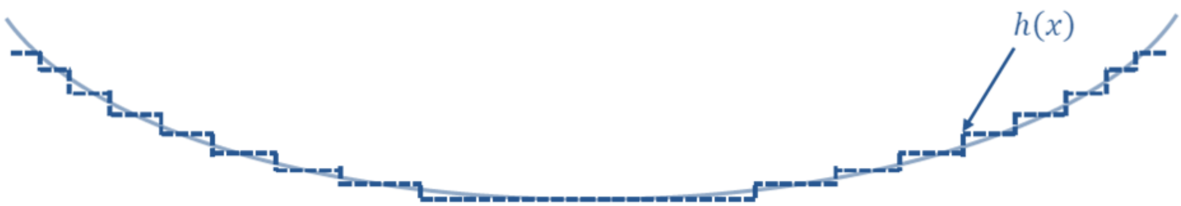

Figure 3-1(b) – Profile of the punch.

Thinking about the normal contact problem first, Figure 3-1(b), the general idea is to replace the smooth front face of the contact defining punch by one consisting of a lot of steps - in the limit infinitesimal steps - and to find the effect of a set of load increments corresponding to each of the steps. As the effect of driving the punch in is simply to increase the displacement imposed on the other body by a constant amount, the key first step is to look at traction distributions which give rise to constant surface displacements.

Solution for normal load

In preparation for the incremental solution, we note that substituting the normal pressure distribution

$$p\left(x\right)=f_{0}\left(x,a\right) \tag{3-4}$$

where

$$f_0\left(x,a\right) = \begin{array}{cc} \frac{1}{\sqrt{a^2-x^2}}; & -a < x < a \\ 0; & |x| > a \end{array} \tag{3-5}$$

into the first integral (3-1) and evaluating it produces the combined surface slope

$$\frac{dv}{dx} = \frac{(\kappa+1)}{2\mu} h_0\left(x,a\right), \tag{3-6}$$

where

$$h_0\left(x,a\right) = \begin{array}{cc} 0; & -a < x < a \\ -\frac{\mathrm{sgn}(x)}{\sqrt{x^2-a^2}}; & |x| > a. \end{array} . \tag{3-7}$$

The surface normal pressure and normal surface displacement distribution are shown in Figure 3-1(c).

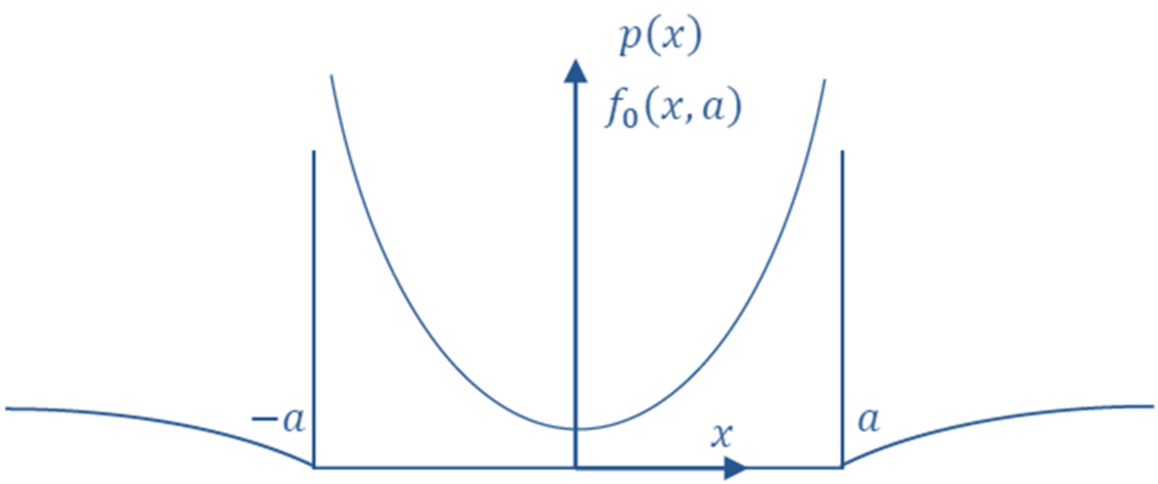

Figure 3-1(c) – Contact pressure distribution produced by a square ended punch, and corresponding surface displacement.

Thus, we know the contact pressure which must be applied over the interval $[-a \quad a]$ to produce a constant displacement over the same range, the force required to obtain this is given by

$$P = \int_{-a}^{a} p\left(x\right) dx = \int_{-a}^{a} \frac{dx}{\sqrt{a^2 - x^2}} = \pi. \tag{3-8}$$

We are now in a position to define the indentation problem in a different way from that conventionally employed. Suppose that we have already pressed the indenter, which has a profile whose slope is defined by $g_0'\left(x\right)$, in so as to make contact over the interval ($-a \leq x \leq a$). Now increase the normal load by a small amount so that, within the existing contact, the bodies suffer a further small constant compression. Additionally, the contact width increases and the compression of material within that small region must be consistent with the form of the contacting profile. In the limit, when the increment of load, dP, is very small, and the corresponding change in half width is ds, we can write the resultant contact pressure, $p(x, a)$, as the sum of a set of load steps and use superposition of the above solution to give

$$p\left(x, a\right) = \int_{0}^{a} F\left(s\right) f_0\left(x, s\right) ds, \tag{3-9}$$

where the corresponding surface relative slope is given by

$$\frac{dv}{dx} = \frac{(k+1)}{2\mu} \int_{0}^{s} F\left(s\right) h_0\left(x, s\right) ds. \tag{3-10}$$

Notice that if $F(s)$ is a continuous function,the singularity in $f_0(x, s)$ will be integrated out, so that equation (3-9) always defines a distribution that tends to zero at the edges of the contact area $x = \pm a$. In other words, the consistency condition, which has to be imposed separately in the Cauchy equation formulation, is automatically satisfied. Within the contact region the surface slope must match the slope of the profile, and hence

$$\frac{dv}{dx} = -g_0'(x) \qquad -a < x < a. \tag{3-11}$$

Thus

$$\int_0^x \frac{F(s)\,ds}{\sqrt{x^2 - s^2}} = \frac{2\mu g_0'(x)}{(k+1)} \qquad 0 < x < a, \tag{3-12}$$

which is an Abel equation for the unknown function $F(s)$ with solution

$$F(s) = \frac{4\mu}{\pi(\kappa+1)} \frac{d}{ds} \int_0^s \frac{t g_0'(t)\,dt}{\sqrt{s^2 - t^2}}. \tag{3-13}$$

Once $F(s)$ is known for the punch profile under consideration, the pressure distribution may be found from equation (3-9) as

$$p(x,a) = \int_{|x|}^a \frac{F(s)\,ds}{\sqrt{s^2 - x^2}}, \tag{3-14}$$

and, from an imposition overall normal equilibrium, it may be shown that

$$P(a) = \pi \int_0^a F(s)\,ds. \tag{3-15}$$

Tangential loading

The integral equation connecting the direct traction with the surface relative slope (3-1) is exactly the same as that connecting the shear traction with the relative surface tangential strain (3-2). It follows that the results developed above in which the contact pressure distribution needed to achieve a constant normal displacement over the interval $[-a \quad a]$ apply also to shear loading of a pair of elastically similar half planes in glancing contact, free to slide over each other everywhere except the interval ($-a \leq$

$x \leq a$), where they are bonded: the application of a remote shearing force, Q, causes a constant surface tangential displacement relative to the interior of each half-plane to be developed, so that the relative tangential surface strain must vanish. The shearing traction present along the interface, $q(x)$ is then given by

$$q(x) = f_0(x) \tag{3-16}$$

and the difference between the strains induced in the two surfaces ($\epsilon^1_{xx}(x,0) - \epsilon^2_{xx}(x,0) \equiv du/dx$) is

$$\frac{du}{dx} = \frac{(\kappa+1)}{2\mu} h_0(x,a). \tag{3-17}$$

If we apply this result to a contact which is both; (a) advancing, i.e. the normal load is a monotonically increasing function of time, and (b) where the coefficient of friction is sufficient to prevent all slip between surface particles as they are pressed into contact, we see, by analogy with the solution for normal load, that the integral equation specifying the shear traction is given by

$$q(x,a) = \int_{|x|}^{a} \frac{G_0(s)\,ds}{\sqrt{s^2 - x^2}}, \tag{3-18}$$

and the corresponding shearing force is given by

$$Q(a) = \pi \int_0^a G_0(s)\,ds. \tag{3-19}$$

When use is being made of these results in solving a contact problem, the loading history must be specified, and hence, if P,Q, are known functions of t, it follows that

$Q(P)$ is specified, $Q(a)$ must also be known, and hence

$$G_0(a) = \frac{1}{\pi}\frac{dQ}{da}. \tag{3-20}$$

Influence of remote tensions

We now introduce the possibility of surface interfacial shearing tractions arising from a different source, *viz.* the application of remote tensions to the contacting bodies. These frequently arise in practical problems and are important in controlling surface slip and fretting fatigue. A fundamental solution which provides a connexion between surface shear tractions and the corresponding surface strains is needed first. Suppose that we impose a remote tension σ_1 to the upper half-plane and a bulk tension σ_2 to the lower half-plane, whilst they remain bonded over the interval ($-a \leq x \leq a$), Figure 3-1(a). The difference in remote surface tangential strain, $\epsilon(x,t)$, due to the remote tension at time t, $\sigma(t)$, is dependent on the out of plane behaviour, but can be given generally using Bulk modulus μ and Kolosov's constant, ν, as

$$\epsilon(x,t) = \frac{(\kappa+1)\,\sigma_0(t)}{8\mu}, \tag{3-21}$$

where $\sigma_0(t) = \sigma_1(t) - \sigma_2(t)$. This, we will show, will demand a constant surface strain within the contact, and associated shearing tractions. We therefore turn, again, to equation (3-2), but now substitute the shearing traction distribution

$$q(x) = f_1(x), \tag{3-22}$$

where

$$f_1(x,a) = \begin{array}{cc} \frac{x}{\sqrt{a^2-x^2}}; & -a < x < a \\ 0; & |x| > a. \end{array} \tag{3-23}$$

which, because this shear traction is odd in x, produces no resultant force, but gives a relative direct surface strain

$$\frac{du}{dx} = \frac{(\kappa+1)}{2\mu} h_1(x,a), \tag{3-24}$$

where

$$h_1(x,a) = \begin{array}{cc} 1; & -a < x < a \\ -\left(\frac{|x|}{\sqrt{x^2-a^2}} - 1\right); & |x| > a \end{array} \tag{3-25}$$

The relative surface strain for a general, advancing, adhered contact problem (which is analogous to the surface slope in the normal contact problem), is given by

$$\epsilon(x,a) = \frac{(\kappa+1)\,\sigma_0(a)}{8\mu} - \frac{(\kappa+1)}{2\mu}\int_0^a G_1(s)\,h_1(x,s)\,ds. \tag{3-26}$$

where the first term arises from the strains produced by the remote tensions themselves. The adhesion condition demands that the total strain is constant within the contact, as it develops, and therefore that

$$\frac{\partial \epsilon(x,a)}{\partial a} = 0, \tag{3-27}$$

so that

$$G_1(a) = \frac{1}{4}\frac{d\sigma_0(a)}{da}. \tag{3-28}$$

Again, we note that the loading trajectory specifies $P(t)$ and $\sigma_0(t)$, so that $\sigma_0(P)$, and hence $\sigma_0(a)$ are given. In the general case, as material is laid down both an external shearing force and an external difference in remote tensions may be present, specifying both $G_0(s)$, $G_1(s)$. The complete shearing traction and surface strain distributions may then be found as

$$q(x,a) = \int_{|x|}^{a} \frac{G_0(s)\,ds}{\sqrt{s^2-x^2}} + \int_{|x|}^{a} \frac{xG_1(s)\,ds}{\sqrt{s^2-x^2}}. \tag{3-29}$$

$$\begin{aligned} \epsilon(x,a) &= \frac{(\kappa+1)}{2\mu}\left[\frac{\sigma_0(a)}{4} - \mathrm{sgn}(x)\int_0^{|x|}\frac{G_0(s)\,ds}{\sqrt{x^2-s^2}} + \int_0^a G_1(s)\,ds - |x|\int_0^{|x|}\frac{G_1(s)\,ds}{\sqrt{x^2-s^2}}\right] \\ &= \frac{(\kappa+1)}{2\mu}\left[\frac{\sigma_0(a)}{2} - \mathrm{sgn}(x)\int_0^{|x|}\frac{G_0(s)\,ds}{\sqrt{x^2-s^2}} - |x|\int_0^{|x|}\frac{G_1(s)\,ds}{\sqrt{x^2-s^2}}\right] \end{aligned} \tag{3-30}$$

To summarise; the solution to the problem - in the sense of the surface tractions and direct strain, are fully specified by the three functions $F(s)$, $G_0(s)$, $G_1(s)$. The first of these is, in turn, defined by the geometry of the indenter, equation (3-7), whilst the other two are defined by the loading trajectory - the relative rates at which the shearing force and differential bulk tension are developed. To illustrate the method, three example geometries - the Hertz problem, a ‘flat punch with rounded edges’ punch and a shallow symmetric wedge are now evaluated explicitly.

Example Problems

Hertz Problem

For a cylinder of radius R, where the slope of the indenter varies linearly with position

$$g_0'(x) = \frac{x}{R}, \tag{3-31}$$

so that

$$F(s) = \frac{2\mu s}{(\kappa+1)R} \tag{3-32}$$

and

$$p\left(x,a\right) = \frac{2\mu\sqrt{a^2-x^2}}{\left(\kappa+1\right)R}, \tag{3-33}$$

$$P = \frac{\pi\mu a^2}{\left(\kappa+1\right)R} \tag{3-34}$$

Flat and rounded punch

This is the problem of a punch having a central flat face of half-length b, with edge radii R, so that

$$g_0'\left(x\right) = 0 \qquad |x| < b \tag{3-35}$$

$$= \frac{|x|-b}{R}\operatorname{sgn}\left(x\right) \qquad |x| > b. \tag{3-36}$$

Therefore

$$F(s) = 0 \qquad s < b \tag{3-37}$$

$$F\left(s\right) = \frac{4\mu}{R(1+\kappa)} s\cos^{-1}\frac{b}{s} \qquad |s| > b \tag{3-38}$$

and

$$p\left(x,a\right) = \frac{4\mu}{R\left(\kappa+1\right)}\left(I_1\right) \tag{3-39}$$

$$P = \frac{2\mu\pi}{R(1+\kappa)}\left(a^2\cos^{-1}\frac{b}{a} - b\sqrt{a^2-b^2}\right), \tag{3-40}$$

where

$$
\begin{aligned}
I_1 \;&\equiv\; \int_x^a \frac{s\cos^{-1}\frac{b}{s}ds}{\sqrt{s^2-x^2}} && \text{(3-41)}\\
&= \left[\begin{array}{c} \sqrt{a^2-x^2}\cos^{-1}\frac{b}{a} - x\log a - \frac{1}{2}(b+x)\log\left(x^2-b^2\right) \\ +\frac{b}{2}\log\left(2a^2-b^2-x^2-2\sqrt{(a^2-b^2)(a^2-x^2)}\right) \\ +\frac{x}{2}\log\left(a^2\left(b^2+x^2\right)+2bx\sqrt{(a^2-b^2)(a^2-x^2)}-bx\right) \end{array}\right] - a < x < a
\end{aligned}
$$

Wedge Problem

The slope of the indenter is constant and of external (shallow) angle ϕ, so that

$$g_0'(x) = \phi\,\mathrm{sgn}(x). \tag{3-42}$$

so that

$$F(s) = \frac{4\mu\phi}{\pi(1+\kappa)} \tag{3-43}$$

and

$$
\begin{aligned}
p(x,a) \;&=\; \frac{4\mu\phi}{\pi(1+\kappa)}\cosh^{-1}\frac{a}{|x|}, && \text{(3-44)}\\
P \;&=\; \frac{4\mu\phi a}{(1+\kappa)} && \text{(3-45)}\\
a \;&=\; \frac{P(1+\kappa)}{4\mu\phi} && \text{(3-46)}
\end{aligned}
$$

Proportional Loading and the condition for full-stick

We return to the general formulation and proceed to the next stage. Suppose that a pair of contacting bodies is subject to a set of loads $P(t)$, $Q(t)$, $\sigma_0(t)$. Consider now what happens during a time step Δt, when there are corresponding changes in the load ΔP (> 0), $\Delta Q, \Delta\sigma_0$. The necessary and sufficient condition for complete adhesion is that $|\Delta q| < f\Delta p$ at all points within the contact. The above formulation lends itself extremely well to a consideration of this condition, because we see immediately (from 3-14,3-15) that

$$\Delta p\left(x\right) = \frac{\Delta P}{\pi\sqrt{a^2 - x^2}}, \tag{3-47}$$

where a is the current contact length, and this result is independent of the punch geometry (i.e. of $a\left(P\right)$). Similarly, we have also shown that a change in the shearing force and relative remote tensions produces a change in shearing traction given by

$$\Delta q\left(x\right) = \frac{\Delta Q}{\pi\sqrt{a^2 - x^2}} + \frac{x\Delta\sigma_0}{4\sqrt{a^2 - x^2}}, \tag{3-48}$$

from equations (3-28-3-29). The maximum ratio of $\Delta\left|q\left(x\right)\right|/\Delta p\left(x\right)$ will occur at one of the two end points, $x = \pm a$, depending on the relative signs of ΔQ and $\Delta\sigma_0$, and the condition for no slip at any point within the contact is clearly

$$\frac{|\Delta Q|}{\Delta P} + \frac{\pi\Delta\sigma_0 a}{4\Delta P} < f. \tag{3-49}$$

This result is independent of the form of the indenter generating the contact and is both necessary and sufficient for sustained full stick.

We now consider what happens when a contact is gradually loaded so that the elements of loading are proportional, i.e. so that

$$\frac{dP}{P} = \frac{dQ}{Q} = \frac{d\sigma_0}{\sigma_0}. \tag{3-50}$$

when equation (3-49) becomes

$$\frac{|Q|}{P} + \frac{\pi\sigma_0 a}{4P} < f. \tag{3-51}$$

where P, Q, σ_0 are their current values, and a is the contact width corresponding to P for the particular contact geometry being considered. The result found is geometry independent, but in practice P and a are connected by the contact law.

Examples - Hertz

We now remove the dependent variable, $a(P)$ from the contact algorithm (equation 3-51) using the contact law for Hertzian contact, which gives

$$\frac{|Q|}{P} + \frac{\pi\sigma_0}{4}\sqrt{\frac{R(1+\kappa)}{P\mu\pi}} < f, \tag{3-52}$$

or, the solution could be written in a slightly more familiar form by denoting $p(0)$ by p_0,so that we may specify the loading trajectory by two dimensionless parameters m, n where

$$|Q| = mP \tag{3-53}$$

$$|\sigma_0| = np_0, \tag{3-54}$$

where, for a Hertzian contact

$$p_0 = \frac{2a\mu}{R(1+\kappa)} \tag{3-55}$$

$$P = \frac{a^2\mu\pi}{R(1+\kappa)} \tag{3-56}$$

and the requirement for full adhesion is that

$$|m| + \frac{n}{2} < f. \tag{3-57}$$

This simple result, together with the loading regimes which give rise to partial slip and sliding are shown in Figure 3-2 for both Hertz and 'Flat and Rounded' (which are discussed further on p39).

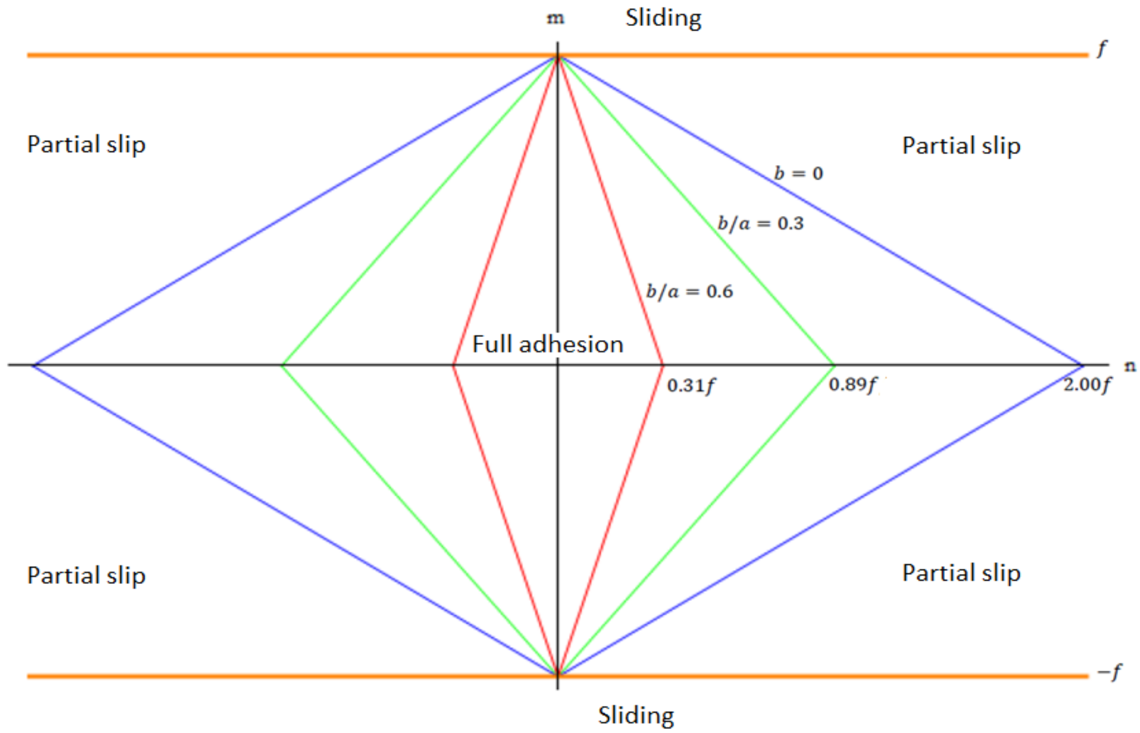

Figure 3-2 – Resulting state of stick and slip for a Flat and Rounded punch, including the Hertz case (b=0).

We can also evaluate the shear traction distribution for a single stage of loading in which the above inequality is satisfied. First write down $G_0(a)$, $G_1(a)$ and σ_0 in terms of m and n, as defined above, so that

$$G_0(a) = m\frac{2a\mu}{R(1+\kappa)} \tag{3-58}$$

$$G_1(a) = \frac{n}{2}\frac{\mu}{R(1+\kappa)} \tag{3-59}$$

$$\sigma_0 = n\frac{2a\mu}{R(1+\kappa)}. \tag{3-60}$$

The shear traction and locked in strain are given by

$$q(x,a) = \frac{\mu}{R(1+\kappa)}\left[2m\sqrt{a^2-x^2}+\frac{n}{2}x\log\left(\frac{a+\sqrt{a^2-x^2}}{|x|}\right)\right] \tag{3-61}$$

$$\epsilon(x,a) = \frac{1}{8R}\left[4na-8mx-|x|\,n\pi\right]. \tag{3-62}$$

Example - Flat and Rounded Punch

The method may also be applied to a punch having the form of a flat face (of half-length b) with rounded edges. This configuration is of particular interest in the gas turbine application, where it approximates the geometry of a fan blade dovetail root. The definition of m and n is the same as for the Hertzian case, but p_0 is defined now given by

$$p_0 = \frac{\pi}{2}\frac{a^2\cos^{-1}\frac{b}{a}+\frac{ab}{2}\log\left(2\frac{a^2}{b^2}-1-\frac{2a}{b^2}\sqrt{a^2-b^2}\right)}{a^2\cos^{-1}\frac{b}{a}-b\sqrt{a^2-b^2}}. \tag{3-63}$$

The condition for full adhesion remains as given in equation (3-57). The shear traction distribution requires $G_0(s)$ and $G_1(s)$, which are given by

$$G_0(s) = \frac{1}{\pi}\frac{dQ}{ds} = \frac{m}{\pi}\frac{dP}{ds} = \frac{4m\mu}{R(1+\kappa)}s\cos^{-1}\frac{b}{s} \tag{3-64}$$

$$G_1(s) = \frac{1}{4}\frac{d\sigma_0(s)}{ds} = \frac{n}{4}\frac{dp_0}{ds} = \frac{n\mu}{\pi R(1+\kappa)}\cos^{-1}\frac{b}{s}. \tag{3-65}$$

so that the locked-in shear traction distribution is

$$q(x,a) = \frac{4\mu}{R(1+\kappa)}\left(\frac{m}{\pi}\int_{|x|}^{a}\frac{s\cos^{-1}\frac{b}{s}}{\sqrt{s^2-x^2}}ds+\frac{nx}{4}\int_{|x|}^{a}\frac{\cos^{-1}\frac{b}{s}}{\sqrt{s^2-x^2}}ds\right). \tag{3-66}$$

The result of the first integral is given by equation (3-41), whilst the second must be evaluated numerically and the condition for full adhesion is portrayed in Figure 3-2 as a function of b/a. An example shear traction distribution for this problem, where the load has been increased until $b/a = 0.8$ is shown in Figure 3-3, for $n/m = 0$ (no bulk load), 0.2, 0.5.

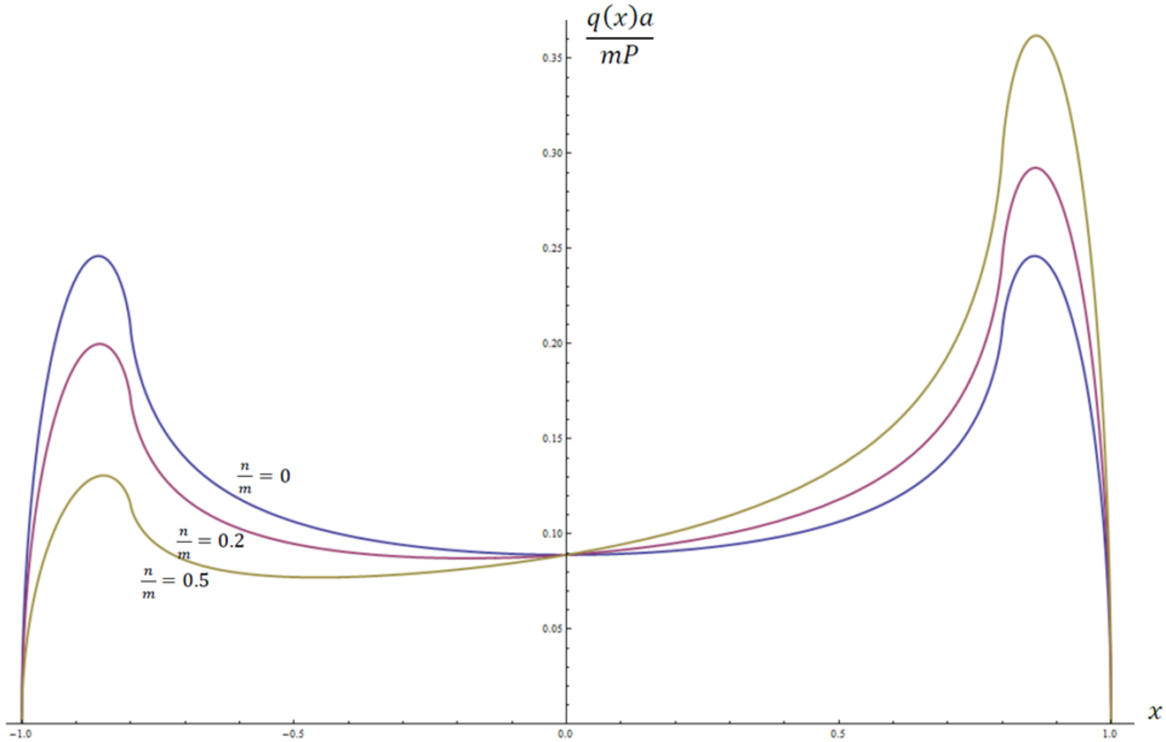

Figure 3-3 Shear traction distribution for a Flat and Rounded punch, b/a=0.8.

Although not directly relevant to the problem at hand, the case of a wedge of external (shallow) angle ϕ, is often considered in literature and so will be considered. The requirement for enduring adhesion for this case, making use of the contact law from equation (3-45), is that

$$\frac{|Q|}{P} + \pi P \sigma_0 \left(\frac{(1+\kappa)}{8\mu\phi} \right)^2 < f \tag{3-67}$$

Conclusion

A method of deriving the contact law and traction distribution for general half-plane contact problems has been developed, from the usual Cauchy relations. The solution, as written, applies to symmetrical contacts and where the contacting bodies have the same elastic constants, so that they are uncoupled. The normal contact solution is therefore independent of the shear traction distribution, and thence of the coefficient of friction, whereas the shear traction distribution derived applies whenever the contact is fully adhered. Excitation of the shearing traction by both an external shear force and differential tensions in the contacting surfaces are considered. The conditions for complete adhesion of the contact are then derived, and example application of the results to Hertzian and other contacting geometries have been carried out. Because the formulation is developed in an incremental fashion it is particularly well suited to application of many frictional contact problems having a complex loading trajectory (not just those where full adhesion is ensured) and many of the intermediate results found are of general interest and applicability. In the next chapter a detailed consideration of cyclic loading in the presence of slip, particularly for a Herztian contact, will be addressed.

4. Example Loading Segments

Introduction

The output from the last chapter provides two sets of results; it enables us, for a general contact, to find the scope of the loading trajectories where full adhesion is maintained. Secondly, it provides us with a means of determining the locked-in interfacial shearing tractions and the locked in surface strains present, at the end of the loading phase. It is the latter which we need if we then wish to find out how the contact evolves when the loading history takes us from a regime of complete adhesion to one of partial slip.

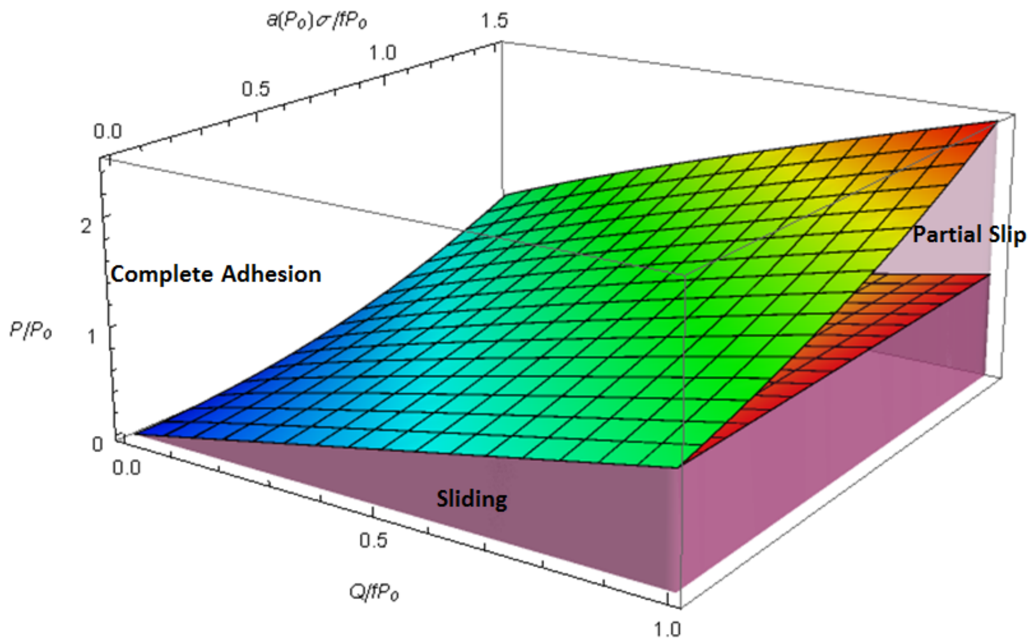

Figure 4-1(a) - 3D plot showing regions of full adhesion, partial slip and full sliding

In the last chapter we used a simplified diagram to visualise the combination of loads which maintain adhesion under proportional loading conditions (Figure 3-2), but now we will use a full three-variable representation in $P - Q - \Delta\sigma$ space. It is clear that the sliding condition, $|Q|/P \to f$ forms a wedge of half-angle f and is independent of geometry and also any bulk tension effects present. However, the condition for partial slip *does* depend on bulk tension and therefore is represented by a curved surface in $P - Q - \Delta\sigma$ space, as shown in Figure 4-1(a). A section through Figure 4-1(a) is shown in Figure 4-1(b).

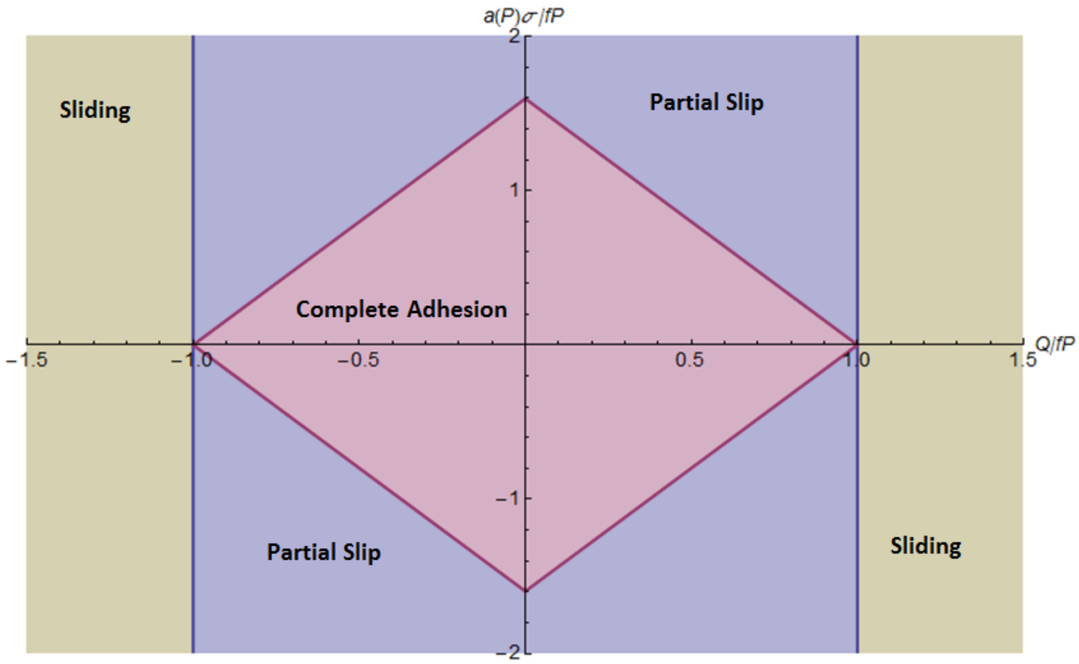

Figure 4-1(b) - 2D slice through 4-1(a) at $P/P_0 = 1$

Results from Chapter 3

In this small sub-section the results found in chapter 3 are collected for reference, as they will be needed at several points in the subsequent sections. The function $F(s)$ is connected to the profile of the punch, $g\prime(x)$, by

$$F(s) = \frac{4\mu}{\pi(\kappa+1)} \frac{d}{ds} \int_0^s \frac{t g_0'(t)\, dt}{\sqrt{s^2 - t^2}}. \tag{4-1}$$

and the corresponding pressure distribution, $p(x,a)$, is

$$p\left(x,a\right)=\int_{|x|}^{a}\frac{F\left(s\right)ds}{\sqrt{s^{2}-x^{2}}}, \tag{4-2}$$

whilst overall equilibrium requires that

$$P\left(a\right)=\pi\int_{0}^{a}F\left(s\right)ds. \tag{4-3}$$

The corresponding results for shear loading are

$$Q\left(a\right)=\pi\int_{0}^{a}G_{0}\left(s\right)ds. \tag{4-4}$$

and the shear traction can be found from

$$q\left(x,a\right)=\int_{|x|}^{a}\frac{G_{0}\left(s\right)ds}{\sqrt{s^{2}-x^{2}}}+\int_{|x|}^{a}\frac{xG_{1}\left(s\right)ds}{\sqrt{s^{2}-x^{2}}} \tag{4-5}$$

where

$$G_{0}\left(a\right) = \frac{1}{\pi}\frac{dQ}{da} \tag{4-6}$$

$$G_{1}\left(a\right) = \frac{1}{4}\frac{d\sigma_{0}\left(a\right)}{da} \tag{4-7}$$

and the corresponding locked-in strains are

$$\epsilon\left(x;a\right)=\frac{\left(\kappa+1\right)}{2\mu}\left[\frac{\sigma_{0}\left(a\right)}{2}-\operatorname{sgn}\left(x\right)\int_{0}^{|x|}\frac{G_{0}\left(s\right)ds}{\sqrt{x^{2}-s^{2}}}-|x|\int_{0}^{|x|}\frac{G_{1}\left(s\right)ds}{\sqrt{x^{2}-s^{2}}}\right]. \tag{4-8}$$

Example Application: two-stage proportional loading, both fully stuck, Hertzian Contact

We have already considered, in Chapter 3, what happens when we have proportional loading (i.e. along a straight trajectory in $P-Q-\Delta\sigma$ space). The range of lines which falls within the cone where there is enduring adhesion is known, and, furthermore, we know both the traction distribution and locked in strains at the end of the phase.

We now look at the implementation of another fully-stuck problem - one where the contact is initially loaded in a proportional manner (step 0) to a dimensionless load (m_0, n_0), and where there is a subsequent phase of proportional loading to a state (m_1, n_1). To ensure that there is never any slip during either phase the following inequalities must be satisfied

$$\left|\frac{dQ}{dP}\right|_i + \frac{\pi a}{4}\left|\frac{d\sigma}{dP}\right|_i < f \qquad i = 0, 1. \tag{4-9}$$

At this point the results apply to an arbitrary punch, but we now specialize to the case of a Hertzian contact for the rest of the section, and use the normalised parameters from the previous chapter, *viz.*

$$\left|\frac{dQ}{dP}\right|_i = m_i\,; \qquad \left|\frac{d\sigma}{dP}\right|_i \frac{\pi a_i}{2} = n_i \qquad i = 0, 1 \tag{4-10}$$

so

$$m_i + \frac{n_i}{2} < f \qquad i = 0, 1. \tag{4-11}$$

Shear traction distribution

In order to find the residual interfacial shearing traction we can, as before, use the result

$$q\left(x, a\right) = \int_{|x|}^{a} \frac{G_0\left(s\right) ds}{\sqrt{s^2 - x^2}} + \int_{|x|}^{a} \frac{x G_1\left(s\right) ds}{\sqrt{s^2 - x^2}} \tag{4-12}$$

but the functions $G_0(s), G_1(s)$ are now defined as follows

$$G_0(s) = \begin{cases} \frac{1}{\pi}\frac{dP}{ds}\left.\frac{dQ}{dP}\right|_0 = \frac{\mu}{R(1+\kappa)}2m_0 s & 0 < s < a_0 \\ \frac{1}{\pi}\frac{dP}{ds}\left.\frac{dQ}{dP}\right|_1 = \frac{\mu}{R(1+\kappa)}2m_1 s & a_0 < s < a_1 \end{cases} \tag{4-13}$$

$$G_1(s) = \begin{cases} \frac{1}{4}\frac{dP}{ds}\left.\frac{d\sigma}{dP}\right|_0 = \frac{\mu}{R(1+\kappa)}\frac{n_0}{4} & 0 < s < a_0 \\ \frac{1}{4}\frac{dP}{ds}\left.\frac{d\sigma}{dP}\right|_1 = \frac{\mu}{R(1+\kappa)}\frac{n_1}{4} & a_0 < s < a_1 \end{cases} \tag{4-14}$$

where the instantaneous contact half-width s has replaced the parameter a. The shear traction distribution induced is therefore given by

$$q(x; a_i) = \frac{2\mu}{R(1+\kappa)} \times \tag{4-15}$$

$$\left[\begin{array}{c|cc} a & 0 < x < a_0 & a_0 < x < a_1 \\ \hline a_0 & m_0 \int_{|x|}^{a_0} \frac{s ds}{\sqrt{s^2-x^2}} - \frac{n_0 x}{4} \int_{|x|}^{a_0} \frac{ds}{\sqrt{s^2-x^2}} & 0 \\ a_1 & \left[\begin{array}{c} m_0 \int_{|x|}^{a_0} \frac{s ds}{\sqrt{s^2-x^2}} + m_1 \int_{a_0}^{a_1} \frac{s ds}{\sqrt{s^2-x^2}} \\ -\frac{n_0 x}{4b_0} \int_{|x|}^{a_0} \frac{ds}{\sqrt{s^2-x^2}} - \frac{n_1 x}{4b_1} \int_{a_0}^{a_1} \frac{ds}{\sqrt{s^2-x^2}} \end{array}\right] & \left[\begin{array}{c} m_1 \int_{|x|}^{a_1} \frac{s ds}{\sqrt{s^2-x^2}} \\ -\frac{n_1 x}{4b_1} \int_{|x|}^{a_1} \frac{ds}{\sqrt{s^2-x^2}} \end{array}\right] \end{array}\right]$$

where the integrals have the results

$$\begin{array}{ll} \int_{|x|}^{a_i} \frac{s ds}{\sqrt{s^2-x^2}} = \sqrt{a_i^2 - x^2} & 0 < x < a_i \\ \int_{a_0}^{a_1} \frac{s ds}{\sqrt{s^2-x^2}} = \sqrt{a_1^2 - x^2} - \sqrt{a_0^2 - x^2} & 0 < x < a_0 \\ \int_{|x|}^{a_i} \frac{s ds}{\sqrt{s^2-x^2}} \equiv \log\left[\frac{a_i + \sqrt{a_i^2 - x^2}}{|x|}\right] = F_1(a_i, |x|) & 0 < x < a_i \\ \int_{a_0}^{a_1} \frac{s ds}{\sqrt{s^2-x^2}} \equiv \log\left[\frac{a_1 + \sqrt{a_1^2 - x^2}}{a_0 + \sqrt{a_0^2 - x^2}}\right] = F_1(a_1, a_0) & 0 < x < a_0 \end{array} \tag{4-16}$$

so

$$q(x; a_i) = \frac{\mu}{2R(1+\kappa)} \times \tag{4-17}$$

$$\left[\begin{array}{c|cc} a & 0 < x < a_0 & a_0 < x < a_1 \\ \hline a_0 & 4m_0\sqrt{a_0^2 - x^2} - n_0 x F_1(a_0, x) & 0 \\ a_1 & \begin{array}{c} 4(m_0 - m_1)\sqrt{a_0^2 - x^2} + m_1\sqrt{a_1^2 - x^2} \\ -n_0 x F_1(a_0, |x|) - n_1 x F_1(a_1, |x|) \end{array} & \begin{array}{c} 4m_1\sqrt{a_1^2 - x^2} \\ -n_1 x F_1(a_1, |x|) \end{array} \end{array}\right].$$

The shear traction distribution for an example series of load cases exhibiting this behaviour is shown in Figure 4-2, in which the first load phase is represented by the red line, and the second by the blue line.

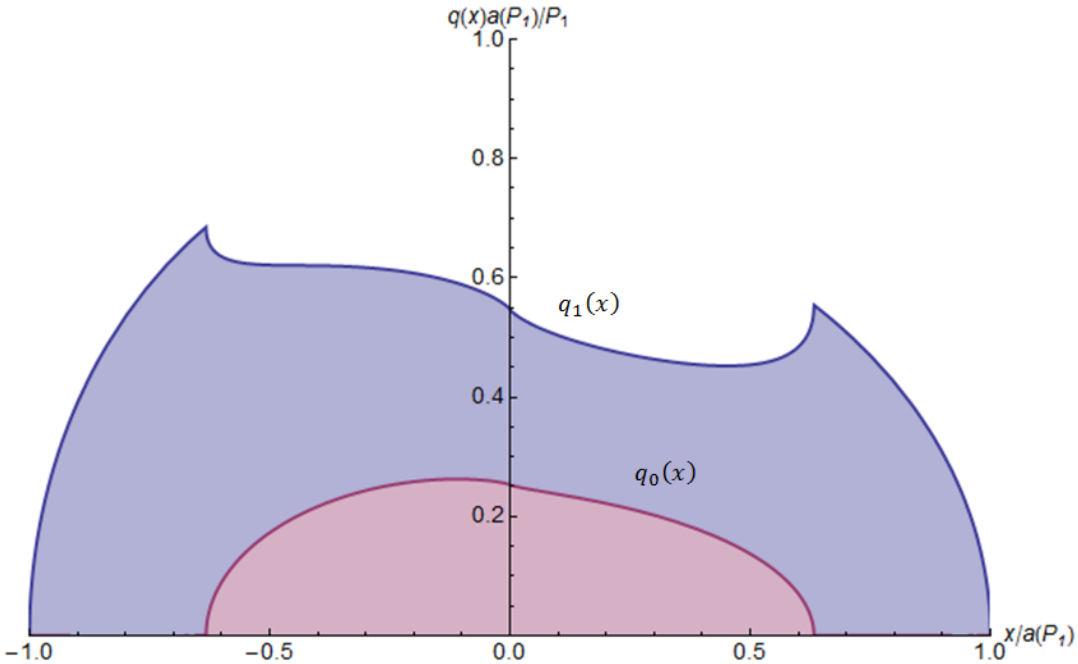

Figure 4-2 Example shear traction distribution for $P_0 = 0.4P_1$, $m_0 = 0.2$, $m_1 = 0.4$, $n_0 = 0.05$, $n_1 = 0.1$

Surface Strain distribution

We also need to know the locked in surface direct strain, for use in any subsequent calculation involving partial slip. This will be preserved in the stick region, and is given by

$$\epsilon\left(x,a\right)=\frac{\left(\kappa+1\right)}{2\mu}\left[\frac{\sigma}{2}-\mathrm{sgn}\left(x\right)\int_0^{|x|}\frac{G_0\left(s\right)ds}{\sqrt{x^2-s^2}}=|x|\int_0^{|x|}\frac{G_1\left(s\right)ds}{\sqrt{x^2-s^2}}\right] \tag{4-18}$$

We can therefore write

$$\epsilon(x,a) \;=\; \frac{1}{R}\times \tag{4-19}$$
$$\left[\begin{array}{c|cc}
a & 0<|x|<a_0 & a_0<|x|<a_1 \\
\hline
a_0 & \begin{array}{c}\frac{\sigma_0 R(\kappa+1)}{4\mu} - n_0\frac{|x|}{4}\int_0^{|x|}\frac{ds}{\sqrt{x^2-s^2}} \\ -\operatorname{sgn}(x)\, m_0\int_0^{|x|}\frac{sds}{\sqrt{x^2-s^2}}\end{array} & 0 \\
a_1 & \begin{array}{c}\frac{\sigma_0 R(\kappa+1)}{4\mu} - n_0\frac{|x|}{4}\int_0^{|x|}\frac{ds}{\sqrt{x^2-s^2}} \\ -\operatorname{sgn}(x)\, m_0\int_0^{|x|}\frac{sds}{\sqrt{x^2-s^2}}\end{array} & \begin{array}{c}\frac{\sigma_1 R(\kappa+1)}{4\mu} - \operatorname{sgn}(x)\, m_0\int_0^{a_0}\frac{sds}{\sqrt{x^2-s^2}} \\ -n_0\frac{|x|}{4}\int_0^{a_0}\frac{ds}{\sqrt{x^2-s^2}} - n_1\frac{|x|}{4}\int_{a_0}^{|x|}\frac{ds}{\sqrt{x^2-s^2}} \\ -\operatorname{sgn}(x)\, m_1\int_{a_0}^{|x|}\frac{sds}{\sqrt{x^2-s^2}}\end{array}
\end{array}\right]$$

where the bulk tension in the 1st phase is

$$\sigma_0 = \frac{2\mu}{R(1+\kappa)} n_0 a_0 \tag{4-20}$$

and in the second phase is

$$\sigma_1 = \frac{2\mu}{R(\kappa+1)}\left(n_0 a_0 + n_1\left(a_1 - a_0\right)\right). \tag{4-21}$$

The integrals needed are given by

$$\begin{array}{rl}
\int_0^{|x|}\frac{sds}{\sqrt{x^2-s^2}} = |x| & 0<|x|<a_0 \\
\int_0^{|x|}\frac{ds}{\sqrt{x^2-s^2}} = \frac{\pi}{2} & 0<|x|<a_0 \\
\int_0^{a_0}\frac{sds}{\sqrt{x^2-s^2}} = |x| - \sqrt{x^2-a_0^2} & 0<a_0<|x| \\
\int_0^{a_0}\frac{ds}{\sqrt{x^2-s^2}} = \frac{\pi}{2} - \cos^{-1}\left(\frac{a_0}{|x|}\right) & 0<a_0<|x| \\
\int_{a_0}^{|x|}\frac{sds}{\sqrt{x^2-s^2}} = \sqrt{x^2-a_0^2} & 0<a_0<|x| \\
\int_{a_0}^{|x|}\frac{ds}{\sqrt{x^2-s^2}} = \frac{\pi}{2} - \sin^{-1}\left(\frac{a_0}{|x|}\right) & 0<a_0<|x|
\end{array} \tag{4-22}$$

and so, finally,

$$\epsilon(x,a) = \frac{1}{R}\times \left[\begin{array}{c|cc} a & 0<x<a_0 & a_0<x<a_1 \\ \hline a_0 & \frac{n_0 a_0}{2} - \frac{n_0}{8}|x|\pi - m_0 x & 0 \\ a_1 & \frac{n_0 a_0}{2} - \frac{n_0}{8}|x|\pi - m_0 x & \left[\begin{array}{c} \frac{1}{2}\left(n_0 a_0 + n_1\left(a_1 - a_0\right)\right) - x m_0 \\ +\mathrm{sgn}(x)\left(m_0 - m_1\right)\sqrt{x^2 - a_0^2} \\ -n_1\frac{|x|}{4}\left(\frac{\pi}{2} - \sin^{-1}\left(\frac{a_0}{|x|}\right)\right) \\ -n_0\frac{|x|}{4}\left(\frac{\pi}{2} - \cos^{-1}\left(\frac{a_0}{|x|}\right)\right) \end{array}\right] \end{array}\right] \tag{4-23}$$

As a small, partial, check on the algebra we note that if we make the two line segments collinear, so that $n_1 = n_0$ and $m_1 = m_0$

$$\epsilon(x,a_0) = \frac{1}{8R}\left[4n_0 a_0 - |x|\, n_0 \pi - 8 m_0 x\right].$$

which is the same as the result for a single phase of proportional loading with the contact width given by a_1, in agreement with chapter 3 equation (3-62).

Example Application: two-stage proportional loading, first stage sliding, second fully stuck, Hertzian Contact

We now consider the case of a contact which, as it is gradually pressed together, is slid along and with the possible simultaneous development of a differential in-plane tension between the two contacting components. This is not a fanciful situation; it is almost certainly the regime which exists within a gas turbine fan blade dovetail when the engine is run up from a standstill. The displacement between the dovetail and its socket is controlled by the overall dilatation of the disk, and crude finite element analyses show that limited sliding occurs until the blade 'jams' with subsequent loading arising principally from vibration.

It follows that, the instant that the loading trajectory moves off the sliding condition, *viz.* $\left|\frac{dQ}{dP}\right|_0 = f$, there will be instantaneous stick, and the shear tractions and surface strains present at that instant will be locked in. If the trajectory continues in a straight line then there must be enduring stick; this phase of loading is given the subscript 1. Therefore, in terms of the dimensionless parameters already defined, we have

$$m_0 = f \qquad m_1 = \left|\frac{dQ}{dP}\right|_1 < f \tag{4-24}$$

$$n_i = \left|\frac{d\sigma}{dP}\right|_i \frac{\pi b}{2} \qquad i = 0, 1 \tag{4-25}$$

and

$$m_1 + \frac{n_1}{2} < f, \tag{4-26}$$

but note that, in contrast to the previous section,

$$m_0 + \frac{n_0}{2} \geq f. \tag{4-27}$$

Shear traction distribution

The locked-in shearing tractions are independent of n_o, so that this quantity does not appear in the results at the end of the sliding phase, and hence we can use the solution already found but choose $n_0 = 0$, giving

$$q(x, a_i) = \frac{\mu}{2R(1+\kappa)} \times \tag{4-28}$$

$$\left[\begin{array}{c|cc} a & 0 < x < a_0 & a_0 < x < a_1 \\ \hline a_0 & 4f\sqrt{a_0^2 - x^2} & 0 \\ a_1 & \begin{array}{c} 4(f - m_1)\sqrt{a_0^2 - x^2} \\ +4m_1\sqrt{a_1^2 - x^2} - n_1 x F_1(a_1, x) \end{array} & 4m_1\sqrt{a_1^2 - x^2} - n_1 x F_1(a_1, x) \end{array}\right]$$

The shear traction distribution for an example series of load cases exhibiting this behaviour is shown in Figure 4-3, again the red line represents the shear traction at the end of the first loading phase, and the blue line at the end of the second load phase.

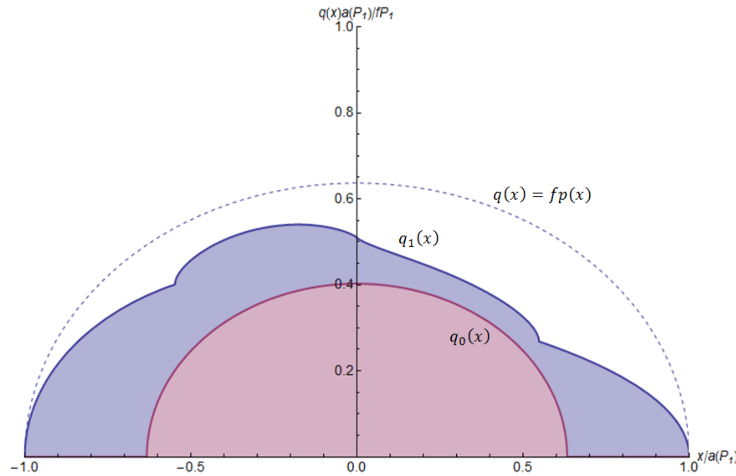

Figure 4-3 Example shear traction distribution for $P_0 = 0.3P_1$, $f = 0.3$, $m_1 = 0.2$, $n_1 = 0.1$

Surface Strain distribution

The strains present at the point of stick must be preserved, and they *do* include a contribution from the bulk tension effect, with the result

$$\epsilon(x, a_i) = \frac{1}{R} \times \tag{4-29}$$

$$\left[\begin{array}{c|cc} a & 0 < x < a_0 & a_0 < x < a_1 \\ \hline a_0 & \frac{n_0 a_0}{2} - \frac{n_0}{8}|x|\pi - fx & 0 \\ a_1 & \frac{n_0 a_0}{2} - \frac{n_0}{8}|x|\pi - fx & \left[\begin{array}{c} \frac{1}{2}\left(n_0 a_0 + n_1 (a_1 - a_0)\right) \\ -n_0 \frac{|x|}{4}\left(\frac{\pi}{2} - \cos^{-1}\frac{a_0}{|x|}\right) \\ -n_1 \frac{|x|}{4}\left(\frac{\pi}{2} - \sin^{-1}\frac{a_0}{|x|}\right) \\ -(m_1 - f)\,\mathrm{sgn}(x)\sqrt{x^2 - a_0^2} - fx \end{array}\right] \end{array}\right]$$

Example Problem III: Full stick then Partial slip

We now turn our attention to the case when the first phase of loading is proportional, and where we will maintain or add a postscript 0 to relevant quantities, $q_0(x; a_0)$, $e^0_{xx}(x; a_0)$.

There is now a further phase of proportional loading, along a different, steeper trajectory in $(Q \quad \sigma \quad P)$ space, where the full-stick inequalities are violated, but where the shearing force present is still less than that needed to cause sliding, and where the locked in tractions modify the subsequent behaviour. In this phase of the solution we will add a subscript 1, and we will, as before, write down the solution in a general form, as far as possible, before applying it to the specific case of a Hertz geometry.

We now expect regions of slip to develop, and we shall restrict our considerations to the case where the sign of slip is the same in both regions ('moderate tension'). Suppose that the contact spans the interval $[-a_1 \quad a_1]$ and the stick region lies in the range ($e_1 - c_1 < x < e_1 + c_1$), within which the strain distribution locked in by the first phase of loading, $\epsilon\left(x, a_0\right)$, will remain, whilst the shear traction in the remainder of the contact is limited by slipping friction, i.e. $q_1 = fp_1\left(x\right)$.

Shear traction distribution

To find the shearing traction within the stick region we first write

$$q_1\left(x\right) = fp_1\left(x\right) - q_1^*\left(x\right) \tag{4-30}$$

where $q_1^*\left(x\right)$ is non-zero only in the stick zone, $[e_1 - c_1 \quad e_1 + c_1]$. In order to preserve the strain in the stick zone, the shearing traction must satisfy the equation

$$\begin{aligned} \epsilon\left(x, a_1\right) &= \epsilon\left(x, a_0\right) = \\ \frac{(\kappa+1)}{2\pi\mu}\int_{-a_1}^{a_1}\frac{q_1\left(\xi\right)d\xi}{(x-\xi)} &= \frac{(\kappa+1)}{2\pi\mu}\left(\int_{-a_1}^{a_1}\frac{fp_1\left(\xi\right)d\xi}{(x-\xi)} - \int_{e_1-c_1}^{e_1+c_1}\frac{q_1^*\left(\xi\right)d\xi}{(x-\xi)}\right) \quad e_1 - c_1 < x < e_1 + c_1, \end{aligned} \tag{4-31}$$

but we recall that the basic normal contact equation is itself given by

$$\frac{\partial g}{\partial x}=\frac{(\kappa+1)}{2\pi\mu}\int_{-a_1}^{a_1}\frac{p_1(\xi)\,d\xi}{(x-\xi)} \qquad a_1<x<a_1, \tag{4-32}$$

where $\frac{\partial g}{\partial x}$ defines the profile of the indenter, by its slope, so that

$$\frac{(\kappa+1)}{2\pi\mu}\int_{e_1-c_1}^{e_1+c_1}\frac{q_1^*(\xi)\,d\xi}{(x-\xi)}=f\frac{\partial g}{\partial x}-\epsilon_0(x,a_0) \qquad e_1-c_1<x<e_1+c_1. \tag{4-33}$$

and for the particular case of one proportional phase of loading,

$$\epsilon(x;a_0)=\frac{1}{8R}\left[4n_0a_0-|x|\,n_0\pi-8m_0x\right]. \tag{4-34}$$

So, for the specific case of a Hertz problem, this becomes

$$\int_{e_1-c_1}^{e_1+c_1}\frac{q_1^*(\xi)\,d\xi}{(x-\xi)}=-\frac{2f\mu x\pi}{(\kappa+1)R}-\frac{\mu\pi}{4(\kappa+1)R}\left(4n_0a_0-|x|\,n_0\pi-8m_0x\right) \qquad e_1-c_1<x<e_1+c_1, \tag{4-35}$$

which may be re-written as

$$\int_{e_1-c_1}^{e_1+c_1}\frac{q_1^*(\xi)\,d\xi}{(x-\xi)}=-\frac{\mu\pi}{4(\kappa+1)R}\left[4n_0a_0+8x(f-m_0)-n_0|x|\pi\right]. \tag{4-36}$$

Inversion gives

$$q_1^*(x) \;=\; -\frac{w(x)\mu}{4(\kappa+1)R}\int_{e_1-c_1}^{e_1+c_1}\frac{8\xi(f-m_0)+4n_0a_0-n_0|\xi|\pi}{w(\xi)(x-\xi)}d\xi \tag{4-37}$$

$$q_1^*(x) \;=\; -\frac{w(x)\mu}{4(\kappa+1)R}\left[\begin{array}{c} 8(f-m_0)\int_{e_1-c_1}^{e_1+c_1}\frac{\xi}{w(\xi)(x-\xi)}d\xi \\ -n_0\pi\int_{e_1-c_1}^{e_1+c_1}\frac{|\xi|}{w(\xi)(x-\xi)}d\xi \\ +4n_0a_0\int_{e_1-c_1}^{e_1+c_1}\frac{1}{w(\xi)(x-\xi)}d\xi \end{array}\right] \qquad e_1-c_1<x<e_1+c_1, \tag{4-38}$$

where $w(x)$ is a 'bounded both ends' type weight function, given by

$$w(x) = \sqrt{(x - e_1 + c_1)(e_1 + c_1 - x)}. \tag{4-39}$$

Two of the integrals can be evaluated for all values of e_1 and c_1 using the formulae

$$\int_{e_1 - c_1}^{e_1 + c_1} \frac{\xi d\xi}{w(\xi)(x - \xi)} \; = \; -\pi \qquad e_1 - c_1 < x < e_1 + c_1 \tag{4-40}$$

$$\int_{e_1 - c_1}^{e_1 + c_1} \frac{d\xi}{w(\xi)(x - \xi)} \; = \; 0 \qquad e_1 - c_1 < x < e_1 + c_1 \tag{4-41}$$

whilst the remaining integral depends on the values of e_1 and c_1:

$$\int_{e_1 - c_1}^{e_1 + c_1} \frac{|\xi|\, d\xi}{w(\xi)(x - \xi)} = \begin{cases} -\int_{e_1 - c_1}^{e_1 + c_1} \frac{\xi d\xi}{w(\xi)(x-\xi)} & e_1 + c_1 < 0 \quad (A) \\ \int_{e_1 - c_1}^{0} \frac{-\xi d\xi}{w(\xi)(x-\xi)} + \int_{0}^{e_1 + c_1} \frac{\xi d\xi}{w(\xi)(x-\xi)} & e_1 - c_1 < 0 < e_1 + c_1 \quad (B) \\ \int_{e_1 - c_1}^{e_1 + c_1} \frac{\xi d\xi}{w(\xi)(x-\xi)} & 0 < e_1 - c_1 \quad (C) \end{cases} . \tag{4-42}$$

The results of A and C can be written down as

$$\int_{e_1 - c_1}^{e_1 + c_1} \frac{|\xi|\, d\xi}{w(\xi)(x - \xi)} = \begin{cases} \pi & e_1 + c_1 < 0 \quad (A) \\ -\pi & 0 < e_1 - c_1 \quad (C) \end{cases} \tag{4-43}$$

but the result of B depends on the position of the observation point, i.e. the value of x:

$$\int_{e_1 - c_1}^{0} \frac{-\xi d\xi}{w(\xi)(x - \xi)} + \int_{0}^{e_1 + c_1} \frac{\xi d\xi}{w(\xi)(x - \xi)} = \begin{cases} \left[\begin{array}{c} \left(\int_{e_1 - c_1}^{0} \frac{-\xi d\xi}{w(\xi)(x-\xi)} \right)_{\text{CPV}} \\ + \left(\int_{0}^{e_1 + c_1} \frac{\xi d\xi}{w(\xi)(x-\xi)} \right)_{\text{REG}} \end{array} \right] & e_1 - c_1 < x < 0 \\ \left[\begin{array}{c} \left(\int_{e_1 - c_1}^{0} \frac{-\xi d\xi}{w(\xi)(x-\xi)} \right)_{\text{REG}} \\ + \left(\int_{0}^{e_1 + c_1} \frac{\xi dt}{w(\xi)(x-\xi)} \right)_{\text{CPV}} \end{array} \right] & 0 < x < e_1 + c_1 \end{cases} \tag{4-44}$$

where the subscripts CPV and REG are used to define the Cauchy Principal Value or

Regular integrals. The results of these are

$$\int_{e_1-c_1}^{0} \frac{-\xi d\xi}{w(\xi)(x-\xi)} + \int_{0}^{e_1+c_1} \frac{\xi d\xi}{w(\xi)(x-\xi)} = \begin{cases} -\pi & e_1-c_1<x<0 \\ -\pi & 0<x<e_1+c_1 \end{cases} \tag{4-45}$$

So the solution to the integral is, in fact,

$$\int_{e_1-c_1}^{e_1+c_1} \frac{|\xi| d\xi}{w(\xi)(x-\xi)} = \begin{cases} \pi & e_1+c_1<0 \\ -\pi & e_1-c_1<0<e_1+c_1 \\ -\pi & 0<e_1-c_1 \end{cases}. \tag{4-46}$$

A general case can be written down

$$\int_{e_1-c_1}^{e_1+c_1} \frac{|\xi| d\xi}{w(\xi)(x-\xi)} = -\pi \mathrm{sgn}(e_1+c_1) \qquad e_1-c_1<x<e_1+c_1. \tag{4-47}$$

By collecting these results, we finally arrive at a corrective shear traction distribution given by

$$q_1^*(x) = \begin{matrix} 0 & x<e_1-c_1 \\ \frac{w(x)\mu\pi}{4(\kappa+1)R}\left[8(f-m_0) - n_0\pi \mathrm{sgn}(e_1+c_1)\right] & e_1-c_1<x<e_1+c_1 \\ 0 & e_1+c_1<x \end{matrix}, \tag{4-48}$$

Finding the location of the stick zone

This can be used in equation (*4-38)* to give the shear traction distribution. Values for e_1 and c_1 can be found from the consistency condition, and contact law. We first examine the requirement imposed by the consistency condition, arising from the integral inversion

$$0 = 8(f-m_0)\int_{e_1-c_1}^{e_1+c_1} \frac{xdx}{w(x)} + 4n_0a_0\int_{e_1-c_1}^{e_1+c_1} \frac{dx}{w(x)} - n_0\pi\int_{e_1-c_1}^{e_1+c_1} \frac{|x| dx}{w(x)} \qquad e_1-c_1<x<e_1+c_1 \tag{4-49}$$

Two of these integrals can be evaluated for all values of e_1 and c_1 using

$$\int_{e_1-c_1}^{e_1+c_1} \frac{xdx}{w(x)} = e_1\pi \quad e_1-c_1<x<e_1+c_1 \tag{4-50}$$

$$\int_{e_1-c_1}^{e_1+c_1} \frac{dx}{w(x)} = \pi \quad e_1-c_1<x<e_1+c_1 \tag{4-51}$$

whilst the remaining integral depends on the value of e_1 and c_1:

$$\int_{e_1-c_1}^{e_1+c_1} \frac{|x|\,dx}{w(x)} = \begin{cases} -\int_{e_1-c_1}^{e_1+c_1} \frac{xdx}{w(x)} & e_1+c_1\le 0 & (A) \\ -\int_{e_1-c_1}^{0} \frac{xdx}{w(x)} + \int_{0}^{e_1+c_1} \frac{xdx}{w(x)} & e_1-c_1<0<e_1+c_1 & (B) \\ \int_{e_1-c_1}^{e_1+c_1} \frac{xdx}{w(x)} & 0\le e_1-c_1 & (C) \end{cases}. \tag{4-52}$$

The integrals can be evaluated to give

$$\int_{e_1-c_1}^{e_1+c_1} \frac{|x|\,dx}{w(x)} = \begin{cases} -e_1\pi & e_1+c_1\le 0 & (A) \\ 2\sqrt{c_1^2-e_1^2}+2e_1\tan^{-1}\frac{e_1}{\sqrt{c_1^2-e_1^2}} & e_1-c_1<0<e_1+c_1 & (B) \\ e_1\pi & 0\le e_1-c_1 & (C) \end{cases} \tag{4-53}$$

so that substituting the integral formulae into the consistency condition gives

$$0 = \begin{cases} 8(f-m_0)e_1+4n_0a_0+n_0\pi e_1 & e_1+c_1\le 0 \\ \left[\begin{array}{c} 8(f-m_0)e_1+4n_0a_0 \\ -n_0\left(2\sqrt{c_1^2-e_1^2}+2e_1\tan^{-1}\frac{e_1}{\sqrt{c_1^2-e_1^2}}\right) \end{array}\right] & e_1-c_1<0<e_1+c_1 \\ 8(f-m_0)e_1+4n_0a_0-n_0\pi e_1 & 0\le e_1-c_1 \end{cases}. \tag{4-54}$$

Cases A and C can be rearranged for e_1

$$e_1 = \begin{matrix} -\frac{4n_0a_0}{8(f-m_0)+n_0\pi} & e_1+c_1<0 \\ -\frac{4n_0a_0}{8(f-m_0)-n_0\pi} & 0<e_1-c_1 \end{matrix}. \tag{4-55}$$

Finding the size of the stick zone

The size of the stick zone, c_1 can be found from the total applied shearing force

$$Q_1 = \int_{-a_1}^{a_1} q_1(x)\,dx = f\int_{-a_1}^{a_1} p(x)\,dx - \int_{e_1-c_1}^{e_1+c_1} q_1^*(x)\,dx \tag{4-56}$$

$$Q_1 = fP_1 - \frac{\mu\pi}{4(\kappa+1)R}\left[8(f-m_0) - n_0\pi\,\mathrm{sgn}(e_1+c_1)\right]\int_{e_1-c_1}^{e_1+c_1} w(x)\,dx \tag{4-57}$$

and

$$\int_{e_1-c_1}^{e_1+c_1} w(x)\,dx = \frac{c_1^2\pi}{2}, \tag{4-58}$$

We now make use of the contact law,

$$a_i^2 = \frac{P_i R}{\pi}\frac{(\kappa+1)}{\mu}, \tag{4-59}$$

and the definition of m_i,

$$Q_i = m_i P_i, \tag{4-60}$$

giving

$$\left(\frac{c_1}{a_1}\right)^2 = \frac{f-m_1}{\pi\left(f-m_0-\frac{1}{8}\mathrm{sgn}(e_1+c_1)\,n_0\pi\right)}$$

Note that the $\mathrm{sgn}(e_1+c_1)$ term must be consistent with the result for c_1 and e_1. Also, this does not depend on a_0, indicating that the **size** of the stick zone depends *only* on the *gradient* of the initial load phase, and not on the point at which the loading angle changes. However, as shown in the previous section, the **location** of the stick zone *does* depend on the first size of the contact at time the load angle changes. The shear traction distribution for an example series of load cases exhibiting this behaviour is shown in Figure 4-4, with the red line again representing the first phase, and the blue line the second.

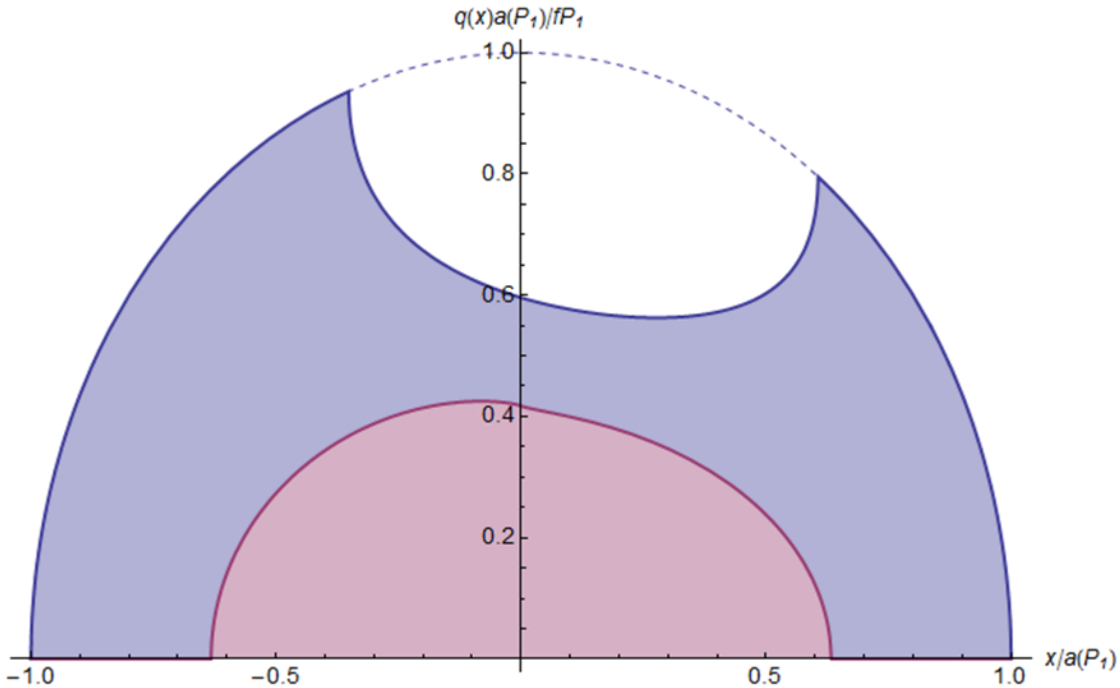

Figure 4-4 Example shear traction distribution for $P_0 = 0.5P_1, m_0 = 0.2,\ m_1 = 0.75,\ n_1 = -0.12, f = 0.5$

Surface Strain distribution

The corresponding surface strain distribution is determined from

$$\epsilon\left(x, a_0\right) = \frac{(\kappa+1)}{2\pi\mu}\left(\int_{-a_1}^{a_1} \frac{f p_1\left(\xi\right)}{(x-\xi)} d\xi - \int_{e_1-c_1}^{e_1+c_1} \frac{q_1^*\left(\xi\right)}{(x-\xi)} d\xi\right) \qquad e_1 - c_1 < x < e_1 + c_1. \tag{4-61}$$

The first integral recovers the punch geometry, as given in equation (4-32) and the latter integral will be Cauchy in the interval $[e_1 - c_1 \ \ e_1 + c_1]$ and regular otherwise.

The solutions are given by

$$\int_{e_1-c_1}^{e_1+c_1} \frac{q_1^*(\xi)}{(x-\xi)} d\xi = \frac{2\pi\mu}{R(\kappa+1)} \left[(f-m_0) - \frac{1}{8} n_0 \pi \operatorname{sgn}(e_1+c_1)\right] \int_{e_1-c_1}^{e_1+c_1} \frac{w(\xi)}{(x-\xi)} d\xi \tag{4-62}$$

$$\int_{e_1-c_1}^{e_1+c_1} \frac{w(\xi)}{(x-\xi)} d\xi = \begin{cases} x - e_1 + \sqrt{(e_1-x)^2 - c_1^2} & x < e_1 - c_1 \\ x - e_1 & e_1 - c_1 < x < e_1 + c_1 \\ x - e_1 - \sqrt{(e_1-x)^2 - c_1^2} & e_1 + c_1 < x \end{cases} \tag{4-63}$$

Definition of moderate bulk tension

The condition required to ensure no reverse slip can be found by ensuring that the strain at either edge of the contact ($x = \pm a$) are of opposite sign, which can be defined by the inequality

$$\epsilon(a;a)\,\epsilon(-a;a) < 0 \tag{4-64}$$

For the Hertz case this means that

$$[4nb - bn\pi - 8mb]\,[4nb - bn\pi + 8mb] < 0 \tag{4-65}$$

so that

$$|n| < \frac{8m}{\pi - 4} \tag{4-66}$$

Conclusion

This chapter contains a derivation for the shear traction distribution and relative surface strains present for two phases of loading in three example cases, representing a complete account of all possible states for two load phases containing moderate bulk tension, these are: (i) two phases of full adhesion, (ii) sliding followed by full adhesion and (iii) full adhesion followed by partial slip. The work can easily be extended to include any number of load phases.

5. Frictional elastic contact with periodic loading

Introduction

In an engineering system comprising elastic components with frictional interfaces, the instantaneous state (in terms of the locations of the stick and slip regions, together with the interfacial tractions within the stick regions) generally depends on the previous loading history. In particular, if the system is subjected to loads that are periodic in time, the steady state may depend on the initial conditions or on an initial transient loading phase. As a result, the effective damping in the system and/or damage due to fretting may exhibit variability due to differences in assembly procedures [28].

It has recently been established that a frictional version of Melan's theorem [29] applies to such systems if and only if the tangential and normal contact problems are uncoupled [30]. By 'uncoupled' means that a change in slip displacements has no effect on the normal contact tractions. The frictional form of the Melan theorem is defined as follows: 'if there exists a set of initial conditions (interfacial shearing tractions) such that the entire contact region can remain in a state of 'stick' without the tractions violating the limiting Coulomb friction conditions at any point of the cycle, then the system will shake down to such a state, regardless of the initial conditions'. For coupled systems, counter examples can always be found in which there exists such a 'safe shakedown state' for a given set of periodic loads, but which may not necessarily be reached from certain combinations of initial conditions (see for example, [31]). Thus, in these cases, movement across to a shaken down state is not guaranteed.

It is conjectured [28] that the frictional Melan theorem is a special case of a more general but unproven result that the steady-state response of an uncoupled frictional system depends on the initial conditions only to the extent of a self-equilibrated set of locked-in tangential tractions in a unique ‘permanent stick zone’ — i.e. a part of the contact area that does not slip during the steady state. In this chapter, we establish this conjecture for the particular case of all uncoupled two-dimensional elastic contact problems for which the bodies may be adequately described as half planes, and subjected to periodic remote loading. We shall also develop techniques for determining the extent of microslip zones and tangential tractions under general periodic loading.

The Cattaneo-Mindlin problem

Earlier in the thesis we have already come across the Cattaneo-Mindlin problem, and looked at more complex loading histories, including the restrictions on those needed to maintain full adhesion, *viz*. $|\Delta Q| < f\Delta P$, where f is the coefficient of friction. The technique was extended to general geometries by Jäger [17], who also developed an algorithm for considering more general loading scenarios as a sequence of straight line segments in PQ-space.

Periodic loading

We consider the case where the contact is subject to a combination of mean and periodic loading, typically as a result of externally driven vibration. For example, the loading might take the form

$$P(t) = P_0 + P_1 \cos(\omega t) \; ; \quad Q(t) = Q_0 + Q_1 \cos(\omega t + \phi) \; , \tag{5-1}$$

where t is time and ϕ is a relative phase angle, so that, in PQ-space, the loading sequence is an ellipse, as shown in Figure 5-1. To ensure that gross sliding never occurs, the trajectory must lie wholly within the 'friction cone', i.e. in this reduced loading space; to within the lines $Q = \pm fP$. The system starts from the unloaded condition $P = Q = 0$ and there is an initial loading phase OA leading to the ellipse. It will become clear that this phase as no bearing on the size of the steady state slip regime, and hence on the frictional energy expenditure. The steady state solution is affected only to the extent that the shearing tractions locked in wholly within the stick zones may vary - and these have no practical influence on the contact's response in terms of damping or damage.

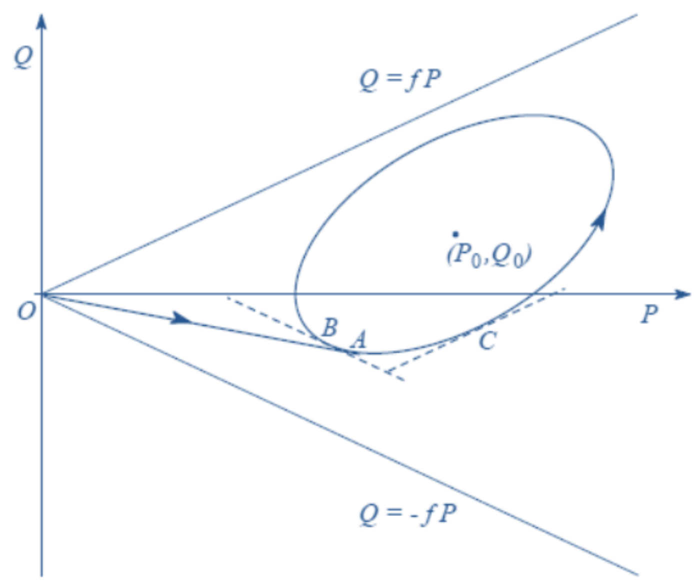

Figure 5-1 - Periodic loading cycle in PQ-space.

The special case $\phi = 0$, collapses the ellipse onto a straight line. If in addition $|Q_1| < fP_1$, the contact will remain in a state of stick throughout the loading phase $dP/dt > 0$ and also during the unloading phase, since the system then passes through the same set of equilibrium states as was traversed during loading. In this case there will therefore be no frictional dissipation and also both wear and fretting damage will be negligible. By contrast, any non-zero phase lag ($\phi \neq 0$) between the normal and tangential loading will mean that slip occurs at least during the unloading period when $dP/dt < 0$.

Evolution of the traction distribution

The contacting materials are similar (or Dundurs constant $\beta = 0$), so the normal contact problem is independent of the tangential tractions, and the contact area $\mathcal{A}$ together with the distribution of normal contact pressure $p(x)$ depend only on the instantaneous normal load P, where x is a coordinate defining position in the contact area. In this chapter we introduce and develop a very compact notation for the size of the contact and load, which we denote by $\mathcal{A}(P), p(x, P)$. These functions depend only on the profiles of the contacting bodies and the composite elastic modulus and can be determined by various classical methods, including reduction to a Riemann-Hilbert problem and solution by Cauchy integral equations as performed by Muskhelishvili [22]§119;[10]), Green's functions [35] or Fourier series [11]§12.5. Also, let

$$p'(x, P) \equiv \frac{\partial p(x, P)}{\partial P} \ . \tag{5-2}$$

The Ciavarella- Jäger result may now be written down in the very compact form

$$q(x) = fp(x, P_2) - fp(x, P_1) \tag{5-3}$$

which satisfies the conditions for slip for all points in the region laid down between 1 and 2 (i.e. $x \in \mathcal{A}(P_2)\backslash\mathcal{A}(P_1)$) and for stick (zero relative tangential displacement) in $x \in \mathcal{A}(P_1)$. Note that the second term makes a contribution only in the stick region

($x \in \mathcal{A}(P_1)$), and is zero, by definition, outside this range.

Tangential traction distribution during full stick

In the loading trajectory shown (Figure 5-1), the full stick condition $|\Delta Q| < f\Delta P$ is satisfied for all infinitesimal loading increments in the segment BC between the two points B, C where the tangent has slope $\mp f$ respectively implying $dQ/dP = \mp f$. Throughout this segment, the tangential contact problem must be solved incrementally. First note that the *change* in normal tractions during a small increase in load ΔP can be written as

$$\Delta p(x, P) = p'(x, P)\Delta P \ , \tag{5-4}$$

and the corresponding change in the tangential force must change by

$$\Delta Q = \frac{dQ}{dP}\Delta P. \tag{5-5}$$

The increment in tangential tractions must ensure that no slip occurs anywhere in the instantaneous contact area $\mathcal{A}(P)$, and from the equivalence between the normal and tangential Green's functions for the elastic half plane, we see that the tangential traction distribution satisfying this condition is proportional to the incremental normal traction distribution and hence

$$\Delta q(x, P) = p'(x, P)\Delta Q = p'(x, P)\frac{dQ}{dP}\Delta P \ . \tag{5-6}$$

This equation (5-6) defines an explicit expression for the increment in tangential tractions during the stick phase, and hence the additional tangential tractions accumulated during the finite stick phase BC can be written down as the integral

$$q_C(x) - q_B(x) = \int_{P_B}^{P_C} p'(x,P) \frac{dQ}{dP} dP \; . \tag{5-7}$$

Partial slip solution

Once point C in the trajectory is passed, the condition $d|Q|/dP < f$ is violated and hence some slip must develop. Suppose that, at point X on the ellipse the corresponding contact area and normal traction distribution are $\mathcal{A}(P_X), p(x, P_X)$ respectively. The tangential tractions can be expressed as the sum of (i) the tangential tractions $q_Y(x)$ that occurred at some earlier stage Y during the preceding full stick phase such that $P_Y < P_X$ and (ii) a generalized Cattaneo-Mindlin distribution, as in equation (5-3) with $P_2 = P_X$ and $P_1 = P_Y$.

For the first loading cycle, the initial loading path is such that full stick is maintained at all times, which gives

$$q_X(x) = \int_0^{P_Y} p'(x,P) \frac{dQ}{dP} dP + fp(x, P_X) - fp(x, P_Y) \; , \tag{5-8}$$

where (5-7) is used to determine $\int_0^{P_Y} p'(x,P) \frac{dQ}{dP} dP$. The unknown normal load P_Y is determined from tangential equilibrium, so that the resultant tangential force be equal to Q, so that

$$Q_X = Q_Y + fP_X - fP_Y \quad \text{or} \quad P_Y - fP_Y = Q_X - fP_X, \tag{5-9}$$

and the points X, Y must both lie on the same line $Q - fP = C$ where C is a constant. We can therefore identify Y by drawing such a line on the loading figure and extending it to cut the initial full stick trajectory, as shown in Figure 5-2.

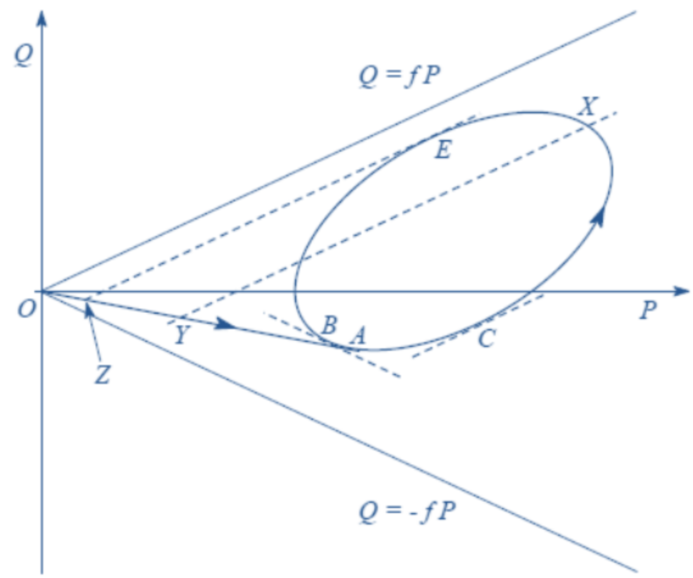

Figure 5-2 - Geometric construction for determining P_Y.

The last two terms in (5-8) comprise a Cattaneo-Mindlin distribution and hence produce no slip in the region $\mathcal{A}(P_Y)$, so the stick boundary condition in this region is satisfied, whilst in the slip region, the tractions are given by $q(x) = fp(x)$. We also require that regions that have once slipped should continue slipping so that there are no 'advancing stick zones' as defined by Dundurs and Comninou [37, 38]) and hence $d\mathcal{A}(P_Y)/dt < 0$. As $\mathcal{A}$ is a non-decreasing function of P, this is equivalent to the requirement that $dP_Y/dt \leq 0$ and it is clear from the geometry of Figure 5-2 that this condition is satisfied from C all the way around to point E, where the tangent has slope f, since X moves around the loop, point Y moves continuously to the left until X reaches E.

To determine the direction of slip in the postulated slip regions, the incremental tangential tractions during a small loading increment are obtained by differentiating (5-8), which gives

$$\Delta q(x) = p'(x, P_Y)\frac{dQ}{dP}\bigg|_{P_Y} \Delta P_Y + fp'(x, P_X)\Delta P_X - fp'(x, P_Y)\Delta P_Y \ . \tag{5-10}$$

The second term of the RHS in this expression is proportional to the normal pressure distribution under a flat punch of planform $\mathcal{A}(P_X)$ which therefore produces a uniform tangential displacement throughout this area, and which corresponds to a rigid-body displacement without slip. The remaining two terms can be grouped as

$$p'(x, P_Y)\left(\frac{dQ}{dP}\bigg|_{P_Y} - f\right)\Delta P_Y \tag{5-11}$$

and, as P_Y lies in a full stick phase where $dQ/dP < f$, the incremental tractions will be positive (so producing positive additional slip) if and only if $\Delta P_Y < 0$, and this remains true up to but not beyond point E. We also note that, as we reach point E, expression (5-11) goes to zero for all values of x. It follows that the slip rate due to the incremental shear tractions will go to zero throughout the slip region and hence the *entire* slip region will transition simultaneously at E to a state of stick.

Reverse slip phase (EB ***)***

Although the system sticks instantaneously at point E, it cannot remain in this state for a finite load interval, because P is decreasing at E and hence the condition $d|Q|/dP < f$ is not satisfied. Starting from E, a region of reverse slip extends from the edges of the contact area. To analyze this phase of the slip process, note first that the tangential tractions at E are defined by

$$q_E(x) = \int_0^{P_Z} p'(x, P)\frac{dQ}{dP}dP + fp(x, P_E) - fp(x, P_Z) \ , \tag{5-12}$$

from (5-8) with X replaced by E. Note, too, that at this point the only 'memory' of the initial loading phase OA is contained in the first and last terms, which are non-zero only in the region $\mathcal{A}(P_Z)$, which corresponds to point Z where the tangent line at E crosses the initial loading line OA. This memory is never erased and so this shows that the final steady state is, to this extent, influenced by the shape of the load trajectory in the range OZ. Further, the total tangential force associated with the first and last terms in (5-12) is $Q_Z - fP_Z$ and this represents the intercept between the tangent line at E and the Q-axis which is independent of the initial loading path.

At a general point between E and B, the corrective tractions $q_{\text{corr}}(x)$ must do three things - (i) cancel the term $fp(x, P_E)$ in (5-12) in the region $\mathcal{A}(P_E) \setminus \mathcal{A}(P)$ (as this region loses contact as P decreases), (ii) satisfy stick conditions in a region $\mathcal{A}_S$ (as yet undetermined), and (iii) convert the shear traction to backward slip $-fp(x, P_E)$ in $\mathcal{A}(P) \setminus \mathcal{A}(P_S)$. Note that if $P_B > P_E$, there will be points in EB for which $\mathcal{A}(P_E) \setminus \mathcal{A}(P)$ is null, in which case only conditions (ii,iii) need to be satisfied.

These requirements are all satisfied by the sum of two Cattaneo-Mindlin distributions defined by

$$q_{\text{corr}}(x) = -\left[fp(x, P_E) - fp(x, P_S)\right] - \left[fp(x, P) - fp(x, P_S)\right] \;, \qquad (5\text{-}13)$$

where P_S is the load (to be determined) that defines the stick region $\mathcal{A}_S$ through the relation $\mathcal{A}_S = \mathcal{A}(P_S)$. Note that, in (5-13), both terms satisfy the stick condition in $\mathcal{A}(P_S)$. The first term cancels the term $fp(x, P_E)$ in equation (5-12) and the second establishes the required reverse slip traction $-fp(x, P)$ in $\mathcal{A}(P) \setminus \mathcal{A}(P_S)$. The traction at a general point between E and B is therefore obtained by adding (5-12, 5-13) to give

$$q(x) = \int_0^{P_Z} p'(x,P)\frac{dQ}{dP}dP - fp(x,P) + 2fp(x,P_S) - fp(x,P_Z). \tag{5-14}$$

As before, P_S and hence $\mathcal{A}_S$ is determined from the corresponding tangential equilibrium condition, which is here

$$Q = Q_Z - fP + 2fP_S - fP_Z \quad \text{or} \quad P_S = \frac{1}{2}\left(\frac{Q}{f} + P - \frac{Q_Z}{f} + P_Z\right). \tag{5-15}$$

This load can also be given a simple geometrical description as shown in Figure 5-3. If we extend a line of slope $-f$ from point (P,Q) it will cut the P-axis at G, where $P_G = P + Q/f$, and similarly the line EZ cuts the P-axis at F, where $P_F = P_Z - Q_Z/f$. It follows that P_S is midway between F and G and hence is defined by the P-coordinate of the intersection point S in Figure 5-3. This construction shows that the inequality $P > P_S > P_Z$ is satisfied for all points between E and B, so the tangential displacements locked in the region $\mathcal{A}(P_Z)$ are not changed during this process. Also, P_S (and hence the stick zone $\mathcal{A}(P_S)$) decrease continuously as we move from E to B, which is important if advancing stick is to be avoided. An argument exactly parallel to that used in the forward slip phase can be used to show that the slip direction in $\mathcal{A}(P) \setminus \mathcal{A}(P_S)$ is consistent with the assumed frictional tractions (5-14). As the the tangent point B is reached the entire slip zone sticks simultaneously.

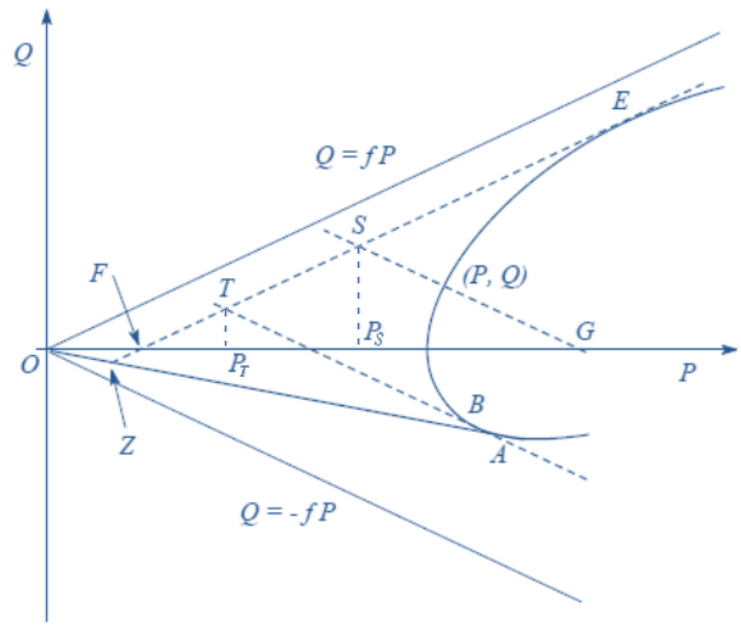

Figure 5-3 - Geometric construction for determining the stick zone during the reverse slip phase EB.

At this point, the traction distribution is

$$q_B(x) = \int_0^{P_Z} p'(x, P)\frac{dQ}{dP}dP - fp(x, P_B) + 2fp(x, P_T) - fp(x, P_Z), \tag{5-16}$$

where point T is defined in Figure 5-3.

The second (and steady state) cycle

Between B and C,there is once again full stick and the incremental tractions can be obtained by integration as before, giving

$$q(x) = q_B(x) + \int_{P_B}^{P} p'(x, P)\frac{dQ}{dP}dP\ . \tag{5-17}$$

In particular, when C is reached for the second time, we have

$$q_C(x) = \int_0^{P_Z} p'(x,P)\frac{dQ}{dP}dP + \int_{P_B}^{P_C} p'(x,P)\frac{dQ}{dP}dP - fp(x,P_B) + 2fp(x,P_T) - fp(x,P_Z)\ , \tag{5-18}$$

from (5-16, 5-17).

As in the first cycle, partial slip will start at C and the corrective traction is constructed in the same way as in (5-8), except that this time point Y defining the stick area through $\mathcal{A}(P_Y)$ is now obtained from an intersection with the segment BC rather than with the initial loading line OAC. Thus, the traction distribution in the segment CH in Figure 5-4 can be written as

$$q(x) = \int_0^{P_Z} p'(x,P)\frac{dQ}{dP}dP + \int_{P_B}^{P_Y} p'(x,P)\frac{dQ}{dP}dP + fp(x,P_X) - fp(x,P_Y) - fp(x,P_B) + 2fp(x,P_T) - fp(x,P_Z)\ . \tag{5-19}$$

This distribution applies only as long as $\mathcal{A}(P_Y) > \mathcal{A}(P_B)$ and hence $P_Y > P_B$. As point H is passed on the second cycle, the slip zone starts to erase the reverse slip tractions locked in at B and a new solution is necessary.

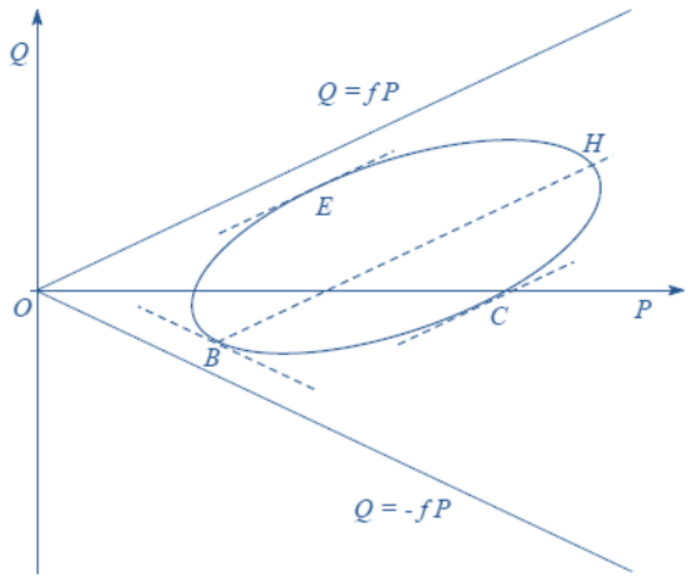

Figure 5-4 - Tractions accumulated during the reverse slip phase start to be erased after point H.

Phase HE

At point H, the second integral term in (5-19) goes to zero, $Y \to B$ and hence

$$\begin{aligned} q_H(x) \;=\; & \int_0^{P_Z} p'(x,P)\frac{dQ}{dP}dP + fp(x,P_H) - 2fp(x,P_B) + 2fp(x,P_T) \\ & - fp(x,P_Z)\ . \end{aligned} \tag{5-20}$$

During the phase HE, the contact area is shrinking and forward slip is therefore to be anticipated near the edges of this region, surrounding a shrinking stick zone. However, the extent of this stick zone cannot now be found by intersecting a line of slope f with the other side of the load loop, because reverse slip was accumulating during the phase EB, and a further development is needed.

Express the stick area as $\mathcal{A}(P_K)$, where P_K is some (as yet unknown) normal load in the range $P_T < P_K < P_B$. A correction for the reduced size of the contact area can be made by subtracting the Cattaneo-Mindlin distribution $fp(x,P_H) - fp(x,P)$, which gives the traction distribution

$$q(x) = \int_0^{P_Z} p'(x,P)\frac{dQ}{dP}dP + fp(x,P) - 2fp(x,P_B) + 2fp(x,P_T) - fp(x,P_Z)\ . \quad (5\text{-}21)$$

This satisfies the stick condition in $\mathcal{A}(P_K)$ and the forward slip condition in $\mathcal{A}(P) \setminus \mathcal{A}(P_B)$, but the slip condition in $\mathcal{A}(P_B) \setminus \mathcal{A}(P_K)$ is *not* satisfied because of the term $-2fp(x,P_B)$. However, this can be corrected, whilst preserving the remaining boundary conditions, by adding a further Cattaneo-Mindlin term $2fp(x,P_B) - 2fp(x,P_K)$, so that

$$\begin{aligned} q(x) \ &= \ \int_0^{P_Z} p'(x,P)\frac{dQ}{dP}dP + fp(x,P) - 2fp(x,P_K) + 2fp(x,P_T) \\ &\qquad - fp(x,P_Z)\ , \end{aligned} \quad (5\text{-}22)$$

for the tractions during the phase HE. As before, the unknown force P_K is obtained from the tangential equilibrium condition

$$Q = Q_E + fP - 2fP_K + 2fP_T - fP_Z\ , \quad (5\text{-}23)$$

or

$$P_K = P_T + \frac{1}{2}\left(P - \frac{Q}{f} - P_Z + \frac{Q_Z}{f}\right)\ . \quad (5\text{-}24)$$

The term in brackets must be positive, as point (P,Q) lies to the right of the tangent line EZ which implies that $P - Q/f > P_Z - Q_Z/f$. Therefore $P_K > P_T$, as assumed, and also that the two become equal as E is reached. At this point, the forward slip zone has completely erased the tractions accumulated during the reverse slip phase EB and the traction distribution is identical to that at the same point during the first cycle, being given by equation (5-12). Therefore, all subsequent loading cycles will follow the same path, so the steady state is reached after one cycle of periodic loading.

The permanent stick zone

The smallest extent of the stick zone is represented by $\mathcal{A}(P_T)$, where point T is identified in Figure 5-3 as the intersection of two lines of slope $\pm f$ tangential to the load loop. It is clear that this point is independent of the initial loading path OA and thus the extent of the permanent stick zone is unique. The tractions locked into the permanent stick zone *are* influenced by the initial loading path, but the total tangential force transmitted through this zone at any given point in the cycle depends only on the steady state loading cycle. For example, at point E, the tangential tractions are given by equation (5-12) and the sum of the tractions in the permanent stick zone $\mathcal{A}(P_T)$ is

$$\int_{\mathcal{A}(P_T)} q_E(x)dx = Q_Z - fP_Z + f\int_{\mathcal{A}(P_T)} p(x, P_E)dx \ . \tag{5-25}$$

The last term in this equation is independent of the initial loading path and it has already been noted that the first two terms define the intercept of the tangent line at E with the Q-axis, which clearly depends only on the periodic part of the loading.

Further, the values of P_T, P_E and hence $\mathcal{A}(P_T)$ would be unchanged if the load loop were to be displaced in the Q-direction whilst preserving its shape and orientation, (assuming that this displacement did not violate the ‘no-sliding’ condition that the entire loop lie between the bounding lines $Q = \pm fP$). In other words, the extent of the permanent stick zone is independent of Q_0 in (5-1), subject to this restriction. It also follows that the last term in (5-25) is independent of Q_0, but the intercept defined by the first two terms will increase by the increment in Q_0. Thus, changing the mean tangential load merely causes the tractions locked into $\mathcal{A}(P_T)$ to increase by an equal amount, whilst the tangential tractions *outside* $\mathcal{A}(P_T)$ are always independent of Q_0, even during periods of stick.

Energy dissipated in friction

During periods of slip, work will be done by the tangential tractions in the slip regions, moving through the corresponding slip displacements $u(x)$. The dissipation rate can be written

$$\dot{W} = \int_{\mathcal{A}(P)} q(x)\dot{u}(x)dx \ , \tag{5-26}$$

where the dot denotes differentiation with respect to time. Now, the slip displacement can be written down as an integral of the tangential tractions, and its time derivative $\dot{u}(x)$ depends only on the time derivative of these tractions, which we have established is independent of the initial conditions. It follows that the energy dissipated in friction per cycle depends only on the periodic loading cycle and is also independent of Q_0 in equation (5-1)

More general load cycles

Most practical loading cycles will result from machine vibration (possibly at a single dominant frequency) and will therefore be quasi-elliptical, as defined by equation (5-1). However,the arguments here developed apply to any scenario in which the corresponding loop has a monotonically turning tangent. In fact, more complex curves can also be allowed without a change in the procedure, as long as they do not precipitate an additional change from forward slip to backward slip, or slip to stick, and this condition will be satisfied as long as the load loop has just four points of tangency with lines of slope $\pm f$.

Conclusion

In this chapter, it is shown that if two two-dimensional elastically similar bodies are subjected to far-field periodic loading, the following properties of the steady-state frictional behaviour are independent of the initial conditions or an initial transient loading phase, provided only that the tangential and normal contact problems are uncoupled:-

- The extent of the permanent stick zone, comprising points that do not slip or separate during the steady state.
- The tractions at all points outside the permanent stick zone.
- The slip velocities at all such points.

The complete stick-slip pattern and shearing traction distribution at all points during the loading cycle may also be found by a sequence of superpositions, and requires very little calculation beyond that of the classical Cattaneo solution. It was also noted that there was no period of advancing stick.

6. Energy expended against friction - damage and damping

Introduction

The procedure for determining the traction distributions and stick-slip zone mix is given in full in chapter 5, for a partial slip contact idealized by uncoupled half-plane theory, Figure 6-1. In this chapter we look at irreversible energy dissipation, with two objectives; we know that irreversible energy losses are deleterious in the sense that, where energy is dissipated the conditions are ripe for crack nucleation. Therefore, as discussed in Chapter I, one of our objectives will be to determine the maximum *density* of frictional losses, and we expect this to correlate at least reasonably well with the conditions - location and number of cycles - to crack nucleation. However, the loss of energy is not wholly deleterious; it also absorbs energy present because of harmonic (vibrational) excitation of loading at, for example, blade roots at various stages in the gas turbine rotor.

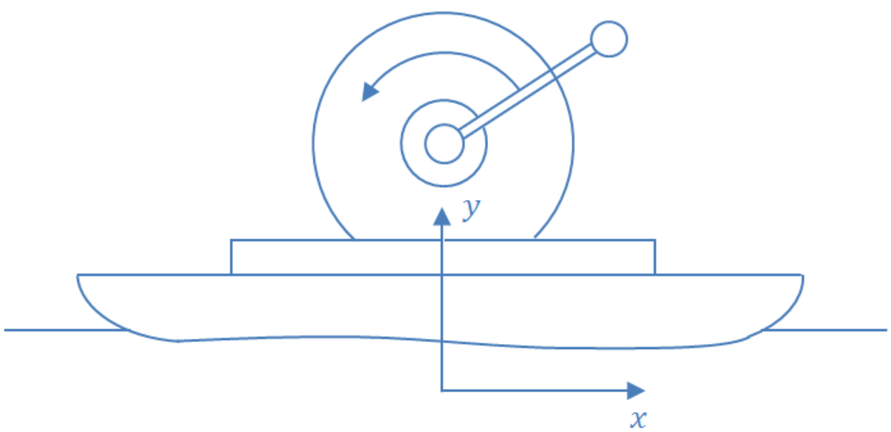

Figure 6-1 – Contact suppourting a motor with an eccentric weight

The philosophy is one of using a superposition of shearing tractions corresponding to scaled values of the normal load and hence extent of the contact, as the contact problem is taken from an unloaded state to a point on the loop, Figure 6-2, and then around the loop .

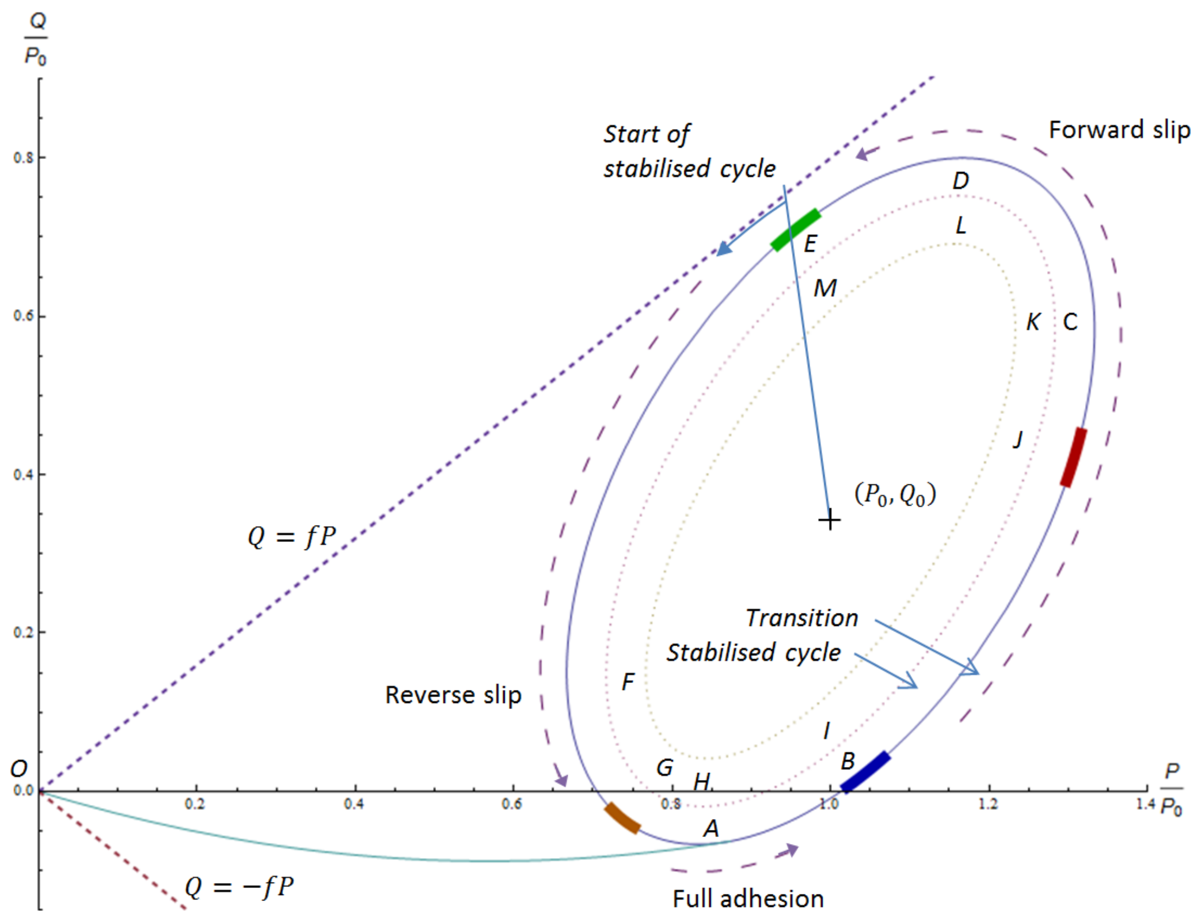

Figure 6-2 – Definition of load history

The first step is to establish the contact law relating the contact half-width, a, to the normal load, P, and a description of the contact pressure distribution. For example, for a Hertzian contact of relative radius of contact, R_0, and where the composite plane strain modulus is E^*, these two equations take the forms

$$a(P) = \sqrt{\frac{8PR_0}{\pi E^*}} \tag{6-1}$$

$$\begin{aligned} p(x,P) &= \frac{E^*}{4R}\sqrt{a(P)^2 - x^2} \qquad |x| < a(P) \\ &= 0 \qquad |x| > a(P). \end{aligned} \tag{6-2}$$

This compact notation enables us to write down solutions very simply; for example, the shear traction distribution for a stationary contact subject to a monotonically increasing shear (where the Hertz problem gives rise to the Cattaneo Mindlin problem, but the solution as now written applies to any uncoupled half-plane problem, as demonstrated by Jäger and Ciavarella [17, 18]) is

$$q(x) = f[p(x,P) - p(x;Q-P)], \tag{6-3}$$

where f is the coefficient of friction and Q is the applied (increasing) shearing force. It is understood that the terms are evaluated only when the observation point falls within the contact corresponding to that particular load, so that, in the above expression, the second term contributes only when the observation point falls with the range where the same punch, subject to a normal load $Q-P$, forms a contact. To proceed to the next stage we introduce also the notation that the derivative of the contact pressure, $p(x)$, with respect to the normal load, P, is denoted by $p'(x)$, i.e.

$$p'(x) \equiv \frac{\partial p(x,P)}{\partial P}. \tag{6-4}$$

The form of the loading history actually studied here is given in Figure 6-2. It consists of an initial phase from an unloaded state along a parabolic arc until the first point on the circle, point A, is reached. The load point then moves anticlockwise around a circle, centred on (P_0, Q_0) and of radius R.

At all points during the initial loading we must have that $d\left|Q\right|/dP < f$, so that stick endures throughout. This state persists not only during the parabolic transient, but until the loading point moves around to a point B, when $dQ/dP = f$. We have shown (chapter 5 and [26]) that, for a general segment of loading trajectory, subject to an increasing normal load, with initial state (P_1, Q_1) and final state (P_2, Q_2) the change in traction is given by

$$q_2\left(x\right) = q_1\left(x\right) + \int_{P_1}^{P_2} p'\left(x, P\right)\frac{dQ}{dP}dP. \tag{6-5}$$

This may be used to establish the tractions first at the end of the transient loading ($P_1 = Q_1 = 0$, and the end point given by $P_2 = P_A, Q_2 = Q_A$ and $P_2 = P_B, Q_2 = Q_B$). Figure 6-3 shows the evolving contact size, pressure distribution, and shear traction distribution during the whole load cycle. The $x-$coordinate is normalised with respect to the contact half width when the normal contact load is P_0, and this is also used to normalise the tractions. The example characteristics chosen are; $Q_0/P_0 = 1.1/3, R/P_0 = 1/3, P_{A/}P_0 = 3.05/3$. Figures 6-3A and 6-3B include, in particular, the shearing tractions while the contact remains adhered.

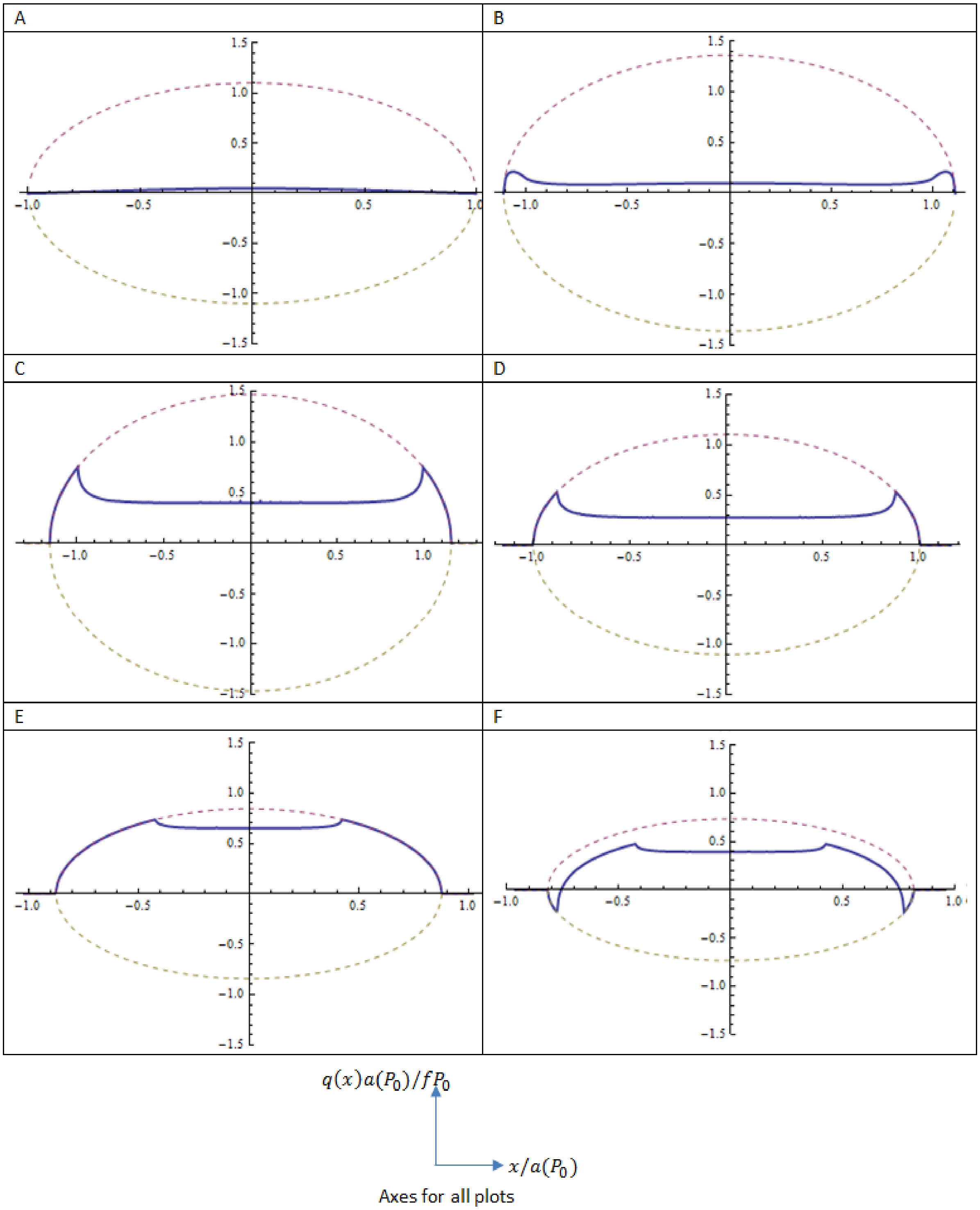

Figure 6-3 – Shear traction distribution beneath a Hertzian contact at various stages in the load cycle – first cycle

During the next phase of loading forwards slip regions develop attached to the contact edges, and grow. The contact itself clearly initially gets bigger, up to point C, but then contracts. Note, though,that the stick slip boundaries recede continuously, so that the slip zone is formally advancing, right the way through to point E, when $dQ/dP = f$ (note $dP < 0, dQ < 0$). During this time, the traction distribution at a general point X has been shown to be given by

$$q_X(x) = \int_0^{P_Y} p'(x, P) \frac{dQ}{dP} dP + f(p(x, P_x) - p(x, P_Y)), \quad \text{(6-6)}$$

where point Y is defined by a line drawn through X, of gradient f, and denotes the intersection of this line with the initial full stick trajectory. Figures 6-3C,D,C show the shearing traction during this phase - point C is the point where the maximum normal load occurs, Point D where the shear force reaches a maximum, and point E the maximum extent of forward slip. When point E is reached the whole contact sticks instantaneously, and then as we move further around the loop, a region of reverse slip develops, and the shear traction is given by

$$q(x) = \int_0^{P_Z} p'(x, P) \frac{dQ}{dP} dP + f(-p(x, P) + 2p(x, P_S) - p(x, P_Z)), \quad \text{(6-7)}$$

where P_Z is the load on the initial loading line where a line of gradient f and passing through E intersects it, and P_S is given by

$$P_S = \frac{1}{2}\left(\frac{Q}{f} + P - \frac{Q_Z}{f} + P_Z\right). \quad \text{(6-8)}$$

This solution remains correct until we reach point G, where $dQ/dP = -f$. Figure 6-3F,G depicts the shear traction in this regime - 3F when the normal load reaches its minimum value and point G the instant before full stick again occurs.

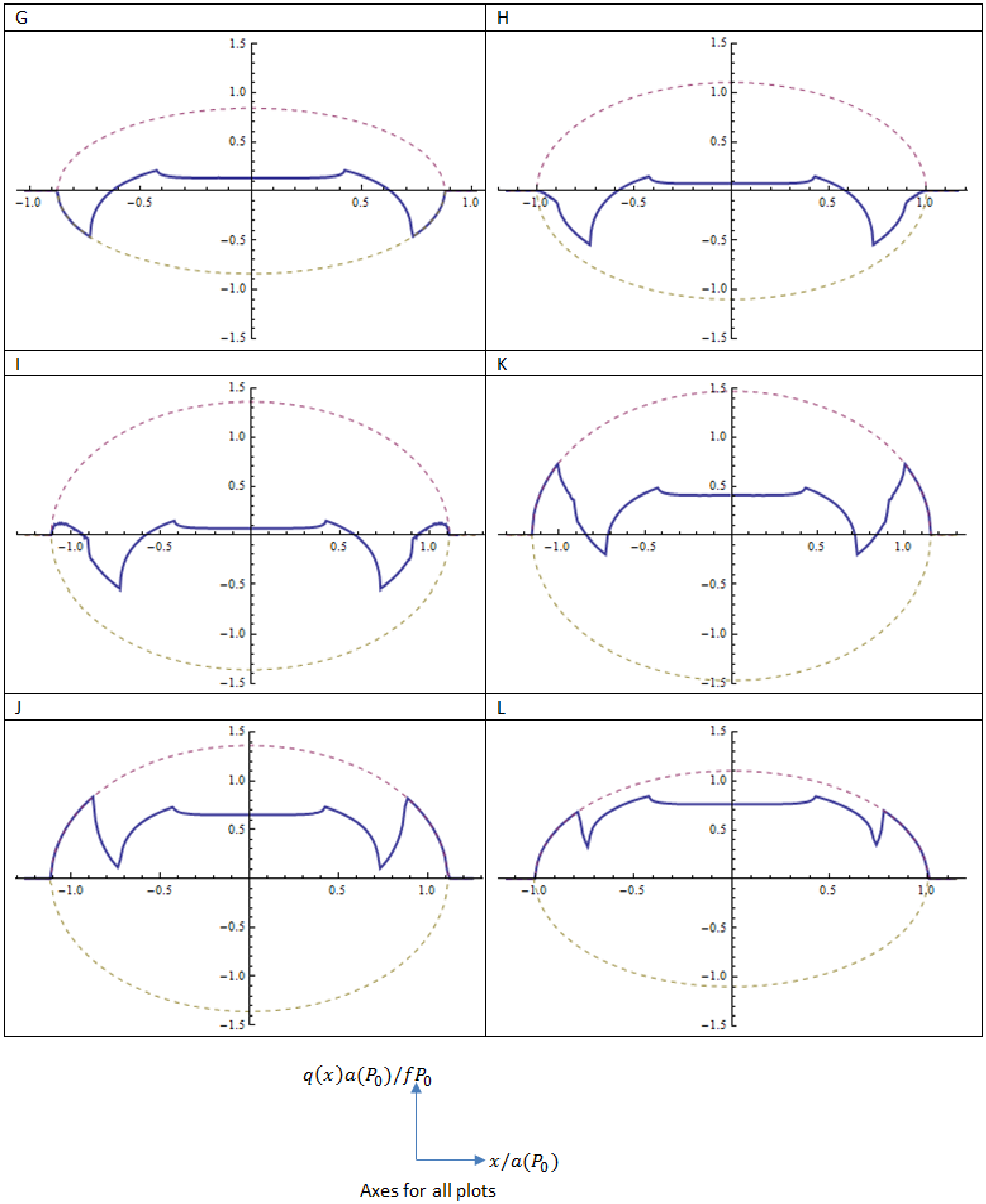

Figure 6-3 – Shear traction distribution beneath a Hertzian contact at various stages in the load cycle – stabilised cycle

These figures include the familiar ‘hooks’ observed in Cattaneo-Mindlin distributions at the point where forward slip reached its maximum value and became locked in. At the point where full stick occurs (G) the shearing traction is, explicitly

$$q_G(x) = \int_0^{P_Z} p'(x,P)\frac{dQ}{dP}dP + f(-p(x,P_B) + 2p(x,P_T) - p(x,P_Z)), \tag{6-9}$$

and point T is defined in Chapter 5

$$P_T = \frac{1}{2}\left(\frac{Q_B}{f} + P_B - \frac{Q_E}{f} + P_E\right). \tag{6-10}$$

During the second cycle of loading the general procedure remains the same, save that the locked in traction is now that established at point G, and that, when we carry out the constructions needed, the intersection is now with a point on the loop rather than the transient initial curve. For full details refer to the original article.

As point G is passed, with full adhesion we observe that, as expect, the full contact remains adhered until point B is reached (denoted I in the is cycle,because the tractions present are different. See Figures 6-3H (where the normal load reaches is minimum value), and 3I. From then on we observe advancing slip zones, as in the first cycle, and denoted by J (max normal load), K (where the tractions being erased change from full stick to reverse slip), L (maximum shear load) and M (incipient stick, and corresponding to point E in the first cycle). From then on the cycle remains stable and the stick and slip zones, together with the tractions and contact size, all remain identical from cycle to cycle.

Evolving Stick Slip Patterns

Figure 6-3 implicitly gives the size of the contact and extent of slip as snapshots through the cycle, but a fuller picture is provided in figure 6-4(a). The abscissa gives the progression of load, or angular position, θ, as described in Figure 6-2. On the ordinate we show, for half of the contact, its size ($a(P)/a(P_0)$), and the size of the stick region ($c\,(P)\,/a\,(P_0)$). This clearly shows that the slip zone is much bigger during the transient first cycle (points B to E) than it is during the steady state (the second cycle, regions I to M). This also shows that, in the steady sate, the extent of slip penetration from the contact edges is more or less the same during forward and reverse slip, although, of course, the contact spends a bigger fraction of the time undergoing forwards slip than reverse slip. The contact is always fully adhered during the interval G to I.

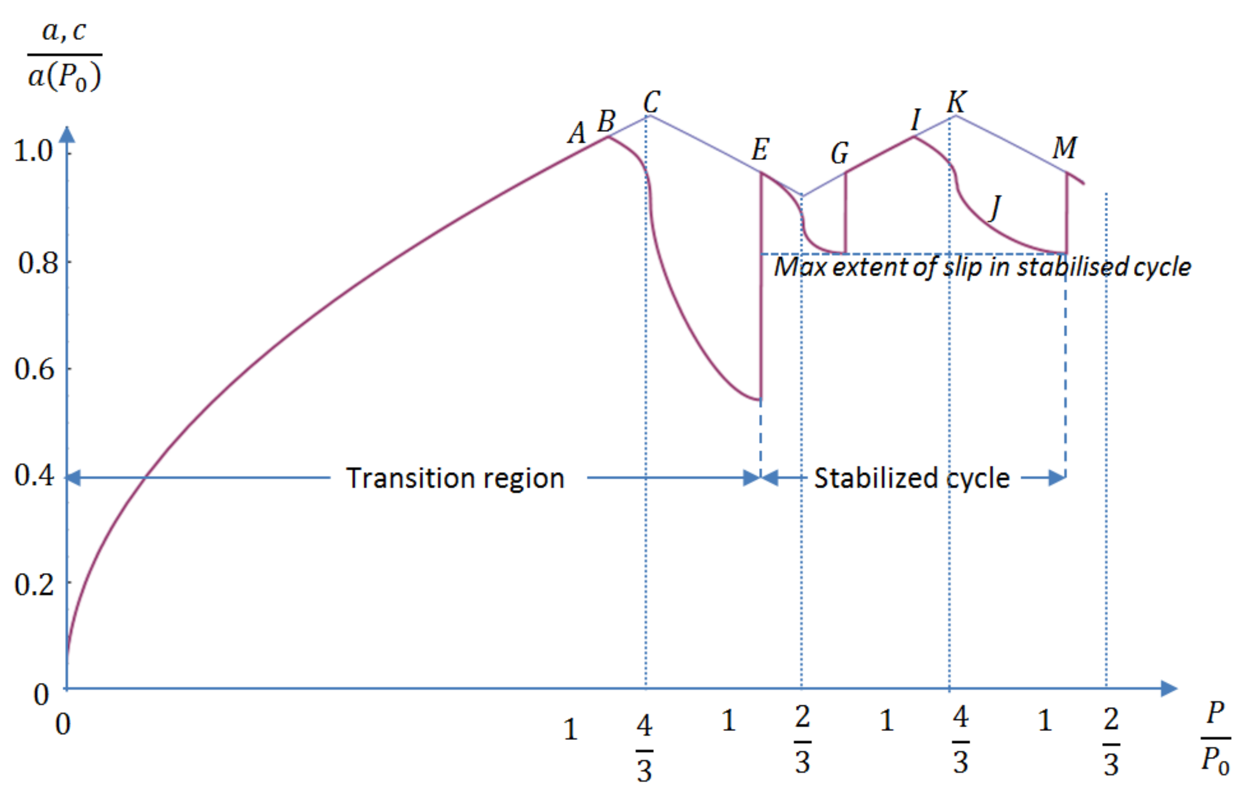

Figure 6-4(a)-Contact size and stick zone size through cycle for Hertzian contact

The variation of stick zone size with θ during the stabilised cycle for several values of the coefficient of friction is shown in Figure 6-4(b).

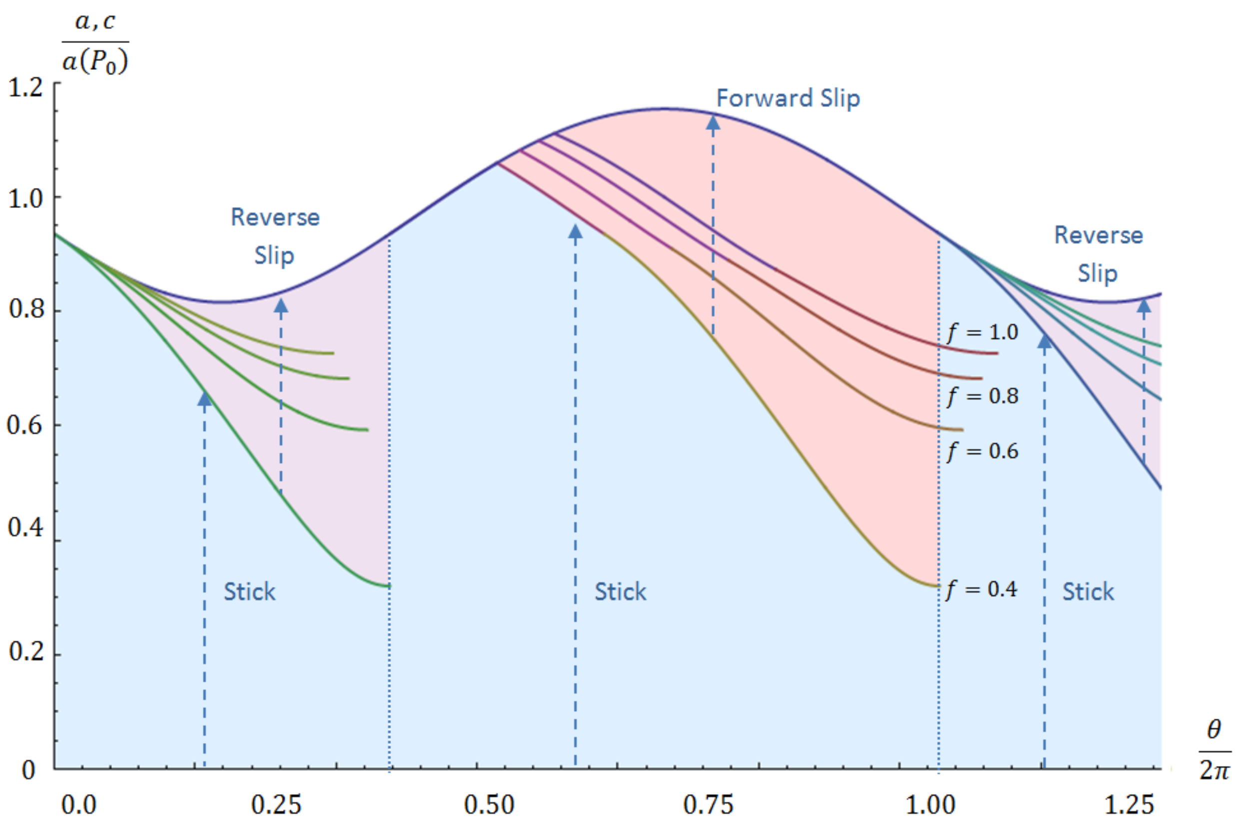

Figure 6-4(b)-Contact size and extent of slip zone during stabilised cycle for various values of friction

Energy expenditure

It has been shown in chapter 5 that, whilst the locked in shearing tractions within the stick region depend on the mean shear force, Q_0, the stick and slip zone distributions, and consequently the shearing tractions in the slip region, are independent of this quantity. Consequently, the work done against friction is also independent of the mean shearing force. The rate of doing frictional work, per unit area, is given by

$$\dot{W} = f \int_{\text{slip region}} p(x)\,\dot{u}(x)\,dx. \tag{6-11}$$

The irreversible work done is useful for two reasons; first, if we determine the rate of doing frictional work per unit area and then integrate this quantity over a steady state loading cycle this will reveal how the work done per unit area and per cycle of loading varies with position. It will clearly be zero within that part of the contact which is always adhered and it will also fall smoothly to zero at the edges of the contact at its maximum extent, because the contact pressure falls smoothly to zero at the contact edges- it must therefore take a maximum somewhere within the steady state slip zone and, as the damage due to frictional energy expenditure may sensibly be assumed to be directly controlled by the irreversible work, the maximum value (with respect to position), could be used as a simple first approximation of a crack nucleation parameter, as discussed in Chapter I. The second quantity of interest is the integral of this quantity with respect to position, which them gives us the total work done per cycle of loading, and hence gives a good measure of the damping provided by the contact when the excitation force is in the form of vibration.

Note that, although the total forwards and backwards displacements of any pair of particles must be equal during the forward and reverse slip phases of the loading cycle, it does not follow that the work done in each phase of slip is the same, because the size of the contact, and hence the magnitude of the contact pressure, may not be the same at corresponding slip zone extents.

We now turn our attention to the incremental slip displacement associated with the incremental tangential traction, given by

$$Cfp'(x, P_1)\,\Delta P, \tag{6-12}$$

where P_1 refers to the load on the 'corrective punch' and applies within the stick region. The constant (for this segment of loading history) C is the multiplier on the incremental traction in each region and takes the following values around the stabilised cycle (see Figure 6-2)

$$C = \begin{cases} \frac{1}{f}\frac{dQ}{dP} + 1 & \text{in } EG \\ \frac{1}{f}\frac{dQ}{dP}(P_Y) - 1 & \text{in } IK \\ \frac{1}{f}\frac{dQ}{dP} - 1 & \text{in } KM \end{cases}. \tag{6-13}$$

No slip, and hence, no frictional dissipation occurs in GI. In chapter 4 and a second recent paper [27] extensive notes on the evaluation of locked-in surface displacements and their variation with the corresponding shear traction were given and we showed that the duality between the normal and shear tangential displacement governing equations enables us to write

$$\dot{u}(x) = Cf\Delta P\frac{(\kappa+1)}{2\pi\mu}\int_c^x h_0(x,c)\,dx, \tag{6-14}$$

where $h_0(x)$ is the function describing the initial gap between the punch and half plane. For Hertz contact

$$\dot{u}(x) = -Cf\Delta P\frac{(\kappa+1)}{2\pi\mu}\cosh^{-1}\frac{x}{c}. \tag{6-15}$$

The total energy dissipation for a given position, x, beneath a Hertzian contact is

$$W(x) = -\frac{f^2}{\pi R}\int_{P_E}^{P_M}\sqrt{a(P)^2 - x^2}C\cosh^{-1}\left(\frac{x}{c}\right)dP, \tag{6-16}$$

where P_E and P_M specify the same location on the ellipse, separated by one complete revolution, as shown in Figure 6-2. The remainder of the integrals in the problem have been evaluated numerically. The load has been redefined as an angular variable, to avoid numerical errors at the minimum and maximum values of P. For the example problem looked at in detail above, the stick/slip/out of contact history and relative displacement during the cycle for four locations that are, at some point, in contact is shown in Figure 6-5.

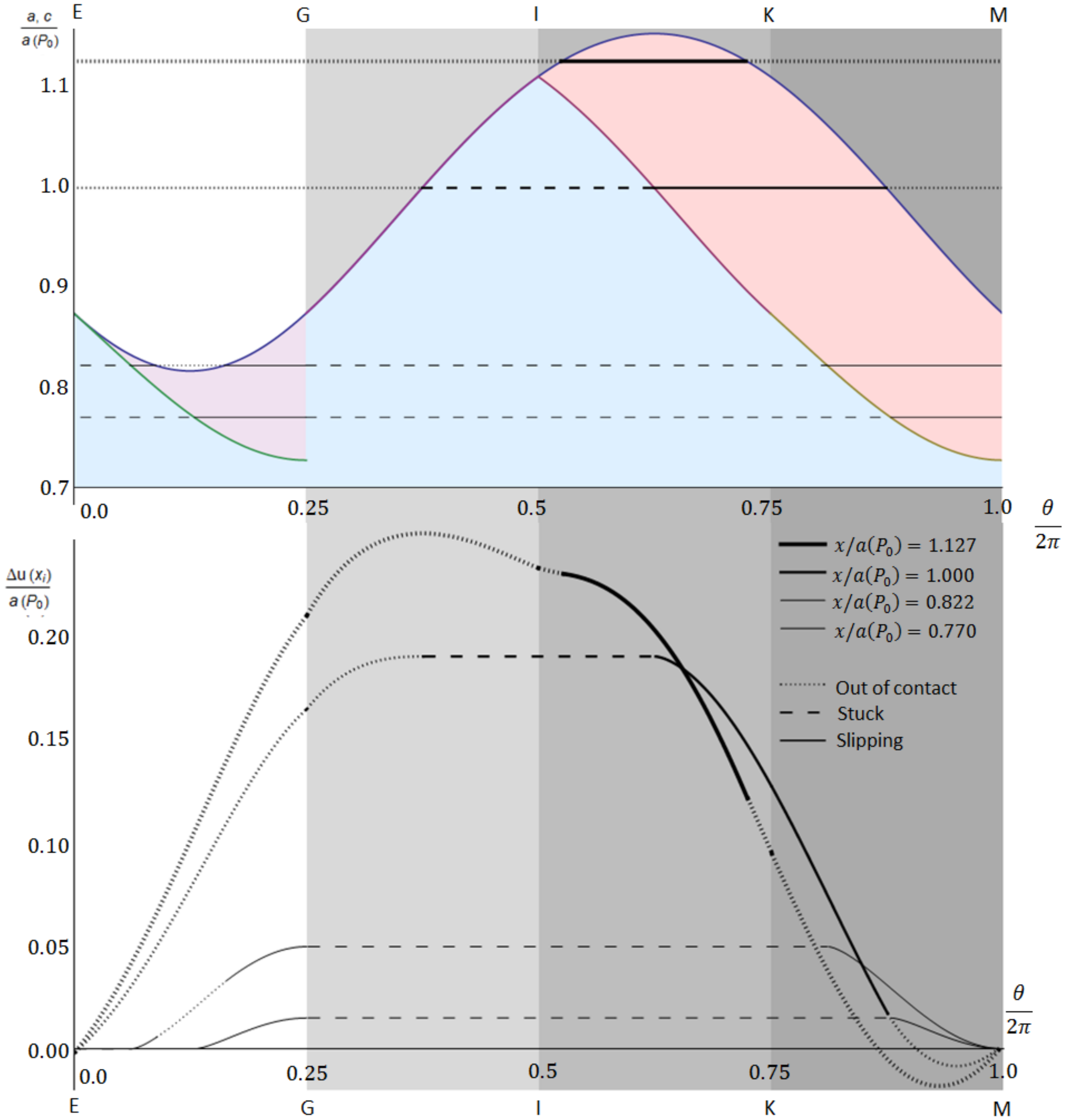

Figure 6-5– Stick/Slip/Out of contact and displacement stabilized cycle history plot for four points

The spatial distribution of work done per cycle, for each of the cycle phases that involve slip, and for the complete cycle (blue line) is shown in Figure 6-6.

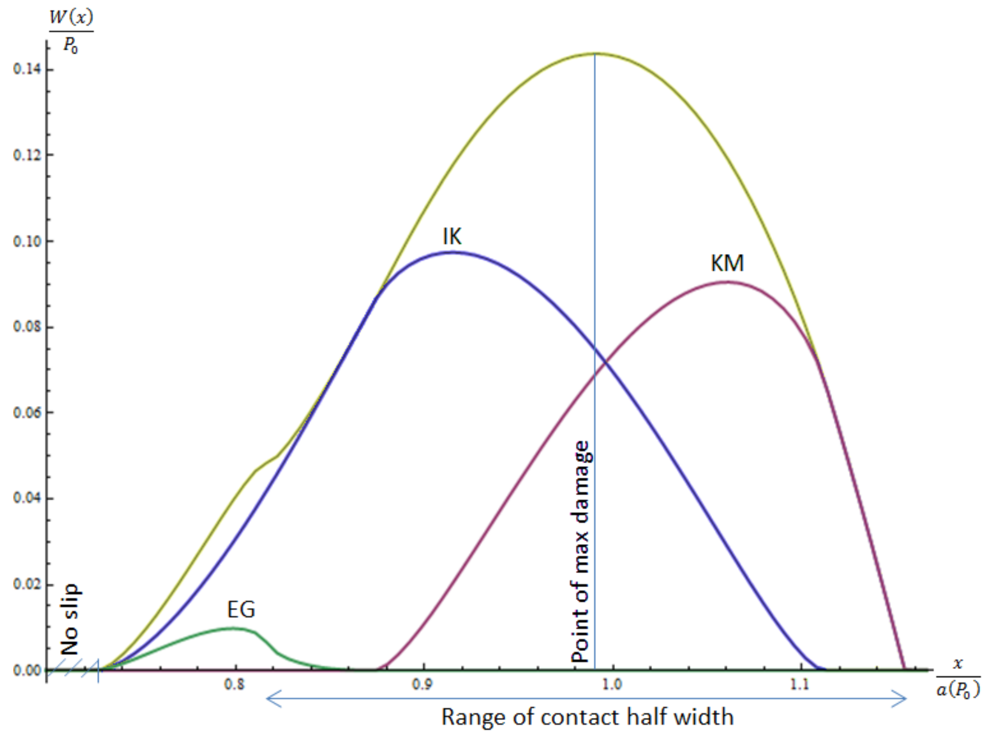

Figure 6-6 - Pointwise dissipation for a Hertzian contact

In order to optimise the contact without affecting the vibration performance, I hypothesize that the peak work done per unit length (as shown by the 'point of maximum damage' on Figure 6-6) should be minimised. However, it can be assumed that any vibrational damping provided by the contact will depend on the overall dissipation, which should therefore not be reduced. As an aid to this, Figure 6-7(a) shows the total energy dissipated and Figure 6-7(b) shows the peak dissipation per unit length,for various combinations of $\overline{P}$ and coefficient of friction.

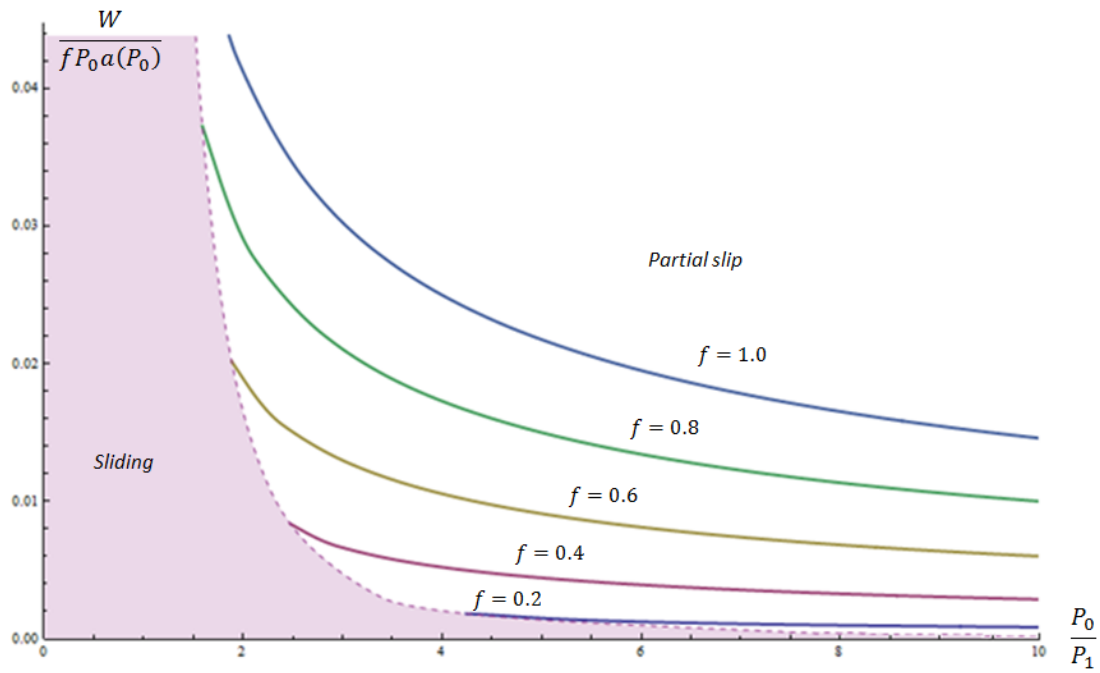

Figure 6-7(a) – Global dissipation experienced by a Hertzian contact during one cycle of load.

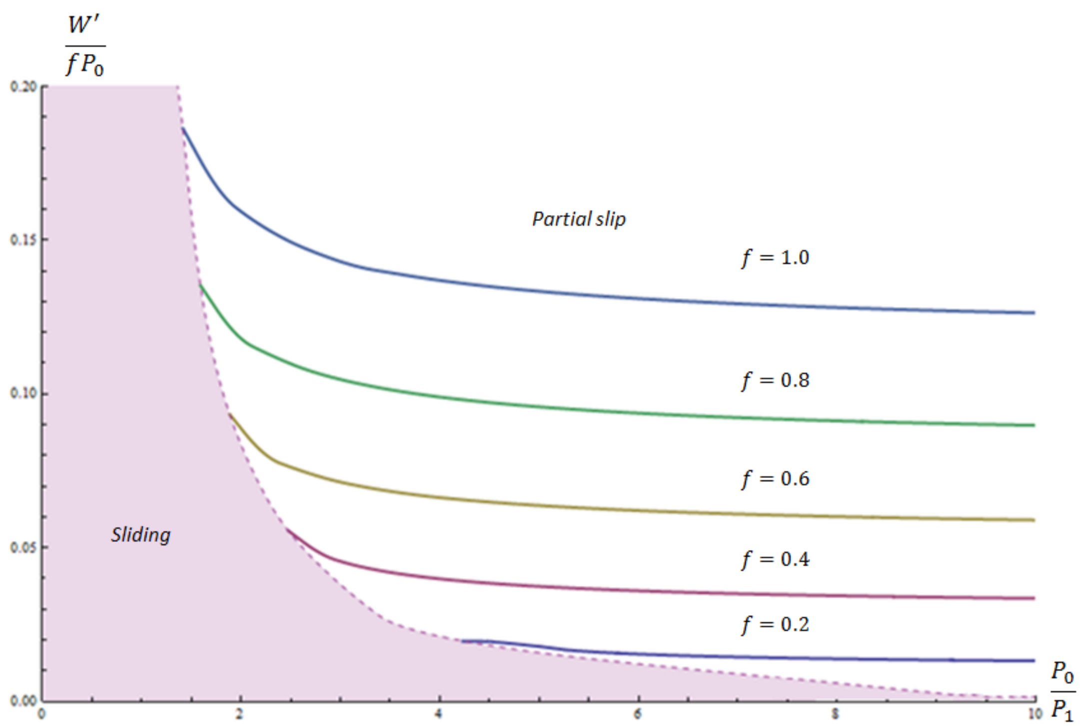

Figure 6-7(b) – Peak Pointwise dissipation experienced by a Hertzian contact during one cycle of load.

Any slip occurring within the portion of the contact that remains in contact for the entire cycle will have to be identical in the forward and reverse slip regions, which can be written as

$$\int_{P_E}^{P_M} \dot{u}\left(x, P\right) dP = 0; \qquad \forall \left|x\right| < a\left(\overline{P} - R\right). \tag{6-17}$$

Flat and Rounded Punch

The energy equations have been repeated for a flat punch with rounded edges. The stick zone size history for an example flat and rounded contact with $b/a\left(\overline{P}\right) = 0.505$ is shown in Figure 6-8.

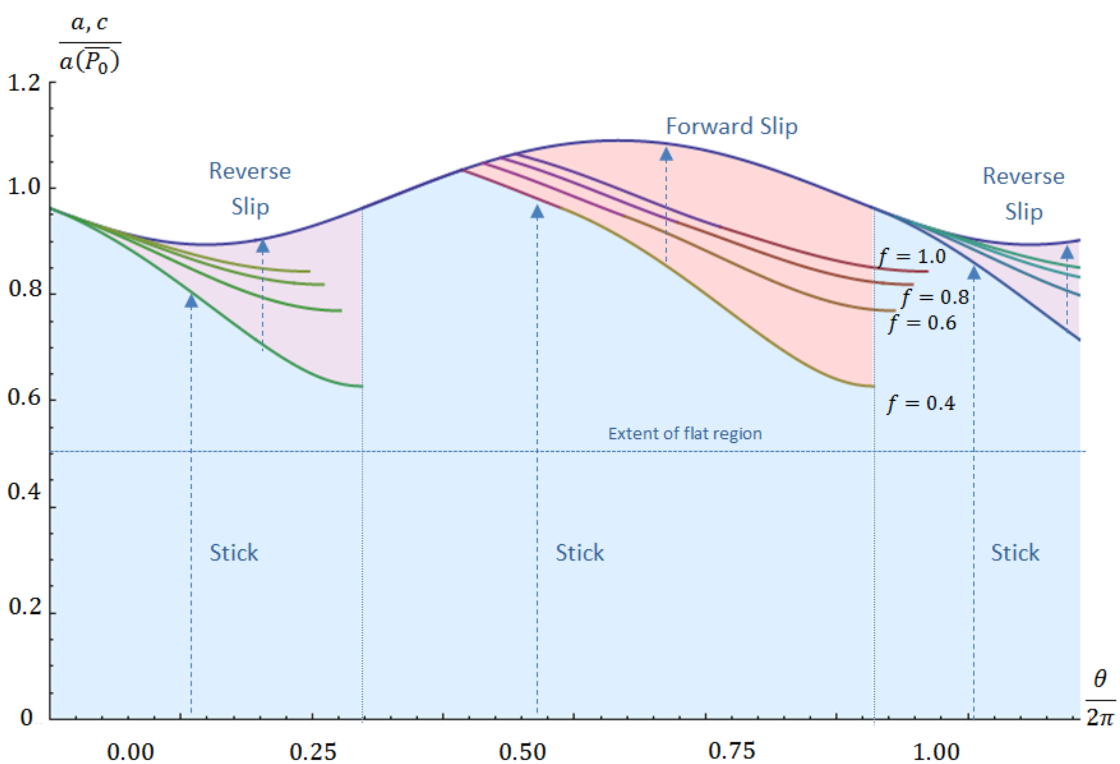

Figure 6-8 – Variation of a and c for flat and rounded contact ($b/a(\bar{P}) = 0.505$)

The results for the energy dissipated per unit length around a complete cycle for the flat and rounded contact example in Figure 6-8 is shown in Figure 6-9.

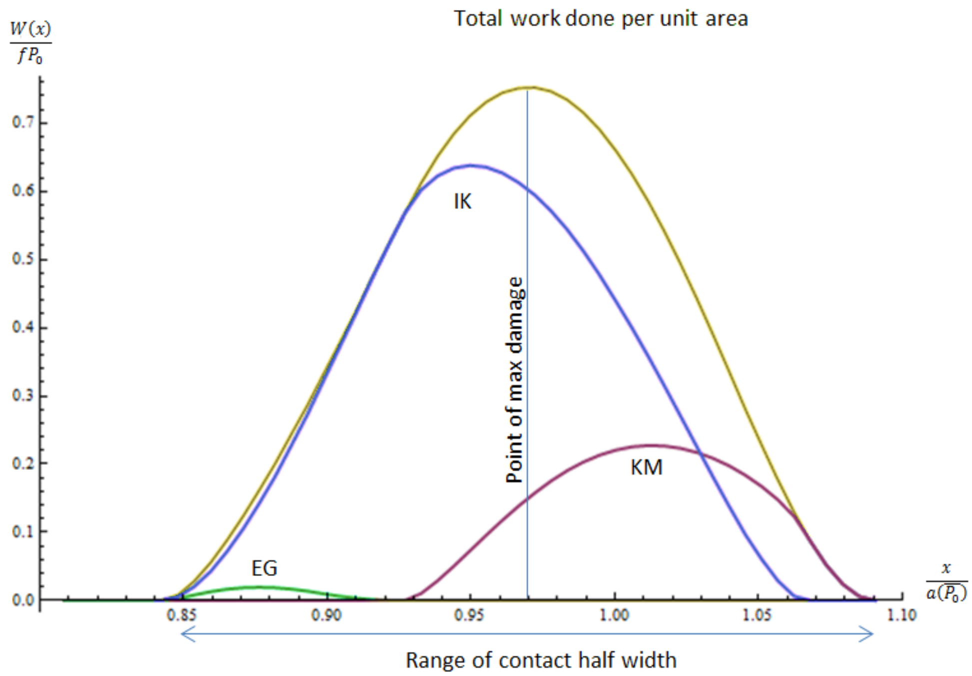

Figure 6-9 – Pointwise dissipation for a flat and rounded contact, $b/a(P_0) = 0.505$

The total energy dissipation and maximum energy dissipation per unit length during one complete cycle for the flat and rounded contact example in Figure 6-8 are shown in Figure 6-10(a) and (b) respectively.

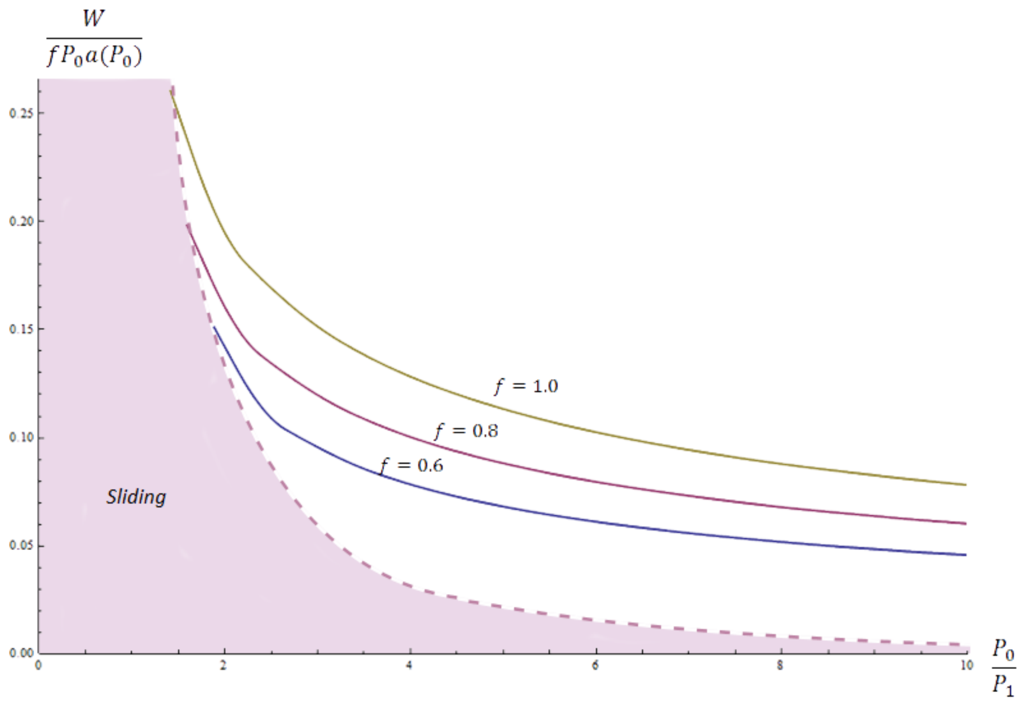

Figure 6-10(a) - Global dissipation experienced by a flat and rounded contact during one cycle of load. $b/a(P_0) = 0.505$

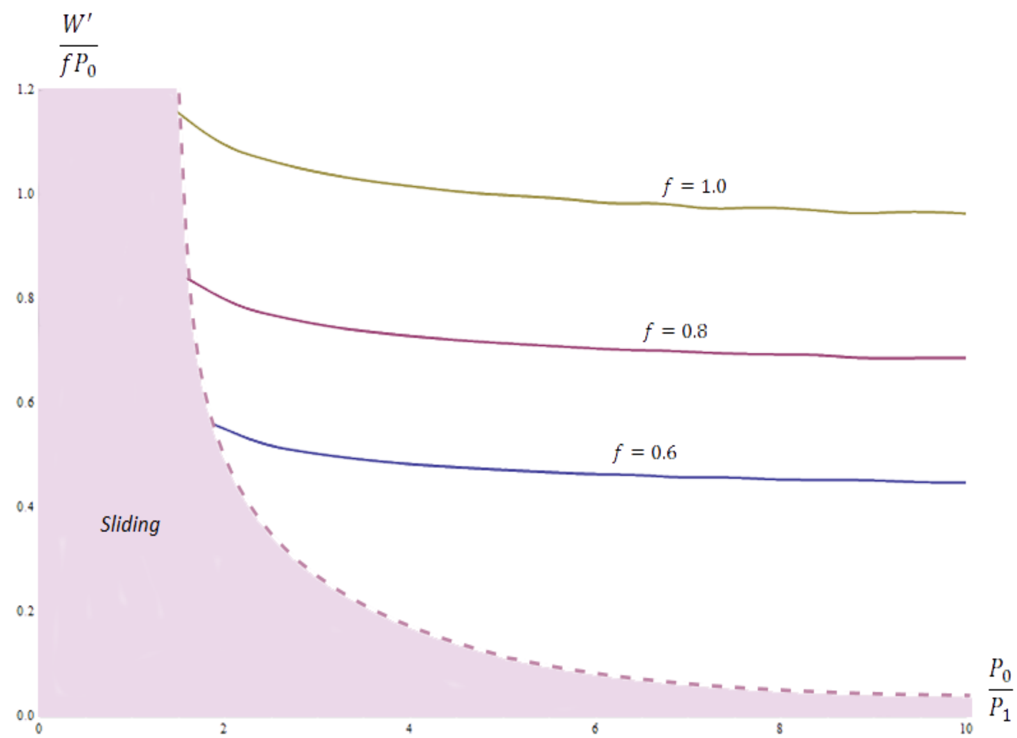

Figure 6-10(b)- Peak Pointwise dissipation experienced by a flat and rounded contact during one cycle of load $b/a(P_0) = 0.505$

A Mathematica code, which can be used to process either a Hertzian or flat and rounded punch has been submitted for publication alongside a paper based on this chapter. The user guide for this code is included in Appendix B.

Conclusion

A well defined, easily implemented procedure for the evaluation of both frictional energy expenditure per unit area and its integral over the slip regions (giving damping data) has been developed. This does not require an explicit prescription of the contact law. As an example the solution has been developed for a Hertzian contact(which is explicit) and where the excitation is in the form of a constant normal load together with a harmonically varying normal contact component and shear loading. Further results have been found for the case of a ‘flat and rounded’ punch which is, perhaps, of greater relevance to the intended application, and where an explicit description of the contact law is impossible.

7. Half-plane contacts subject to cyclic shear and tension forces in the steady state

Formulation

The Cattaneo-Mindlin [14, 15] procedure, extended by Ciavarella and Jäger[18, 17] to further geometries beyond the Hertz solution, was further developed to allow for the inclusion of differential bulk tension effects present in the surface [19]. All these articles look at the development of the stick-slip pattern from an unloaded state, and may be used or developed in a 'marching-in-time' sense to deduce what happens, in the steady state, when the remote loading is periodic in nature. This chapter, by contrast, details the development of a solution for the steady state response *without* solving the transient problem. In chapter 5 it was shown that, for problems of this kind, the transient history serves only to modify the locked in tractions present in the permanent stick region, which have no practical bearing on the performance of the contact in terms of frictional energy expended, nor the slip displacements present in the slipping parts of the contact. The method may be applied to any uncoupled contact capable of idealisation within the framework of half-plane idealisations of the bodies, although its implementation is easier when the contact law may be developed explicitly, such as the Hertzian contact, and this example geometry is therefore treated fully.

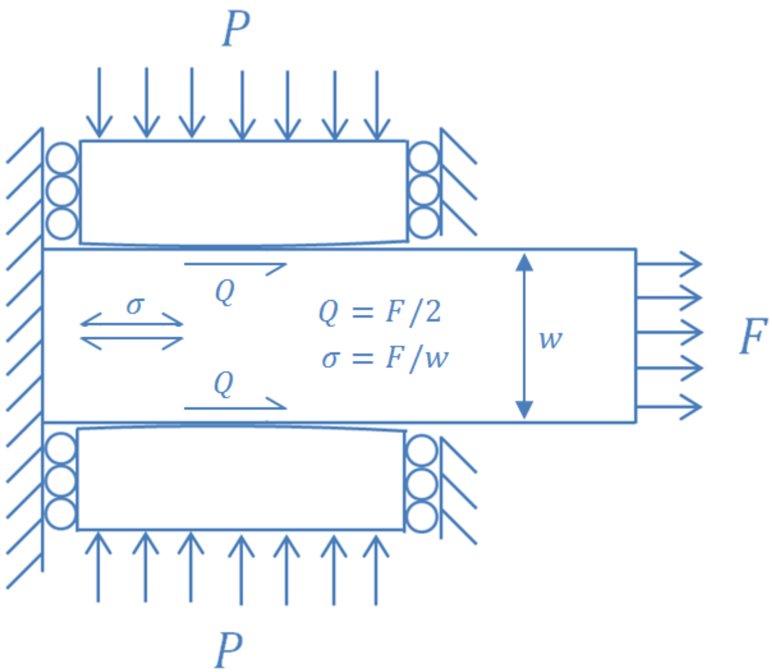

Figure 7-1 – Example problem geometry

In a later part of the chapter we shall examine the behaviour of the assembly shown in Figure 7-1, in which the contact is taken around a smooth loop in $Q-\sigma$ space for constant P, where $Q(t)$ is he shearing force present as a function of time, $\sigma(t)$ is the differential bulk remote tension between the two bodies, again as a function of time and P is the normal load. However, to develop our understanding of the problem, we shall first investigate simplified problems, where the loading history permits a closed form description of the slip history.

Two Phases of Slip

Same sign slip

The first problems we consider are those where, during a cycle of applied load, there are only two phases of slip occurring. Figure 7-2(a) shows an idealisation of the loading loop, and where the performance of the contact is, as we shall show, determined simply by the relative positions of the 'end points', 1 and 2.

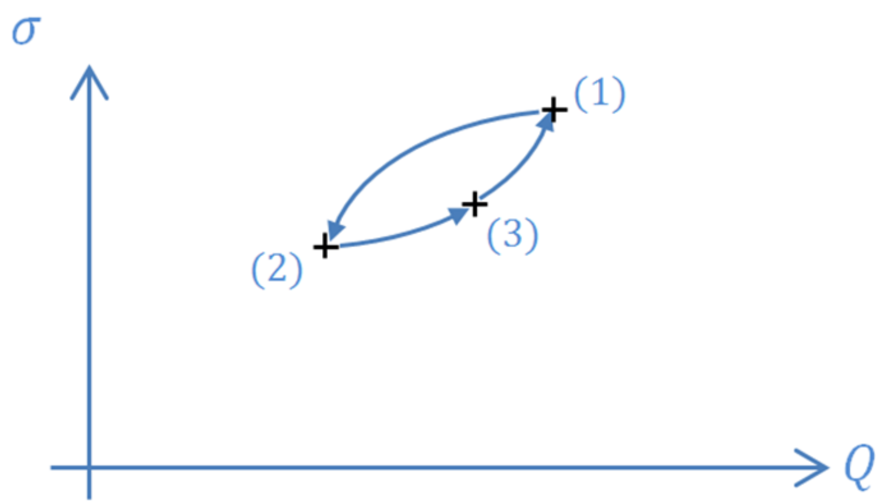

Figure 7-2(a) – Illustrative load path

A normal load, P, is first applied to the contact, and the magnitude of the remote loads is such that the stick-slip history shown schematically in Figure 7-2(b) is traced out, where the slip zones present at opposite ends of the loop (points $1^{-}, 2^{-}$ where the superscript $-$ means immediately *before* the end point is reached) are of the same sign as each other throughout the steady state cycle.

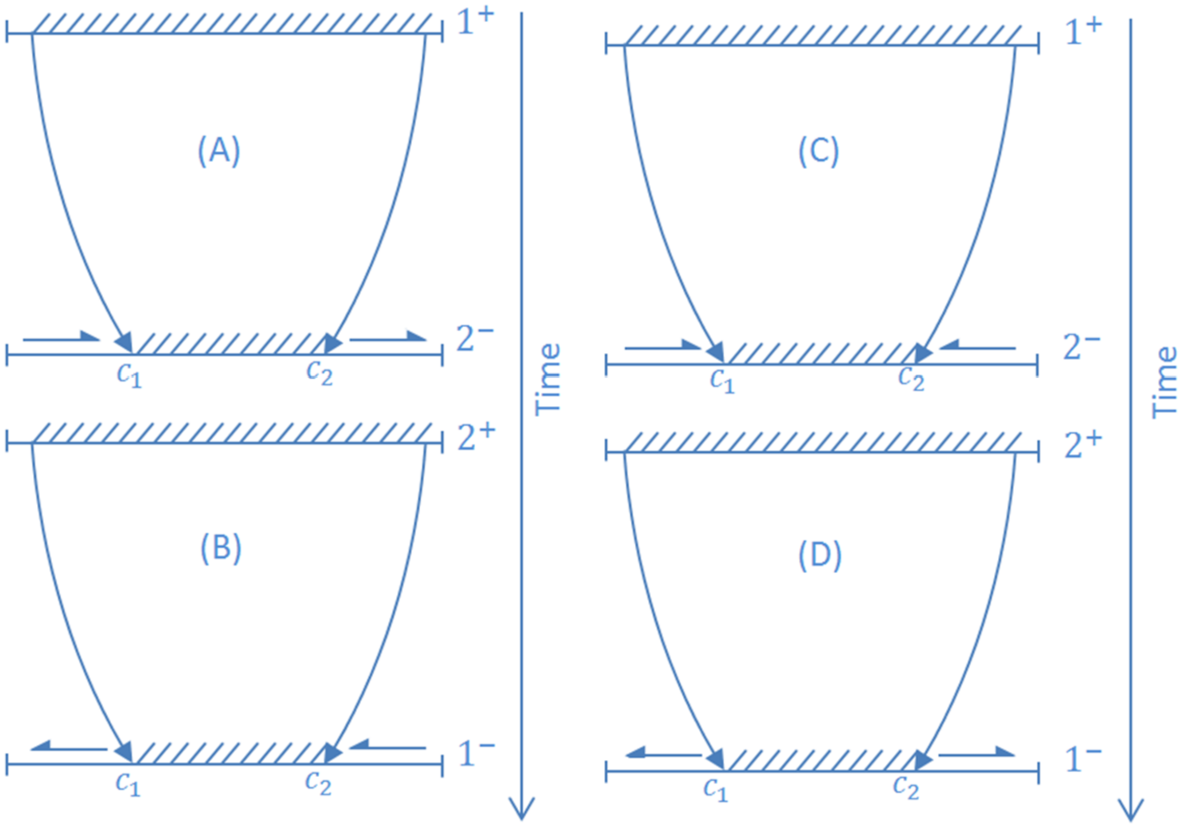

Figure 7-2(b) & (c) – Illustrative stick/slip history for one cycle with (b) same sign and (c) different sign slip throughout

An important feature of this sketch is that, just before each end point is reached, the extent of the permanent stick zone $c_1 < x < c_2$, is the same. This is a necessary condition in order to ensure that there is no build up of slip displacement over the cycle. This observation enables us to write the slip displacement, $g(x)$, at points $1^-, 2^-$ as

$$\frac{2\mu}{(1+\kappa)}\frac{dg}{dx} = \frac{f}{\pi}\int_{-a}^{a}\frac{p(\xi)\,d\xi}{x-\xi} + \frac{1}{\pi}\int_{c_1}^{c_2}\frac{q_1(\xi)\,d\xi}{x-\xi} + \frac{\sigma_1}{4} \qquad c_1 < x < c_2 \text{ at } 1^- \quad (7\text{-}1)$$

$$\frac{2\mu}{(1+\kappa)}\frac{dg}{dx} = -\frac{f}{\pi}\int_{-a}^{a}\frac{p(\xi)\,d\xi}{x-\xi} + \frac{1}{\pi}\int_{c_1}^{c_2}\frac{q_2(\xi)\,d\xi}{x-\xi} + \frac{\sigma_2}{4} \qquad c_1 < x < c_2 \text{ at } 2^- \quad (7\text{-}2)$$

where μ is the modulus of rigidity, κ is Kolosov's constant, $p(x), q(x)$ the direct and shear tractions, σ_i the difference in remote tensions present between the bodies at point i, and a the contact half-width. Therefore

$$0 = \frac{1}{\pi}\int_{c_1}^{c_2} \frac{q_1(\xi)\,d\xi}{x-\xi} - \frac{1}{\pi}\int_{c_1}^{c_2} \frac{q_2(\xi)\,d\xi}{x-\xi} + 2\frac{f}{\pi}\int_{-a}^{a} \frac{p(\xi)\,d\xi}{x-\xi} + \frac{\sigma_1}{4} - \frac{\sigma_2}{4} \qquad c_1 < x < c_2 \tag{7-3}$$

or

$$\int_{c_1}^{c_2} \frac{\Delta q(\xi)\,d\xi}{x-\xi} = h'(x)\,\frac{4\mu f}{(1+\kappa)} - \frac{\pi\Delta\sigma}{4}, \tag{7-4}$$

where we have used the normal contact relationship

$$\frac{2\mu}{(1+\kappa)}\frac{dh}{dx} = \frac{1}{\pi}\int_{-a}^{a} \frac{p(\xi)\,d\xi}{x-\xi}, \tag{7-5}$$

$h'(x) \equiv dh/dx$, and

$$\Delta q(x) = \begin{cases} q_2(x) - q_1(x) & c_1 < x < c_2 \\ 0 & \text{otherwise} \end{cases} \tag{7-6}$$

$$\Delta\sigma = \sigma_2 - \sigma_1. \tag{7-7}$$

Solution

Inverting the integral equation gives

$$\frac{\Delta q(x)\,a}{fP} = \frac{w(x)}{\pi}\left[\frac{4}{\pi}\int_{c_1/a}^{c_2/a} \frac{(h'(\xi)/a)\,d\xi}{w(\xi)(x-\xi)} - \frac{\pi}{4}\frac{a\Delta\sigma}{fP}\int_{c_1/a}^{c_2/a} \frac{d\xi}{w(\xi)(x-\xi)}\right] \tag{7-8}$$

where

$$w(x) = \frac{1}{a}\sqrt{(c_1 - x)(x - c_2)} \tag{7-9}$$

and the second integral always evaluates to zero

$$\int_{c_1/a}^{c_2/a} \frac{d\xi}{w(\xi)(x-\xi)} = 0. \tag{7-10}$$

So the shear traction difference between the two extremes in the cycle, $\Delta q(x)$, is given by

$$\frac{\Delta q\left(x\right)a}{fP}=\frac{4w\left(x\right)}{\pi^{2}}\int_{c_{1}/a}^{c_{2}/a}\frac{\left(h'\left(\xi\right)/a\right)d\xi}{w\left(\xi\right)\left(x-\xi\right)} \tag{7-11}$$

The ‘bounded both ends’ solution demands that the following consistency condition is satisfied

$$0=\frac{4\mu f}{\left(1+\kappa\right)}\int_{c_{1}}^{c_{2}}\frac{h'\left(x\right)dx}{w\left(x\right)}-\frac{\pi\Delta\sigma}{4}\int_{c_{1}}^{c_{2}}\frac{dx}{w\left(x\right)} \tag{7-12}$$

or

$$\int_{c_{1}}^{c_{2}}\frac{h'\left(x\right)dx}{\sqrt{\left(c_{1}-x\right)\left(x-c_{2}\right)}}=\frac{\pi^{2}\Delta\sigma\left(1+\kappa\right)}{16f\mu} \tag{7-13}$$

whilst overall equilibrium in the x direction shows that

$$\Delta Q=-2fP+\int_{c_{1}}^{c_{2}}\Delta q\left(x\right)dx \tag{7-14}$$

where

$$\Delta Q=Q_{2}-Q_{1}. \tag{7-15}$$

and finally

$$\Delta Q=-2fP+\frac{4\mu f}{\left(1+\kappa\right)}\int_{c_{1}}^{c_{2}}\frac{w\left(x\right)}{\pi}\int_{c_{1}}^{c_{2}}\frac{h'\left(\xi\right)d\xi}{w\left(\xi\right)\left(x-\xi\right)}dx. \tag{7-16}$$

Opposite sign slip

When the shear traction in the two slip regions is of the opposite sign at all times, as shown schematically in Figure 7-2(c) the same basic formulation procedure may be used. We first assume a distribution with forward slip between $[-a\ c_1]$, reverse slip between $[c_2\ a]$, and a linear variation of shear traction between $[c_1\ c_2]$ together with an unknown corrective traction between $[c_1\ c_2]$. As a result of the form chosen, the corrective traction must be zero at both ends. We start by writing down the x-displacement for the two bodies inside the permanent stick zone, $[c_1\ c_2]$.

$$\begin{aligned}\frac{2\mu}{(1+\kappa)}\frac{dg}{dx} &= \frac{f}{\pi}\int_{-a}^{c_1}\frac{p(\xi)\,d\xi}{x-\xi}+\frac{f}{\pi}\int_{c_1}^{c_2}\frac{p_x(\xi,c_1,c_2)\,d\xi}{(x-\xi)} \\ &\quad -\frac{f}{\pi}\int_{c_2}^{a}\frac{p(\xi)\,d\xi}{x-\xi}+\frac{1}{\pi}\int_{c_1}^{c_2}\frac{q_1(\xi)\,d\xi}{x-\xi}+\frac{\sigma_1}{4} \qquad c_1<x<c_2\end{aligned} \tag{7-17}$$

$$\begin{aligned}\frac{2\mu}{(1+\kappa)}\frac{dg}{dx} &= \frac{-f}{\pi}\int_{-a}^{c_1}\frac{p(\xi)\,d\xi}{x-\xi}-\frac{f}{\pi}\int_{c_1}^{c_2}\frac{p_x(\xi,c_1,c_2)\,d\xi}{(x-\xi)} \\ &\quad +\frac{f}{\pi}\int_{c_2}^{a}\frac{p(\xi)\,d\xi}{x-\xi}+\frac{1}{\pi}\int_{c_1}^{c_2}\frac{q_2(\xi)\,d\xi}{x-\xi}+\frac{\sigma_2}{4} \qquad c_1<x<c_2,\end{aligned} \tag{7-18}$$

where $p_x(x;c_1,c_2)$ provides smooth interpolation, e.g. linear, within the interval ($c_1 < x < c_2$)

$$p_x(x;c_1,c_2)=\frac{[p(c_1)(c_2-x)-p(c_2)(x-c_1)]}{(c_2-c_1)}. \tag{7-19}$$

Again, dg/dx must remain unchanged throughout the cycle in the region $c_1 < x < c_2$. Therefore

$$\begin{aligned}\int_{c_1}^{c_2}\frac{\Delta q(\xi)\,d\xi}{x-\xi} &= \frac{2f}{\pi}\int_{-a}^{c_1}\frac{p(\xi)\,d\xi}{x-\xi}+\frac{2f}{\pi}\int_{c_1}^{c_2}\frac{p_x(\xi,c_1,c_2)\,d\xi}{(x-\xi)} \\ &\quad -\frac{2f}{\pi}\int_{c_2}^{a}\frac{p(\xi)\,d\xi}{x-\xi}-\frac{\pi\Delta\sigma}{4} \qquad c_1<x<c_2,\end{aligned} \tag{7-20}$$

where, again

$$\Delta q(x) = q_2(x)-q_1(x) \tag{7-21}$$

$$\Delta\sigma = \sigma_2-\sigma_1. \tag{7-22}$$

Analytical inversion does not seem possible, so the integral equation in 7-20 must be evaluated numerically to find $\Delta q\left(x\right)$.

Example: Hertzian Contact

It is possible to develop the theory further at this level, using only the contact profile as a descriptor of the problem, but that leads, in the subsequent treatment, to multiple integrals, and it seems preferable to take the solution up to his point and evaluate it for the contact geometry in question before proceeding. For the case of a Hertzian contact, where $h'\left(x\right)=x/R$, we have

$$\Delta q\left(x\right)=-\frac{4\mu f}{R\left(1+\kappa\right)}\sqrt{\left(c_1-x\right)\left(x-c_2\right)}, \tag{7-23}$$

whilst the side condition shows that the *location* of the centre of the stick zone depends only on the range of differential bulk tension, and is given by

$$\frac{c_1+c_2}{a}=\frac{\pi^2}{16}\frac{a\Delta\sigma}{fP}, \tag{7-24}$$

whilst tangential equilibrium shows that the *extent* of the stick zone depends on the range of shear force applied

$$\frac{c_2-c_1}{a}=\sqrt{2}\sqrt{2-\frac{\Delta Q}{fP}}. \tag{7-25}$$

Therefore

$$\frac{c_1}{a} = \frac{\pi^2}{16}\frac{a\Delta\sigma}{fP}-\sqrt{1-\frac{\Delta Q}{2fP}} \tag{7-26}$$

$$\frac{c_2}{a} = \frac{\pi^2}{16}\frac{a\Delta\sigma}{fP}+\sqrt{1-\frac{\Delta Q}{2fP}} \tag{7-27}$$

The requirement that the slip zones be of the same sign demands that $\frac{c_1}{a}>-1$ and

$\frac{c_2}{a} < 1$, i.e.

$$-1+\sqrt{1-\frac{\Delta Q}{2fP}} < \frac{\pi^2}{16}\frac{a\Delta\sigma}{fP} < 1-\sqrt{1-\frac{\Delta Q}{2fP}}. \tag{7-28}$$

Evolution of Slip during a Cycle

The next phase of the solution is to develop an expression for the extent of the slip region during the cycle. Suppose that the current point in the cycle is just before incipient full stick at stage 2, so that the surface slip displacement is given by (7-2) and therefore, when the turning point has been passed, the slip displacement present is locked in, at this value. The external loading (Q, σ) is now changed to some new condition, point 3 on the loop, Figure 7-2(a), so as to give stick over an interval $[b_1\ b_2]$, where $b_1 < c_1 < c_2 < b_2$, and hence the displacement is preserved over this interval, whilst the sign of the shear is reversed external to the slip zone, *i.e.*

$$\frac{2\mu}{(1+\kappa)}\frac{dg}{dx}_3 = \frac{f}{\pi}\int_{-a}^{a}\frac{p(\xi)\,d\xi}{x-\xi}+\frac{1}{\pi}\int_{b_1}^{b_2}\frac{q_3(\xi)\,d\xi}{x-\xi}+\frac{\sigma_3}{4} \qquad -a<x<a. \tag{7-29}$$

The *change* in surface relative strain is therefore

$$\frac{1}{A}\frac{dg}{dx}_3-\frac{1}{A}\frac{dg}{dx}_2 = \frac{2f}{\pi}\int_{-a}^{a}\frac{p(\xi)\,d\xi}{x-\xi}+\frac{1}{\pi}\int_{b_1}^{b_2}\frac{q_3(\xi)\,d\xi}{x-\xi}-\frac{1}{\pi}\int_{c_1}^{c_2}\frac{q_2(\xi)\,d\xi}{x-\xi}+\frac{\sigma_3}{4}-\frac{\sigma_2}{4} \tag{7-30}$$

and $\frac{dg}{dx}_3 - \frac{dg}{dx}_2 = 0 \qquad b_1 < x < b_2$, so that

$$0 = \frac{2f}{\pi}\int_{-a}^{a}\frac{p(\xi)\,d\xi}{x-\xi}+\frac{1}{\pi}\int_{b_1}^{b_2}\frac{q_3(\xi)\,d\xi}{x-\xi}-\frac{1}{\pi}\int_{c_1}^{c_2}\frac{q_2(\xi)\,d\xi}{x-\xi}-\frac{\Delta^*\sigma}{4} \qquad b_1<x<b_2 \tag{7-31}$$

where

$$\Delta^*\sigma = \sigma_2(x)-\sigma_3(x). \tag{7-32}$$

We now define

$$\Delta^{*}q\left(x\right)=q_{2}\left(x\right)-q_{3}\left(x\right)\qquad b_{1}<x<b_{2}, \tag{7-33}$$

and note that, as $q_2\left(x\right)\neq 0$ only in the range $[c_1\ c_2]$, it follows that, outside this interval, $\Delta^{*}q\left(x\right)=-q_{3}\left(x\right)$. and we can write

$$0=\frac{2f}{\pi}\int_{-a}^{a}\frac{p\left(\xi\right)d\xi}{x-\xi}-\frac{1}{\pi}\int_{b_{1}}^{b_{2}}\frac{\Delta^{*}q\left(\xi\right)d\xi}{x-\xi}-\frac{\Delta^{*}\sigma}{4}\qquad b_{1}<x<b_{2}. \tag{7-34}$$

This is an integral equation for $\Delta^{*}q\left(x\right)$ over the interval $[b_1\ b_2]$, which can be inverted for $\Delta^{*}q(x)$, and the solution follows the same sequence as that defining the full range of the cycle, *mutatis mutandis.* Equations (7-16,7-13) continue to hold, with c_i replaced by b_i,and $\Delta Q,\Delta\sigma$ replaced by $\Delta Q^{*},\Delta\sigma^{*}$. We are now in a position to determine the bounds on the permissible shape of the trajectory sketched in Figure 7-2(a). To do this we take the equations defining the location of the stick slip boundaries, and obtain their complete differentials, which are

$$\frac{db_{1}}{a}=\frac{\pi^{2}}{16}\frac{ad\sigma}{fP}+\frac{1}{2\sqrt{2}\sqrt{2-\frac{\Delta^{*}Q}{fP}}}\frac{dQ}{fP} \tag{7-35}$$

$$\frac{db_{2}}{a}=\frac{\pi^{2}}{16}\frac{ad\sigma}{fP}-\frac{1}{2\sqrt{2}\sqrt{2-\frac{\Delta^{*}Q}{fP}}}\frac{dQ}{fP} \tag{7-36}$$

We note that, for slip to be advancing we must have that $db_1>0$, and $db_2<0$. The bounding condition, therefore, on the requirement for advancing slip is when $db_1=db_2=0$, so that the increment must lie in the range

$$\frac{ad\sigma}{dQ}=\pm\frac{8}{\pi^{2}\sqrt{2}\sqrt{2-\frac{\Delta^{*}Q}{fP}}}. \tag{7-37}$$

If we assume that the increments of load just tracked along the extremes of these gradients we would then trace out an envelope of $(\pm a\Delta\sigma^*/fP$ vs. $\Delta^*Q/fP)$ defined by

$$a\Delta\sigma^* = \pm\frac{8}{\pi^2\sqrt{2}}\int_0^{\Delta Q^*}\frac{dQ}{\sqrt{2-\frac{Q}{fP}}}. \tag{7-38}$$

or

$$\frac{a\Delta\sigma^*}{fP} = \pm\frac{8}{\pi^2}\left(1-\sqrt{1-\frac{\Delta Q^*}{2fP}}\right). \tag{7-39}$$

This is a very important characteristic, which defines many of the properties of the system, and is shown in Figure 7-3.

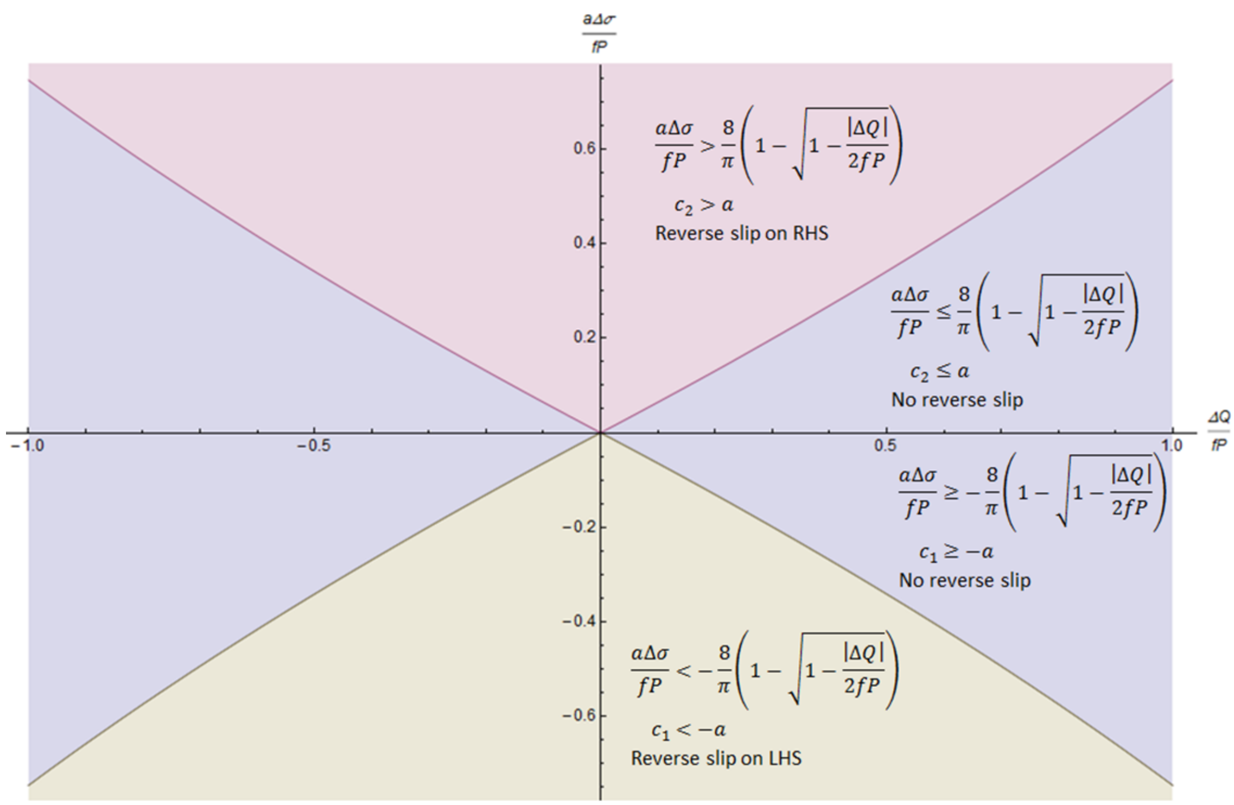

Figure 7-3 – Boundary between same sign and different sign slip behaviour

Note that, in order for a loading trajectory to conform to the requirement that it leads to advancing slip at both stick-slip transition points, it must both (a) lie within the envelope and, at the same time, (b) its gradient at all points must lie within the gradient of the envelope. This figure may be used immediately in conjunction with the schematic of Figure 7-2(a), to show the envelope of load trajectories which fall between this particular pair of points. It is emphasized that only trajectories which satisfy the requirement on bounds of gradient at all points are acceptable. This shows that only trajectories which display a cusp at the end points can be expected to show behaviour where there is only one pair of developing slip regions per cycle of load. An example trajectory for Hertzian contact is shown in Figure 7-4.

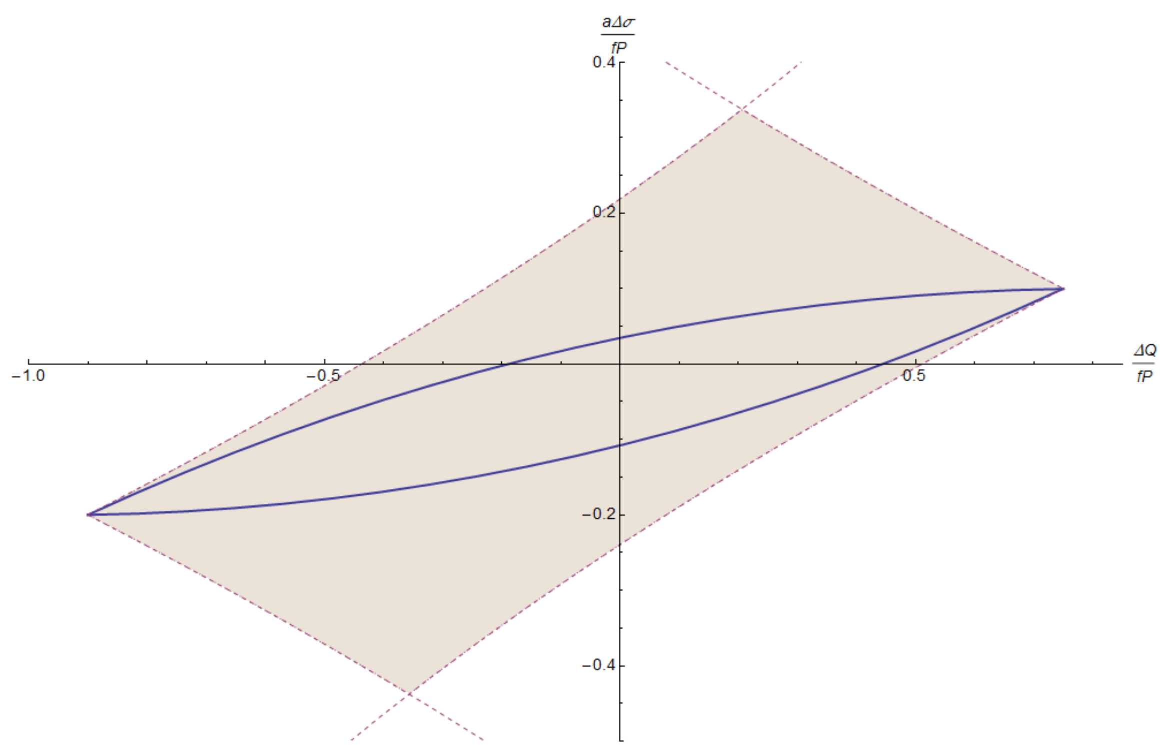

Figure 7-4 – Load for trajectory for same sign slip throughout with point (1)= (-0.9,-0.2) and (2)= (0.75,0.1)

The shaded region indicates where equation 7-28 is upheld, although the condition on the gradient, described above, must also be adhered to for same sign slip behaviour to occur. The slip zone size history for this example is shown in Figure 7-5(a) and the shear traction distribution just before full adhesion, assuming zero locked in strain in the permanent stick zone, is shown in Figure 7-5(b).

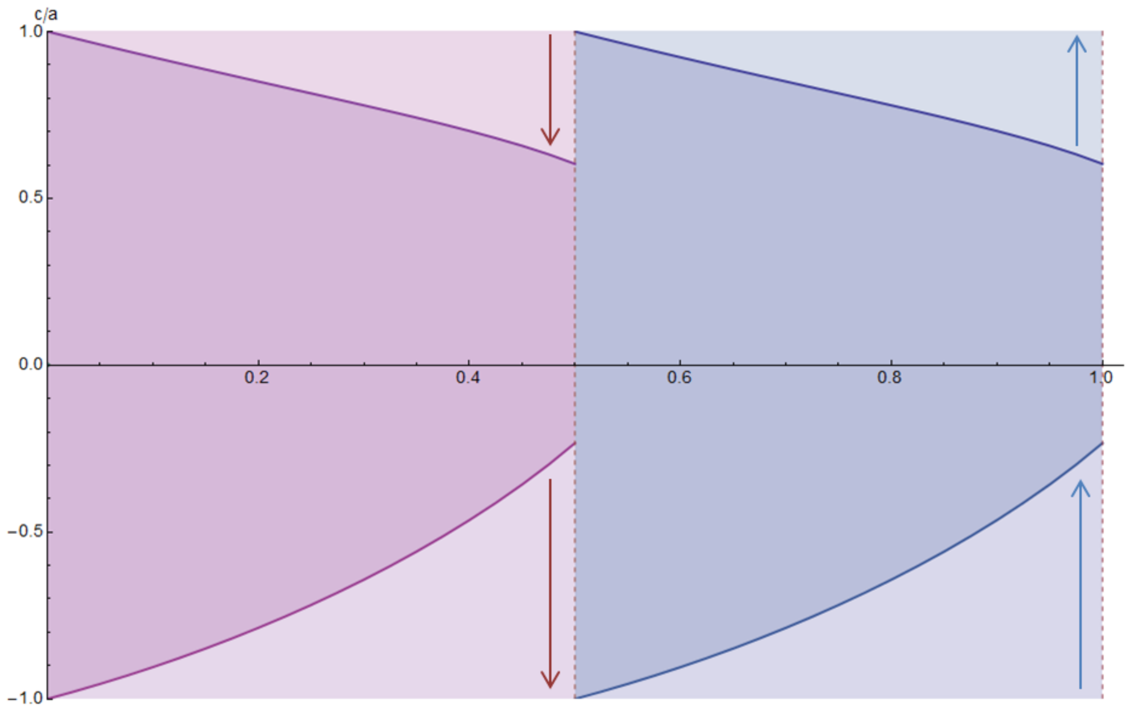

Figure 7-5(a) – Slip zone size history for one cycle shown in figure 7-4

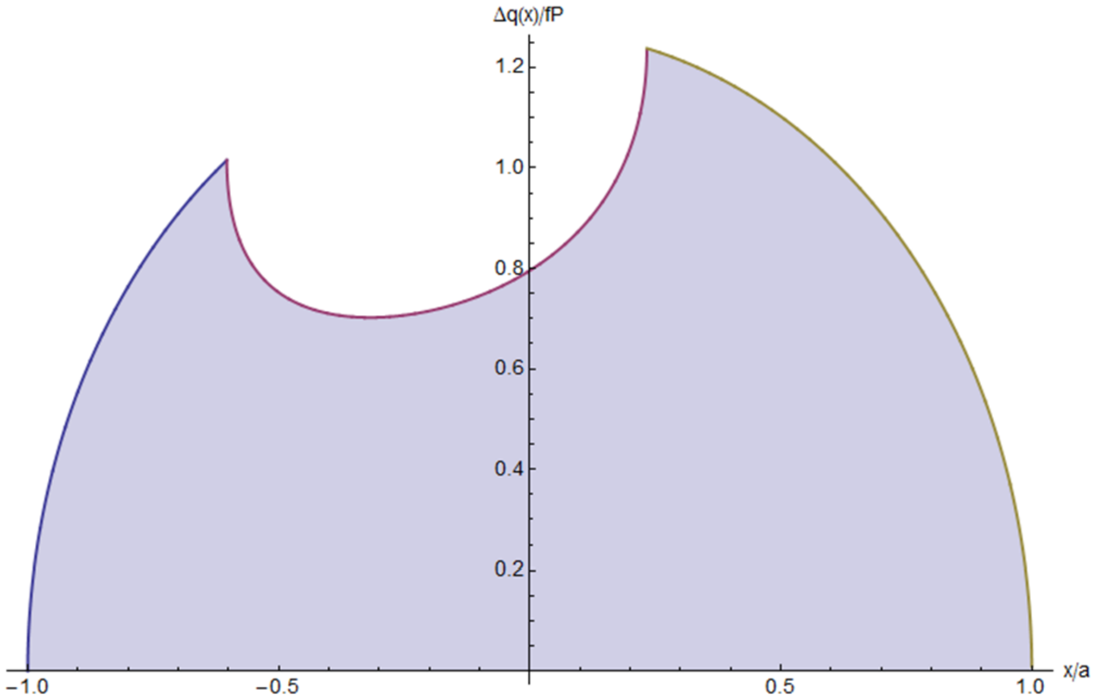

Figure 7-5(b) – Shear traction distribution just before full stick for same sign slip problem shown in Figure 7-4

Opposite Signs of Slip

A solution for the steady state behaviour of the contact where the bulk tension is sufficiently large for the signs of slip in the two slip regions to differ throughout the load cycle is sought. The condition for this behaviour is that the inequality specified by equation 7-28 is not satisfied on one side and that the gradient for all points lies outside the gradient of the envelope. An example trajectory for this behaviour is shown in Figure 7-6. The shaded region again indicates where equation 7-28 is upheld.

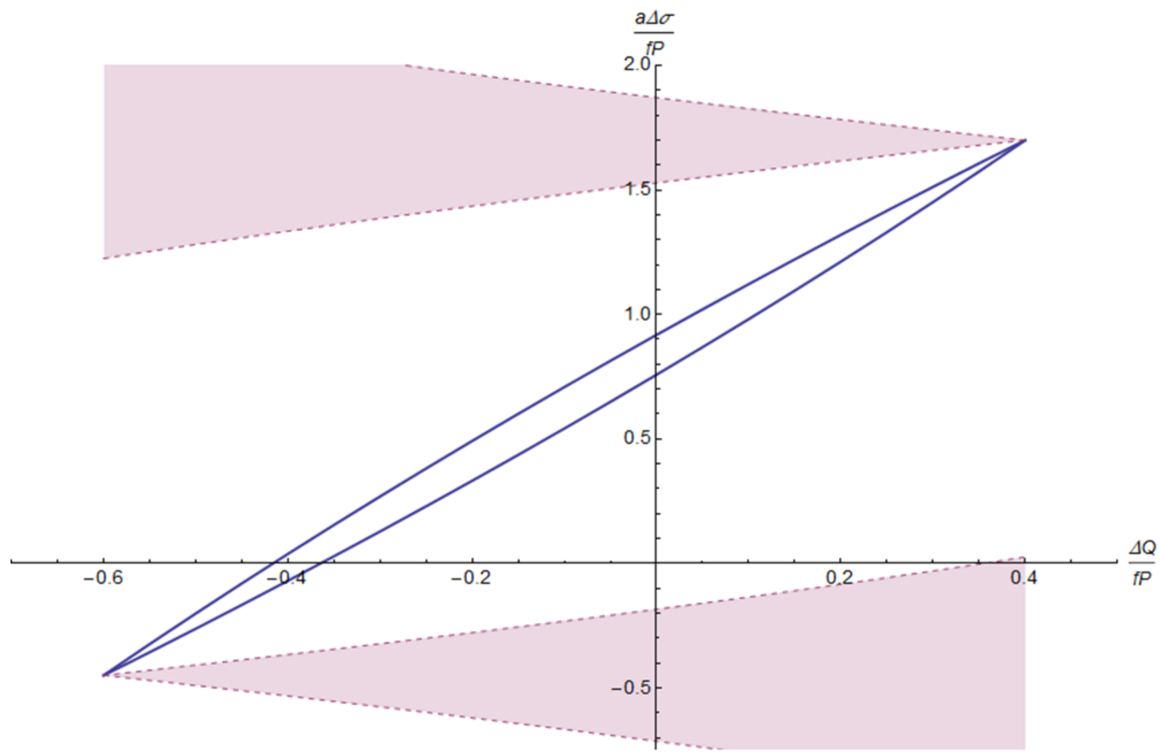

Figure 7-6 – Load for trajectory for different sign slip throughout with point (1)=(-0.6,-0.45) and (2)=(0.4,1.7)

A schematic representation of the slip zone behaviour is shown in Figure 7-2(c). This case has to be treated numerically, using the standard procedure first outline by Erdogan Gupta and Cooke [39], and applied to various forms of this problem, see, e.g. [19], or, for a fuller description [10].

The resulting slip zone size history for the example problem is shown in Figure 7-7(a) and the shear traction distribution just before full adhesion, assuming zero locked in strain in the permanent stick zone, is shown in Figure 7-7(b).

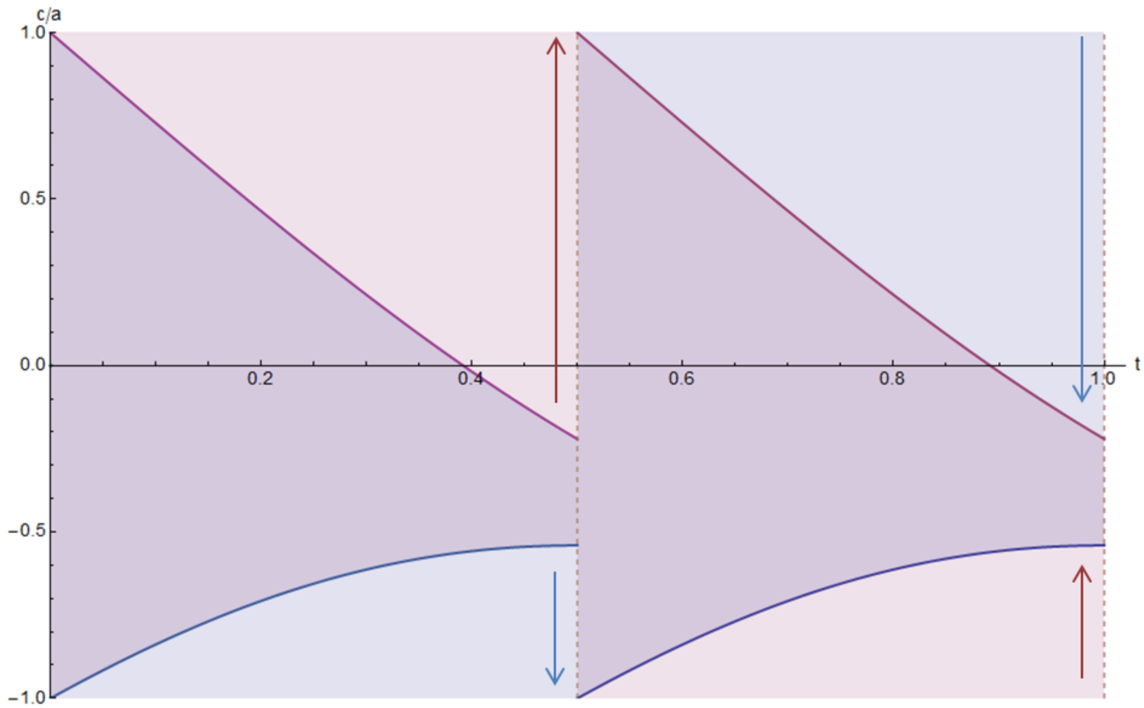

Figure 7-7(a) – Slip zone size history for one cycle shown in figure 7-6

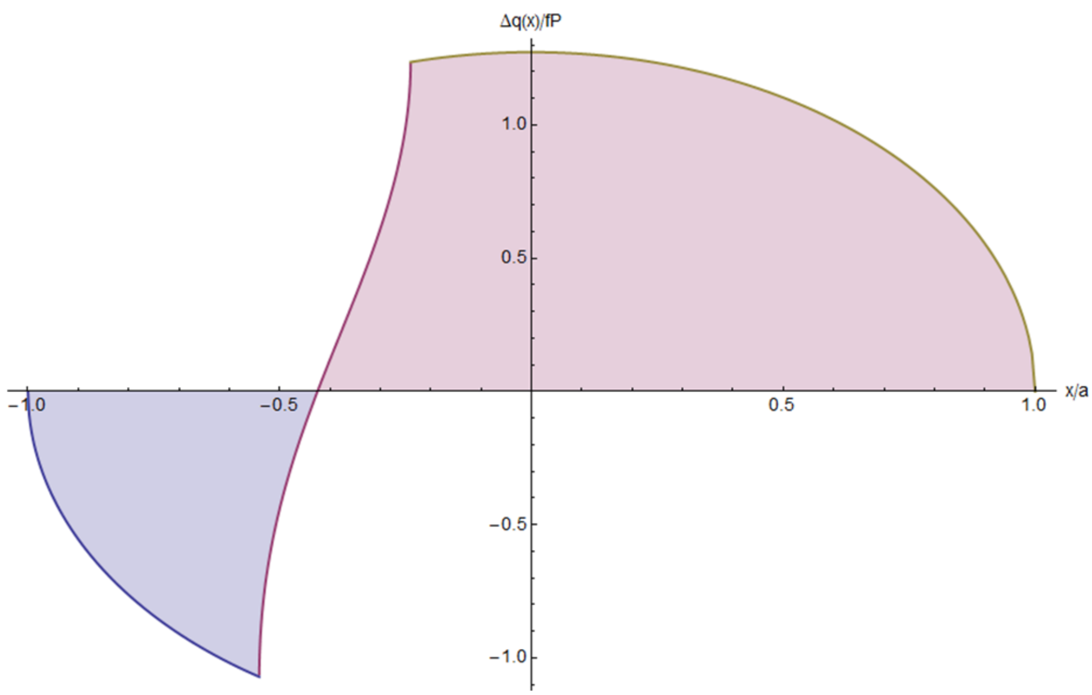

Figure 7-7(b) – Shear traction distribution just before full stick for opposite sign slip problem shown in Figure 7-6

Frictional Energy expended

To complete the solution, we need also to quantify the frictional energy expended, both in a pointwise and global sense. Fortunately, at any point within the contact the pressure is fixed in time, so that, when any point enters the slip state, the shearing traction there is also subsequently constant in time. It follows that, at any point which lies outside the permanent stick region, the work done is simply the product of $fp(x)$ and the slip displacement the instant before full stick again occurs, and the next phase of advancing slip develops. It is therefore very straightforward to work out the density of frictional energy expended at any point, and this is given by

$$W\left(x\right)=fp\left(x\right)\Delta g\left(x\right) \tag{7-40}$$

where the relative displacement since the previous point of full adhesion, $\Delta g\left(x\right)$ is given by

$$\Delta g(x) = \begin{array}{ll} \int_{c_1}^{x}\left[h'\left(\zeta\right)+\frac{1}{\pi}\int_{c_1}^{c_2}\frac{q_1(\xi)d\xi}{\zeta-\xi}+\frac{\sigma_1}{4}\right]d\zeta & -a<x<c_1 \\ \int_{x}^{c_2}\left[h'\left(\zeta\right)+\frac{1}{\pi}\int_{c_1}^{c_2}\frac{q_1(\xi)d\xi}{\zeta-\xi}+\frac{\sigma_1}{4}\right]d\zeta & c_2<x<a \end{array} \tag{7-41}$$

$$\Delta g(x) = \frac{2f}{\pi R}h(x)+\frac{\pi f}{2R}F_1(x;c_1,c_2)+\frac{\Delta\sigma\left(1-\kappa\right)}{8\mu} \qquad \begin{array}{c} -a<x<c_1 \\ c_2<x<a \end{array} \tag{7-42}$$

where, for the Hertz case

$$F_1(x;c_1,c_2)=\left(\begin{array}{c} (x-c_1)(x-c_2)+2c_2\sqrt{x-c_1}\sqrt{x-c_2} \\ +\frac{1}{2}(c_1-3c_2-2x)\sqrt{(x-c_1)(x-c_2)} \\ +\frac{1}{2}(c_1-c_2)(c_1+3c_2)\sinh^{-1}\sqrt{\frac{c_2-x}{c_1-c_2}} \\ +c_2(c_1-c_2)\log\left[\frac{c_2-c_1}{\left(\sqrt{x-c_1}+\sqrt{x-c_2}\right)^2}\right] \end{array}\right) \qquad \begin{array}{c} -a<x<c_1 \\ c_2<x<a \end{array} \tag{7-43}$$

The same relative displacements are locked in at each point of instantaneous stick, so the equations above are valid in both forward and reverse slip regions. As an example, the energy dissipated during a two phase problem with opposite signs of slip during each phase is shown in Figure 7-8.

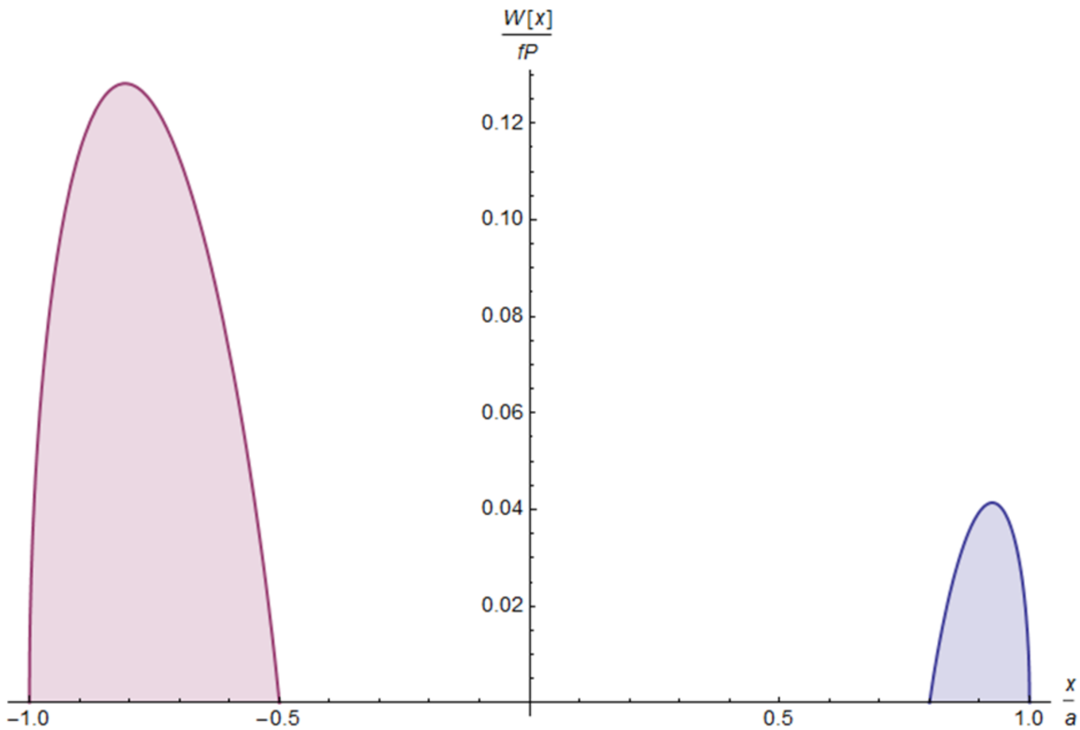

Figure 7-8 – Energy dissipation for two phase problem for $\Delta Q = 1.15, .\Delta\sigma = 0.243.$

Harmonic problem

Formulation

For a contact following a smooth circular trajectory in Q-σ space, the conditions specified in equation 7-28 will be valid as $d\sigma$ approaches zero and will be invalid as dQ approaches zero. Furthermore, it is possible that the two sides of the contact will not stick at the same time, which will invalidate the formulation used to derive equation 7-28. Therefore, this problem is best approached using a 'marching in time' solution. An example has been considered in which the change in shear force and bulk tension are described by the following equations

$$\Delta\sigma = \sigma_0 + \Delta\sigma_0 \sin\theta \quad (7\text{-}44)$$

$$\Delta Q = Q_0 + \Delta Q_0 \sin(\theta + \phi), \quad (7\text{-}45)$$

where θ is a time-like parameter. To simplify the implementation, we assume that $\sigma_0 = Q_0 = 0$ and $\phi = \pi/2$, which gives an ellipse centred on the origin. The implementation procedure is very time consuming[1] and has therefore been solved for a small number of steps along the trajectory, an approach that is valid only when the stick zone is receding. If advancing stick occurs, a new analytical method would need to be developed. Alternatively, numerical solution, such as finite element analysis or 'quadratic programming' (as used by Reina et al.[40], among others) could to be used. An example load trajectory with $\Delta Q_0/fP = 0.825$, $\Delta\sigma_0 a/fP = 0.275$ has been considered, which gives a load trajectory in $Q - \sigma$ space as shown in Figure 7-9.

[1] Numerical methods are required: One to solve the integral equation for the shear traction distribution, because there will be a relative slip locked in to the stick zone. This runs for each iteration in the second numerical method, which gives the the size and location of the stick zone and the direction of slip in each slip zone for the required normal and shear load.

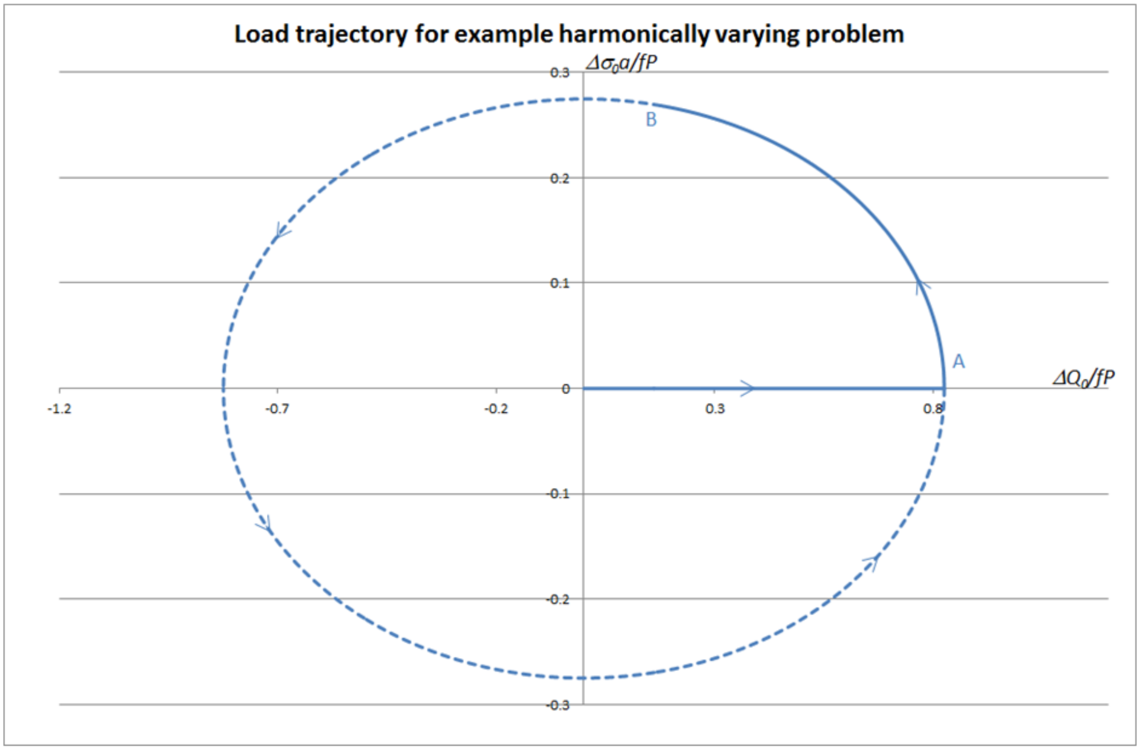

Figure 7-9 – Example load trajectory for harmonic problem, $\Delta Q_0/fP = 0.825$, $\Delta\sigma_0 a/fP = 0.275$.

Solution

The progression of slip zone size for the example problem is shown in figure 7-10(a)[2]. Initially, only a shear load was applied,so that the initial solution is identical to the Cattaneo-Mindlin problem. At point A^+, the $+ve$ side of the contact instantaneously sticks, and a reverse slip region begins to develop. During this time, the forward slip zone on the $-ve$ side of the contact continues to grow. The slip zones now show opposite signs of slip and both continue to grow until point B is reached, after which an advancing stick zone was observed on the $-ve$ side of the contact. At this point, the solution becomes invalid, as a continuous integral representation to account for the effect of laying down stuck material is required, which is unfeasible

[2] Note that this curve is a cubic fit through the five valid points at which a solution was found

using the existing implementation. Furthermore, advancing stick has not previously been observed in any other example partial slip contact problem, so no methods of analysis are available. Derivation of a method to provide a solution is beyond the scope of this thesis, and is therefore recommended as further work. The history of relative strain between the two bodies for the points at which the problem was valid is shown in Figure 7-10(b) and the shear traction distribution history at these points is shown in Figure 7-10(c).

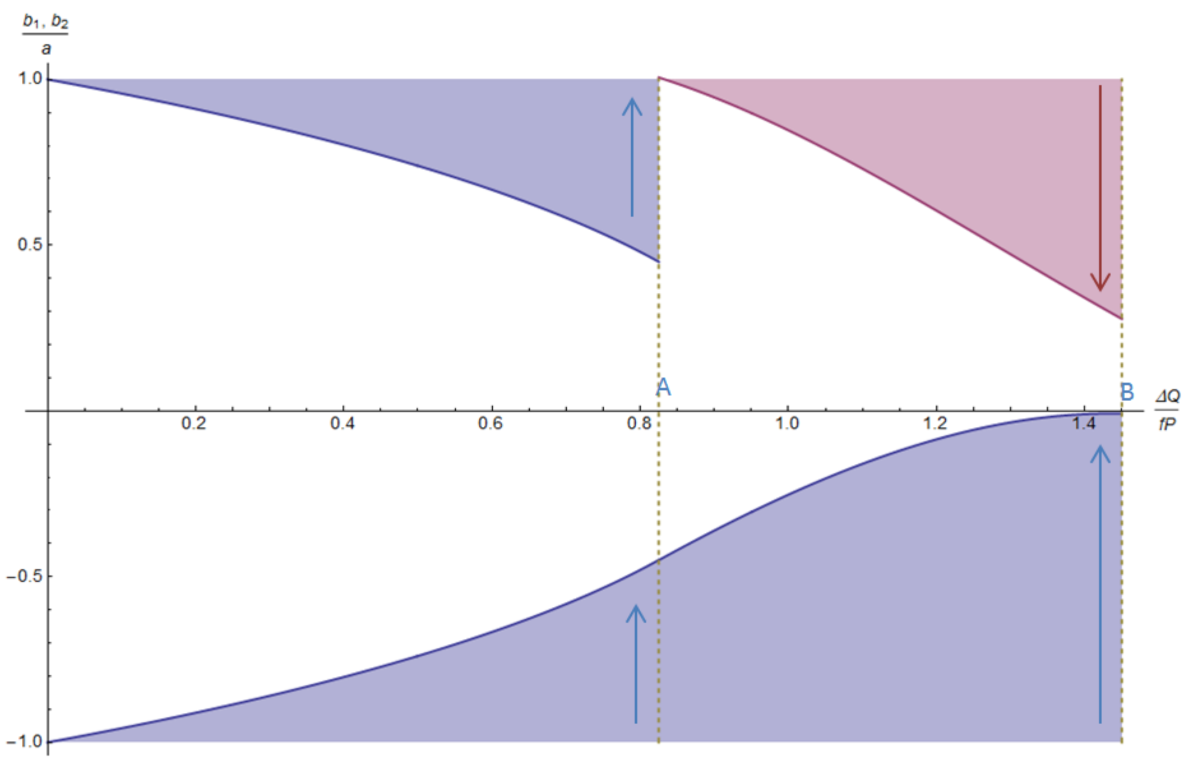

Figure 7-10(a) – Slip zone size history for one cycle shown in figure 7-9 (solved by 'marching in time')

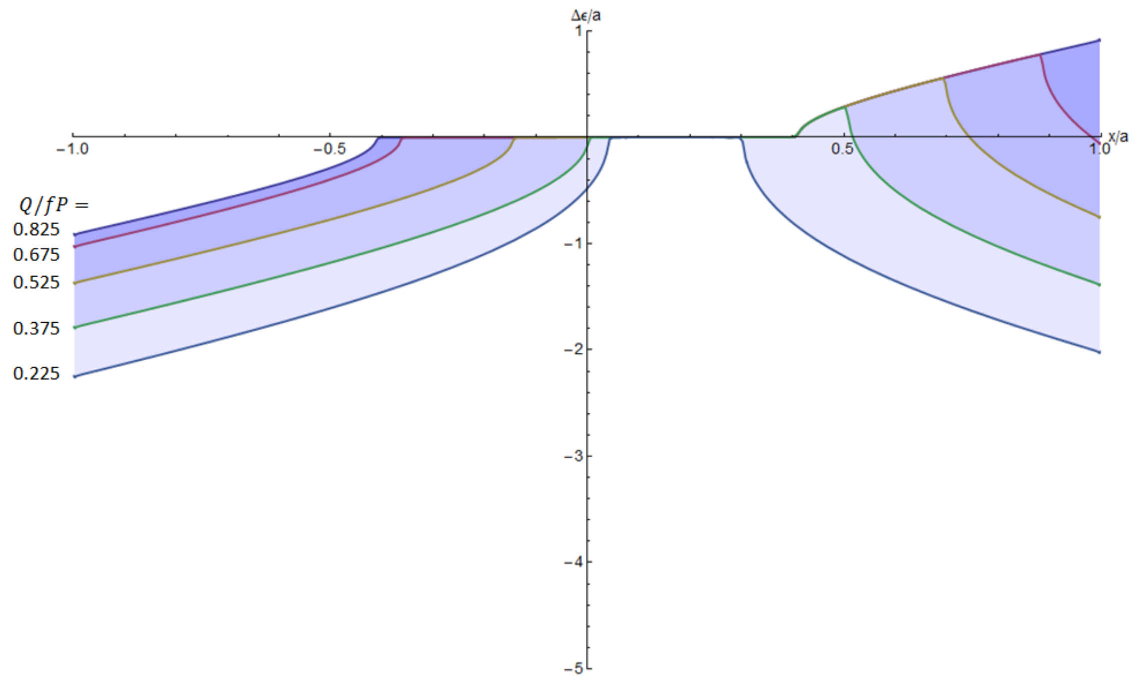

Figure 7-10(b) – Locked in strain history for one cycle shown in figure 7-9 (solved by 'marching in time')

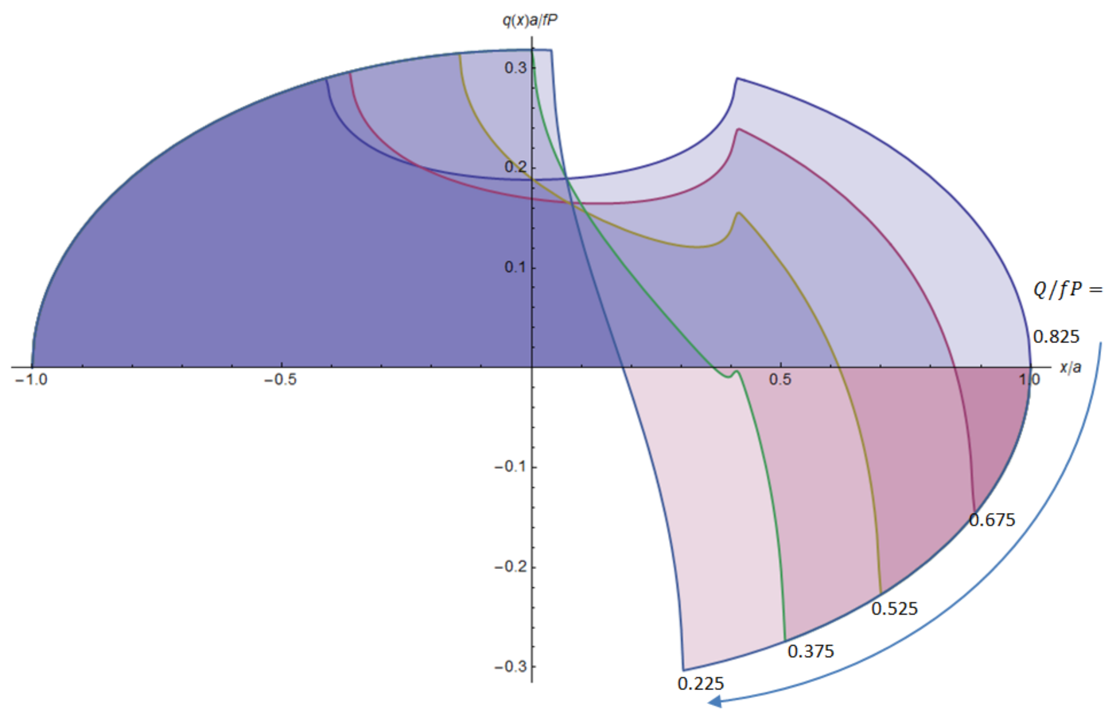

Figure 7-10(c) – Shear traction history for one cycle shown in figure 7-9 (solved by 'marching in time')

Conclusion

A method for obtaining the steady state stick-slip zone evolution for a half-plane contact subject to periodically varying shear and bulk tension has been found, for the 'two slip zone' regime, which implies 'lens like' loci in $Q - \sigma$ space. The most general kind of response to be expected - where there are two periods of advancing slip per cycle of loading have been investigated in detail. The procedure is economical, and applies regardless of any locked in shearing tractions developed during the transient loading phase. A smooth circular path in $Q - \sigma$ space implies four characteristic phases per cycle of load, and requires further work beyond the scope of this thesis, because the occurrence of advancing stick has been demonstrated.

Conclusions

This thesis provides a series of useful tools to aid in the investigation of, and design against fretting fatigue. The formulation for a general incomplete contact, defined as a series of curved segments is provided, along with a Mathematica tool that uses the formulation to generate common contact mechanics expressions for any combination of algebraic and numerical input.

The remainder of the thesis focuses on developing contact formulations that are not restricted to the current ‘sequential’ process, by which a normal load is applied first, followed by a shearing force and bulk tension in proportion. The modified formulation uses a sequence of complete contacts to introduce shear force and bulk tension at the same time as the normal load is applied. Conditions for full adhesion, partial slip and sliding have been developed. The formulation for all possible outcomes from two phases of proportional loading along straight lines is provided along with worked examples.

Cyclic loading is subsequently considered. Restricting the problem to normal and shear load only at first, formulation is provided for the stick zone size for the entire transition problem, and around one complete steady state cycle. The relative velocity between local points and the frictional dissipation energy around the steady state cycle are calculated, and are proved to be independent of the transition problem. A Mathematica tool has been created to provide the complete stick/slip state, energy dissipation per unit length and instantaneous shear tractions for an incomplete contact under a load path described by an ellipse in $P-Q$ space. Any form of incomplete punch can be considered by using the first Mathematica tool to generate the required equations.

Finally, the constant normal load problem is considered. The formulation for two phases of slip, which can be of the same or different sign on either side of the contact, is provided. A harmonic variation in $Q - \sigma$ space, similar to the solution provided in $P - Q$ space, is attempted by a 'marching in time' approach, resulting in an advancing stick zone, which has not been observed previously, but a solution to which is beyond the scope of the thesis.

The techniques developed in this work are intended to allow assessment of i) the likely fretting performance and ii) any impact on vibration damping in a short time for a given incomplete contact. The primary application is in gas turbine dovetail and firtree design: these methods can be used to carry out an optimisation process that will indicate the contact form that will give the most even dissipation of frictional energy for a given flight cycle, without reducing the total energy dissipated. A process which is unfeasible using numerical methods, which are too time consuming for the large number of iterations that will be required. The proposed contact profiles can then be assessed using a method that is less limited, such as quadratic programming, to allow further refinement. Finally the most accurate, but time consuming methods, such as 3D finite element analysis, can be used to approximate closely the exact stress field and calculate the safe operating life for the component.

It is acknowledged that this work is based on an unproven hypothesis, namely that the fretting performance can be characterised using only frictional energy dissipation. Furthermore, the validity of the analysis is restricted to half-plane situations, which, for most blade/disc interface geometries, is not an appropriate model. However, the analysis is required only to calculate the relative performance of one geometry with respect to another, both of the aforementioned limitations are unlikely to be sufficiently erroneous to prevent this completely and the method should give a starting point, which can be fine tuned with a more detailed analysis.

Some of the above limitations could be addressed in further work: In particular, a promising method is being investigated that allows firtree analysis without using a half-plane approximation by initially assuming the blade and disc to be a monolith, before introducing dislocations to model i) the relatively small gaps that exist between the components, and ii) the relative slip along the interface. Development of this method could allow more precise optimisation, which would require less fine tuning.

References

[1] D. Dini, D.A. Hills, A method based on asymptotics for the refined solution of almost complete partial slip contact problems, *European Journal of Mechanics - A/Solids*, **22** (2003), 851-859.

[2] C.-H. Goh, D.L. McDowell, R.W. Neu, Characteristics of plastic deformation field in polycrystalline fretting contacts, *International Journal of Fatigue*, **25** (2003), 1047–1058.

[3] M. Zhang , R.W. Neu, D.L. McDowell , Microstructure-sensitive modeling: Application to fretting contacts, *International Journal of Fatigue*, **31** (2009), 1397–1406

[4] M.P. Szolwinski, T.N. Farris, Mechanics of fretting fatigue crack formation, *Wear*, **198** (1996), 93-107.

[5] N. Banerjee, D.A. Hills, D. Dini, The derivation and application of a semi-infinite flat and rounded asymptotic frictionless contact, *International Journal of Mechanical Sciences*, **51** (2009), 662-666.

[6] M. Porter, D. A. Hills, A flat punch pressed against an elastic interlayer under conditions of slip and separation, *International Journal of Mechanical Sciences*, **44** (2002), 465-474.

[7] A. Mugadu, D.A. Hills, A generalised stress intensity approach to characterising the process zone in complete fretting contacts, *International Journal of Solids and Structures*, **39** (2002), 1327-1335.

[8] H. Hertz, Über die berührung fester elastischer Körper, *J. reine und angewandte Mathematik,* **92** (1882).

[9] G.M.L. Gladwell, *Contact problems in the classical theory of elasticity*, Sijthoff & Noordhoff, 1980, Alphen aan den Rijn, The Netherlands

[10] D.A. Hills, D. Nowell, A. Sackfield, *Mechanics of Elastic Contacts*, Butterworth-Heinemann, 1993, Oxford

[11] J.R. Barber, *Elasticity (3rd ed.)*, 2010, (Springer, Dordrecht).

[12] H. Deresiewicz, Bodies in contact with applications to granular media, in *R.D. Mindlin and applied contact mechanics*, Ed. George Herrmann, 1974, Pergamon,

105-147.

[13] F.W. Carter, On the action of a locomotive driving wheel, *Proc. R. Soc. London. A*, **112** (1926), 151-157

[14] C. Cattaneo, Sul contatto di due corpi elastici: distribuzione locale degli sforzi. *Rendiconti dell'Accademia Nazionale dei Lincei,* **27 (**1938), 342–348, 434–436, 474–478. (In Italian)

[15] R.D. Mindlin, Compliance of elastic bodies in contact. *ASME J.Appl.Mech.,* **16** (1949), 259–268.

[16] R.D. Mindlin, H. Deresiewicz, Elastic spheres in contact under varying oblique forces. *ASME J.Appl.Mech*., **75** (1953), 327–344.

[17] J. Jäger, A new principle in contact mechanics. *ASME J.Tribology*, 1998, **120** (1998), 677–684.

[18] M. Ciavarella, The generalized Cattaneo partial slip plane contact problem. I-Theory, II-Examples. *Int.J.Solids Struct,* **35** (1998), 2349–2378.

[19] D. Nowell, D.A. Hills, Mechanics of fretting fatigue tests, *International Journal of Mechanical Sciences*, **29** (1987), 355-365

[20] J. Vazquez, A. Sackfield, D.A. Hills, J. Dominguez, Mechanical Behaviour of a Symmetrical Punch Having Compound Curvature: Part I-Normal Loading, *Private correspondence*, September 2009

[21] M. Ciavarella, G. Demelio, On non-symmetrical plane contacts *International Journal of Mechanical Sciences*, **41** (1999), 1533 - 1550

[22] N. I. Muskhelishvili, *Some basic problems of the mathematical theory of elasticity*, Noordhoff Layden, 1975.

[23] I.G. Goryacheva, H. Murthy, T.N. Farris, Contact problem with partial slip for the inclined punch with rounded edges, *International Journal of Fatigue*, **24** (2002), 1191–1201

[24] V.I. Mossakovskii, Application of the reciprocity theorem to the determination of the resultant forces and moments in three-dimensional contact problems. (In Russian), *PMM*, **17** (1953), 477–482.

[25] D.A. Spence, An eigenvalue problem for elastic contact with finite friction, *Proceedings of the Cambridge Philosophical Society*, **73** (1973), 249–268.

[26] J.R. Barber, M. Davies, D.A. Hills, Frictional elastic contact with periodic loading, *International Journal of Solids and Structures*, **48** (2011), 2041-2047

[27] D.A. Hills, M. Davies, J.R. Barber, An incremental formulation for half-plane contact problems subject to varying normal load, shear and tension, *J. Strain Analysis*, **46** (2011), 436-443

[28] J.R. Barber, Frictional systems subjected to oscillating loads. *Ann.Solid Struct. Mech*., under review. 2011

[29] E. Melan, Theorie statisch unbestimmter Systeme aus ideal-plastichem Baustoff. Sitzungsber. d.Akad. d. Wiss., Wien 2A(145) (1936), 195–218 (In German).

[30] J.R. Barber, A. Klarbring, M. Ciavarella, . Shakedown in frictional contact problems for the continuum. Comptes Rendus Mecanique, **336** (2008), 34–41.

[31] Y.J. Ahn, E. Bertocchi, J.R. Barber, Shakedown of coupled two-dimensional discrete frictional systems. J. Mech. Phys. Solids **56** (2008), 3433–3440.

[32] M. Ciavarella, 1998. Tangential loading of general three-dimensional contacts. *ASME J.Appl.Mech,* **65** (1998), 998–1003.

[33] J. Jäger, Half-planes without coupling under contact loading. *Arch. Appl. Mech*., **67** (1997), 247–259.

[34] D. Dini, D.A. Hills, Frictional energy dissipation in a rough Hertzian contact. *ASME J.Tribology,* **131** (2009)

[35] K.L. Johnson, *Contact Mechanics*, Cambridge University Press, Cambridge, 1985.

[36] J.R. Barber, Determining the contact area in elastic indentation problems. *J. Strain Analysis* **9** (1974), 230–232.

[37] J. Dundurs, M. Comninou, An educational elasticity problem with friction — Part I: Loading, and unloading for weak friction. ASME J.Appl.Mech. **48** (1981), 841–845.

[38] J, Dundurs, M. Comninou, An educational elasticity problem with friction — Part III: General load paths. ASME J.Appl.Mech. **50** (1983), 77–84.

[39] F. E. Erdogan, G.D. Gupta, T.S. Cook, The numerical solutions of singular integral equations, in Mechanics of Fracture. Volume 1. Methods of Analysis and Solution of Crack Problems, Noordhoff Intern. Publ., Leyden, 1973, 368-425

[40] S. Reinaa, D. Dini, D.A. Hills, On the accurate prediction of interfacial micro-slip in frictional joints using distributed dislocations and quadratic programming techniques, *Procedia Engineering*, **1** (2009), 181–184

Program giving equations for contact between a general piecewise quadratic punch and a half-plane – User guide.

1. Introduction

This documentation covers the Mathematica file "GeneralContact.nbp" which accompanies 'Closed form solutions for a piecewise quadratic half-plane contact problem'. The program generates equations for contact load, contact pressure, Muskhelishvili potential and the consistency condition (arising from inversion of the contact pressure equation) for any given half plane contact problem. The program accepts both numerical and algebraic inputs, and as such lends itself to being used to generate equations which can subsequently be used in an optimisation process. This document serves as a guide to the features of the code, verification is performed against a standard case, and a worked example is given.

2. Running the program

This program is in the Wolfram Mathematica '.nbp' form, as such it can be run either with limited functionality on the freely available 'Mathematica Player', or with full functionality on either of the commercial releases of the software: 'Mathematica' or 'Mathematica Player Pro'. Upon opening, the user will be prompted about dynamic content, in order to function correctly, this should be enabled[1]. No accompanying files are required for execution however a free plug-in is required if the equations are to be exported in Matlab code, see section 4.

3. Operating the program

Once the file has been opened, the screen shows the main console together with a quick reference to identify the required parameters. Figure 1 shows the main console as it will appear initially. Boxes with blue backgrounds or buttons written in grey are locked and cannot be altered by the user.

[1] The program can be opened with dynamic content disabled to allow inspection of the code prior to execution, dynamic content can be subsequently enabled using the evaluation menu, or by reopening the file.

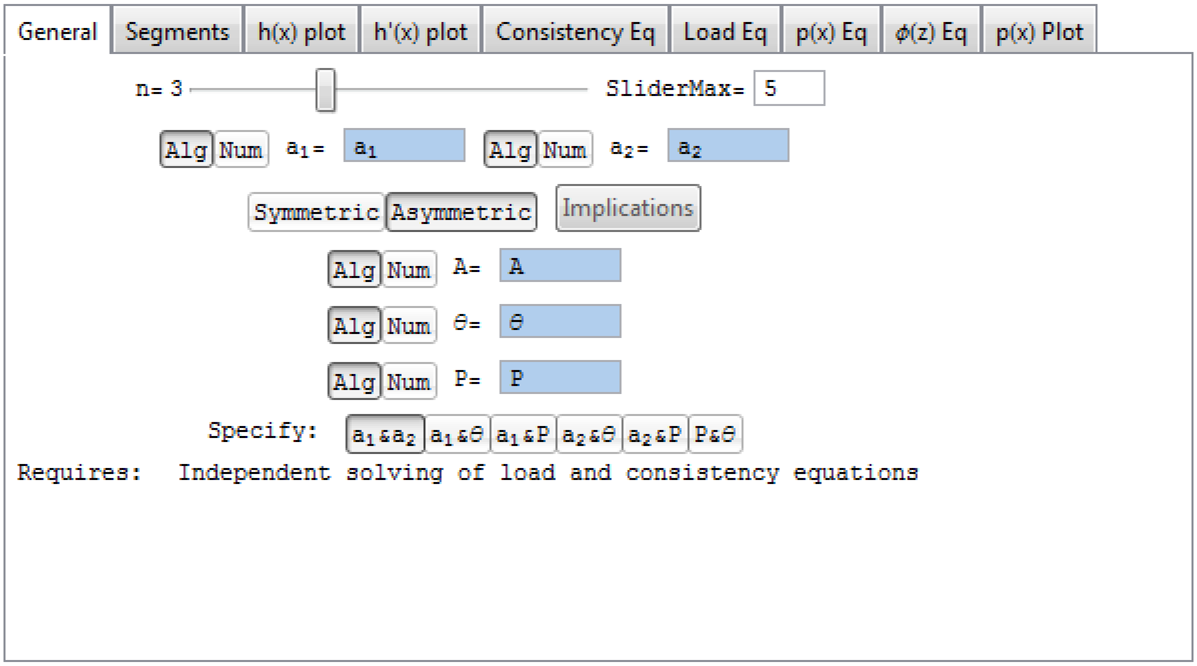

Figure 1 – Main console with 'General' tab active

3.1. 'General' tab

This screen allows the parameters affecting the entire punch and half-plane to be set:

- The first line contains a slider, which is used to define the number of segments in the punch. This is initially constrained to be in the region 2-5, but can be increased by altering the 'Slider Max' input to the right of the slider.
- The second line defines the extent of the contact, which can either be algebraic or numerical. If symmetry is selected, the second field is constrained by the opposing coordinate and cannot be altered.
- The third line is used to define whether if the contact is symmetric or not. A symmetric contact will have constraints applied to various inputs, which will be either locked or hidden to prevent input. To see these constraints, click the 'Implications' button, a drop down list of the applied constraints will be shown.
- The next three lines allow either algebraic or numerical values to be set for the composite compliance, A, the punch rotation, θ, and the applied load, P.
- The final control defines the parameters to which numerical values can be assigned. The extent of contact, rotation of the punch and applied load represent four parameters sharing two degrees of freedom, therefore only two can be independently specified. This selector defines which are locked and which are unlocked. If symmetric contact is specified, only the first and last are selectable as the punch rotation is zero and a_1 and a_2 are constrained. The text beneath these controls specifies how the consistency equation and load equation should be used to determine all the parameters.

3.2. 'Segments' Tab

Once the general parameters have been defined, the parameters affecting the individual segments need to be set. Figure 2 shows the screen displayed when the second tab is activated.

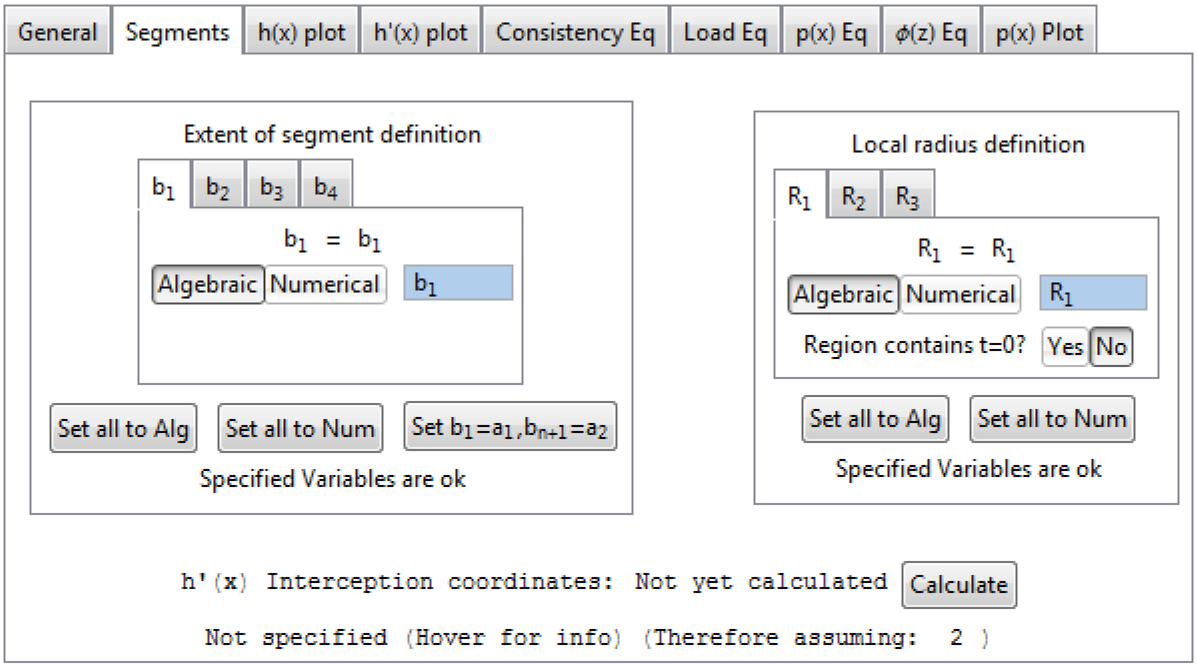

Figure 2 - Main console with 'Segments' tab active

This screen is composed of two main sections, with a different number of tabs, depending on the number of regions, and whether symmetry is enabled:

- The left hand pane defines the extent of each region. Figure 3 below shows how the parameters are interpreted for symmetric and asymmetric punches. This reference is also included in the program itself. There are three buttons beneath the input, these can be used to set all the regions to be algebraic or numeric[2] or to set the outermost coordinates to be equal to the extent of contact, this is useful for verification against known cases, but care should be taken to ensure that $a_1<b_2<b_3...<b_n<a_2$, as this is not checked by the program.
- The right hand pane sets the local radius in each segment, again either algebraic or numeric input can be selected and the same controls for setting each region to be algebraic or numeric2 are present. Flat regions can be introduced using a very large local radius (R>1E9), and concave sections using a negative local radius[3]. Additionally, the region containing the *x=0* coordinate can be set. This is only has an effect on the consistency equation and if it is not specified, is

[2] Setting all values to numerical uses the initial assumption of *n* equally sized segments in the interval [-1,1] with the local radius reducing by a factor of 2 with each region moving outwards from the centre, which has a local radius of 1.

[3] If concave regions are present, P must be sufficient to cause a single contact region, which can be checked by ensuring the p(x) plot is entirely positive.

automatically assumed to be the central region[4]. The region currently assigned to contain x=0 is shown at the bottom of the form, along with a statement regarding how it was determined.

- Finally, the *h'(x)* interception coordinate array needs to be defined. This is an internal array and is automatically calculated; pressing this button will both generate and display it. If any parameter affecting this is changed, it will need to be regenerated. No output is available until this has been run.

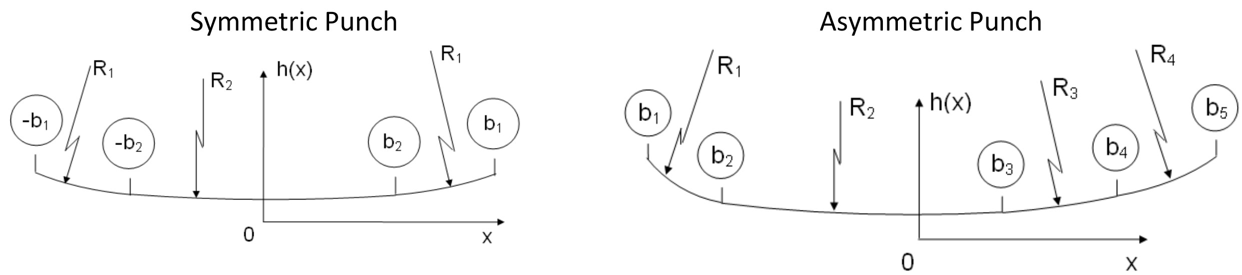

Figure 3 - Punch diagrams

3.3. '*h(x)* plot' and '*h'(x)* plot' tabs

The next two tabs allow the punch profile, *h(x)*, and its first derivative, *h'(x)*, to be viewed graphically providing all values for b_i and R_i in each segment have been defined numerically.

3.4. 'Consistency Eq', 'Load Eq', 'p(x) Eq' and 'ϕ(z) Eq' tabs

These four tabs show the equations for the consistency condition, and load equivalence (which are automatically calculated), and the contact pressure and Muskhelishvili potential (which are calculated after clicking a button, as they can take some time). The equations can be exported as FORTRAN, C++ or Matlab code. More information on exporting can be found in section 4.

3.5. '*p(x)* plot' tab

If numerical values have been specified for a_i, b_i, R_i, θ and A, then a plot of contact pressure across the surface can be viewed on this tab. If the contact is asymmetric, it is not possible to set a_1, a_2 and θ, (as the three are not independent). In this case, θ can be set by the user after manually solving the consistency condition. No checks are made regarding the validity of the value used, so care should be taken when manually specifying θ.

4. Exporting equations

As mentioned in section 3.4, equations can be exported as FORTRAN, C++ or Matlab code. To do this, select the required format, then press export, select the filename and location, then press 'Save'. Exporting equations is not possible if the program is being run using the free 'Mathematica Player' software, to comply with licensing restrictions.

The variables in exported files are the same as in the Mathematica program, except that subscripts have been raised so a_1 would be exported as *a1*.

[4] If *n* is even, the left central region is assumed. If the x-coordinate lies between the central regions, either can be set.

If the Matlab format is required, the free converter must be loaded prior to running this program. This can be obtained from http://library.wolfram.com/infocenter/MathSource/577. To install, open the file and click the 'Run Package' button, the file can then be closed.

5. Verification – Barrelled contact

This section details verification of the code against the Symmetric barrelled contact defined by Vazquez et al. (see paper for Ref.). This contact form has a central region, with a large radius of curvature, bounded both sides by regions with a smaller local radius. These bounding regions are defined as far as the edges of contact.

5.1. Summary of problem variables

n=3

A, θ, a_1 and P all algebraic

$b_1=a_1$, $b_2=b_2$, $b_3=-b_2$ and $b_4=-a_1$

$R_1=R_1$, $R_2=R_2$, and $R_3=R_1$

The assignments on the last two rows can be set by pressing the '*symmetric*' button on the general tab and the '*Set* $b_1=a_1$ *and* $b_{n+1}=a_2$' button on the 'Segments' tab. For detailed instructions, please see appendix A.

5.2. Output screenshots

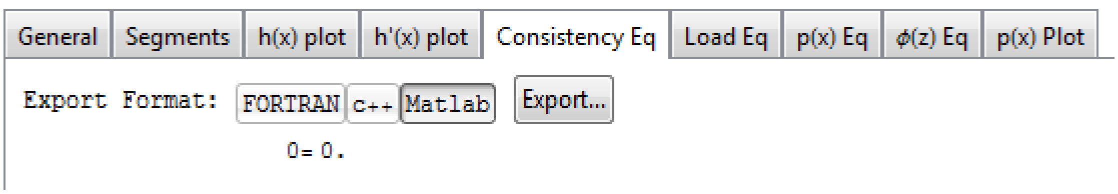

a)

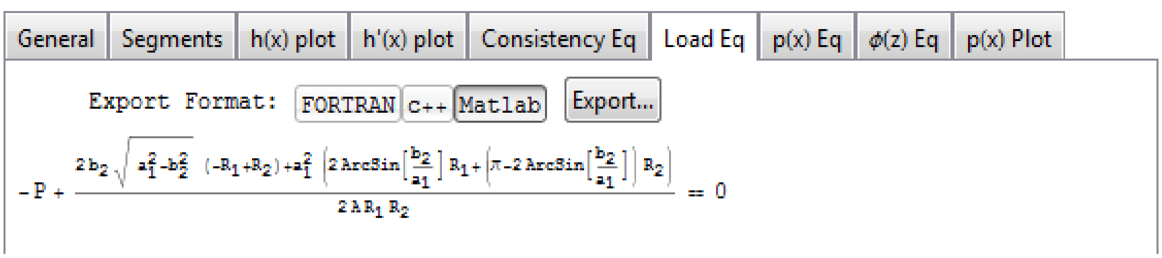

b)

Figure 4 - Output from verification problem

The formula in *a)* shows that the consistency condition is automatically satisfied and therefore provides no new information.

After rearrangement and substituting $k=\left(1-\frac{R_1}{R_2}\right)$, the formula in *b)* agrees with the result in Vazquez et al.

5.3. Numerical comparison of p(x) plot

Continuing the example above, if the algebraic definitions for the parameters are replaced with numerical values (the field can be unlocked by pressing the 'num' button adjacent to the definition, after which the value can be entered) then a contact pressure plot can be generated. For detailed instructions, please see appendix A.

A=1, θ=0 (automatically set by turning symmetry on), a_1=-1, b_2=-0.7, R_1=1, R_2=5.

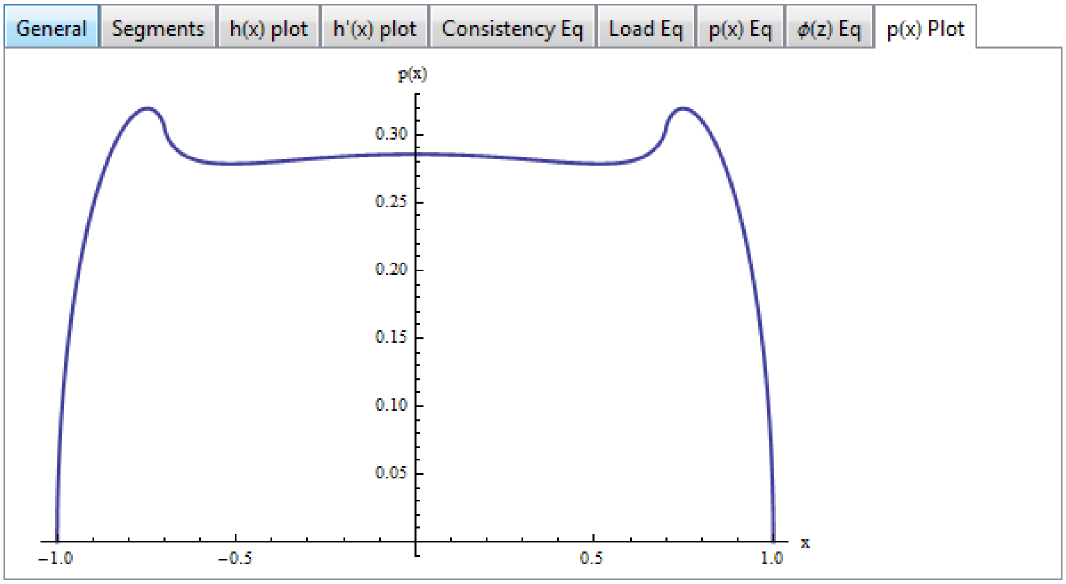

Figure 5 - Numerical p(x) plot from this program

In[1]:= $A = 1;\ R1 = 1;\ R2 = 5;\ b = 0.7;\ k = 1 - \frac{R1}{R2};\ a = 1;$

$$F[t\_, x\_, a\_] := \text{Log}\left[\text{Abs}\left[\frac{\sqrt{\frac{a-x}{a+x}} - \sqrt{\frac{a-t}{a+t}}}{\sqrt{\frac{a-x}{a+x}} + \sqrt{\frac{a-t}{a+t}}}\right]\right]$$

pcheck[x_] :=

$$\frac{1}{\pi\, A\, a\, R1}\left(\sqrt{a^2 - x^2}\left(\pi - 2\,k\,\text{ArcSin}\left[\frac{b}{a}\right]\right) + k\,(b - x)\,F[b, x, a] + k\,(b + x)\,F[-b, x, a]\right)$$

Plot[{pcheck[x]}, {x, -1, 1}, PlotRange → Full, AxesLabel → {"x", "p(x)"}]

Out[4]=

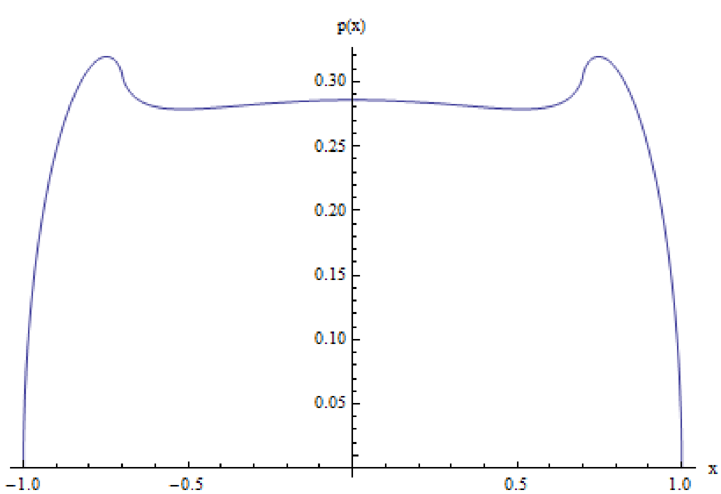

Figure 6 - Numerical p(x) plot from Vazquez et al equation

The above plots can be seen to show very good agreement. An overlaid plot has shown an exact match, but is not included here

6. Example problem – Optimisation of an asymmetric barrelled contact

This section details an example of how this code could be used in a real world problem.

Suppose the shape of contact giving the lowest peak contact pressure for a given contact length and load is sought. Any number of edge radii can be incorporated, but the manufacturing difficulty demands a compromise between the number of discrete regions and the improvement offered by each region. A plot of the number of contact regions against peak contact pressure would be a valuable tool to determine when the 'law of diminishing returns' makes incorporating extra regions undesirable. We present here a method by which this program could be used to generate this plot.

6.1. Problem variables

The program would be executed a number of times with the following sets of input variables.

For all cases:

Symmetric =True, A=1 , $a_1= b_1=-1$, $P=P$, $b_{n+1}=1^*$

Specific case variables:

$n=2$	n=3	n=4	n=4
$b_2=b_2$, $R_1=R_1$, $R_2=-R_2^*$	$b_2=b_2$, $b_3=-b_2^*$ $R_1=R_1$, $R_2=R_2$, $R_3=R_1^*$	$b_2=b_2$, $b_3=b_3$, $b_4=-b_2^*$ $R_1=R_1$, $R_2=R_2$, $R_3=R_2^*$, $R_4=R_1^*$	$b_2=b_2$, $b_3=b_3$, $b_4=-b_3^*$, $b_5=-b_2^*$ $R_1=R_1$, $R_2=R_2$,$R_3=R_3$, $R_4=R_2^*$, $R_5=R_1^*$

**Automatically assumed by the program*

6.2. Problem method

The resulting load and contact pressure equations for each value of *n* can then be exported to Mathematica or Matlab, and optimisation routines within these packages could be used to find the minimum peak contact pressure subject to the constraint implied by the contact load equivalency equation. This allows the graph discussed in the introduction to be produced. The program has removed the need to spend time evaluating the integrals and deriving the equations for each contact type.

7. Final notes

The following issues are acknowledged, and will be resolved in future versions.

- No export is available in Mathematica format – as a workaround, export the file in Matlab format without the plug-in running (ignore the message), then remove 'ToMatlab[' from the start and ']' from the end
- If 'Set $b_1=a_1$ & $b_{n+1}=a_2$' is enabled for a symmetric contact, the Muskhelishvili potential equation returns an error. As a workaround, asymmetry should be selected, and the required assumptions manually set.

8. Contact details

To report any undocumented issues, please contact Mat Davies at mat.davies@rolls-royce.com or Mat Davies (ELT-10), Rolls-Royce Groups plc, PO Box 31, Derby, Derbyshire. DE24 8BJ

Appendix A – Detailed instructions to replicate the examples in sections 5.1 and 5.3

The following method was used in section 5.1

1. Open the file, ensure dynamic content is enabled and the 'General' tab is selected.
2. The default position for the slider should be 'n=3', if not, move the slider to set this value.
3. Click the 'Symmetric' button on the third line, once set, clicking the 'implications' button gives a list of the values that have been constrained by this, which should be the same as specified in section 5.1.
4. Ensure that algebraic definitions are supplied for 'A' and 'P', 'θ should be zero due to the assumption of symmetry.
5. For the 'specify' tab, 'a_1 & a_2' should be selected.
6. Select the 'Segments' tab.
7. In the 'Extent of segment definition' window, click '*Set* $b_1=a_1$ *and* $b_{n+1}=a_2$', which should change '$b_1=b_1$' *to* '$b_1=a_1$'.
8. The remaining values should remain at their default setting.
9. Click the 'calculate' button toward the bottom of the page, the *h'(x)* array should be displayed.
10. Click on the 'Consistency Eq.' tab. The display should show '0=0', which implies that the consistency condition is automatically satisfied (by the assumption of symmetry) and yields no information.
11. Click on the 'Load Eq.' tab. The load equation (contact law) will be displayed
12. Click on the 'p(x) Eq.' tab and press run. The contact pressure equation is displayed

The following additional steps were taken in section 5.3

13. Go back to the 'General' tab, select the button labelled 'Num' next to 'a_1='. The value in the box should change to '-1' and the value in the 'a_2=' box should change to '1'.
14. Click the 'Num' button next to '*A*=', the value in the box should change to '1'.
15. Go to the 'Segments' tab, again click '*Set* $b_1=a_1$ *and* $b_{n+1}=a_2$' the value in the 'b_1=' box should change to '-1' (note: the 'b_{n+1}=' box is not visible)
16. Click on the b2 tab, press the 'numerical button, and change the value in the box to '-0.7'
17. In the 'Local radius definition' box, click the 'numerical' button on the 'R_1' tab, the box should show '1'.
18. Click the 'R_2' tab, and the 'numerical' button, change the value in the box to '5'. Ensure that the 'yes' button is also active in this field.
19. Click the 'calculate' button towards the bottom of the page and then click on the 'p(x) plot' tab, the pressure distribution will be displayed.

Energy Dissipation in a Frictional Incomplete Contact with varying Normal Load – Supplementary Mathematica code user guide

Purpose

This documentation details the Mathematica code accompanying 'Energy dissipation in a frictional incomplete contact with varying normal load'. The code provides an implemented form of the formulae and methods detailed in the paper, and allows modest extension to other incomplete contact forms, including, but not limited to, the commonly studied problem of a flat punch with rounded edges which is discussed as an example in this guide.

The code herein provides the following information for a the steady state behaviour of an incomplete contact under normal and shear load varying as an ellipse.

- Contact size history.
- Relative displacement history for any point that comes into contact during the cycle.
- The energy dissipation per unit length for one complete cycle and total energy dissipated during a cycle.
- The instantaneous shear stress distribution along the interface at any point in the cycle.

Numerical solutions are employed for all of the above and some control over these is provided.

The tool is presented as a series of tabs, within which the intention is to progress from left to right. The first tab defines the loading parameters. The second and third allow individual time frames and positions to be selected for later tabs. The final four tabs provide the output for displacement, energy and shear stress. Each tab is discussed in more detail below.

Requirements

This code has been written using Mathematica version 7.1 and has been tested using this and version 8.0. Compatibility with other versions is untested.

Defining parameters

The first tab is used to define the elliptic load path, the initial values are shown in Figure 1.

The values for P_0, P_1, Q_0, Q_1 and ϕ are discussed in the paper. The coefficient of friction is specified by f. The parameter Q_Z defines the intercept of a line of gradient f and the initial load trajectory for the transient problem. It defines only the locked in relative displacements for the region in which no slip takes place in the steady state problem and has no effect on the displacement or energy dissipation of the steady state displacement and energy dissipation.

The ‘Troubleshooting’ panel at the bottom rarely needs to be changed and will be discussed later.

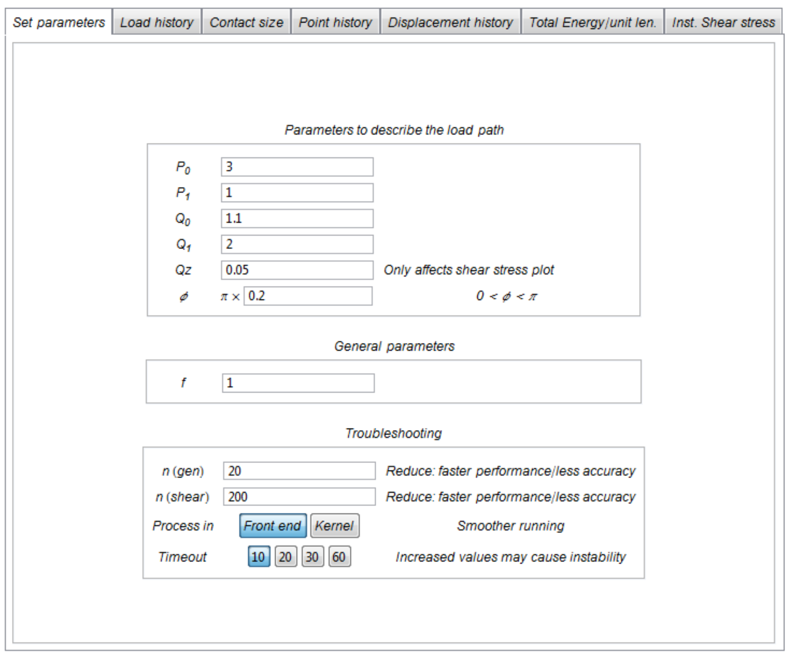

Figure 1 - 'Set parameters' tab with default values

Load cycle and setting θ_{ref}

Once the load history has been defined, the cycle can be seen visually in PQ space on the second tab. Pressing the plot button will plot the values currently entered on the 'Set parameters' tab. Figure 2 shows this tab with the default cycle history.

After plotting, the top row of the tab allows the entire plot to be removed or the construction lines can be hidden.

Placing the mouse cursor over any of the lines will print the behaviour at that point in the cycle (i.e. advancing forward slip, advancing reverse slip or full adhesion) to the row immediately below the plot. Four cycle points are also highlighted, which are referred to in the paper as E, G, I and J. Placing the cursor on one will cause the appropriate label to appear immediately below the plot. If the 'Enable θ_{ref} selection' button is checked, then the timeframe at which the shear stress is shown (on the final tab) can be set using the adjacent slider. The values of P_T, P_Z andP_S, as discussed in the paper, are also shown.

One important check that can be performed on this tab is to ensure that no gross slip will occur during the cycle because there is a requirement that the point at the centre of contact be adhered throughout. If the plotted ellipse crosses either the $Q = fP$ or $Q = -fP$ lines (the dashed lines) then gross slip will occur and the formulation is not valid.

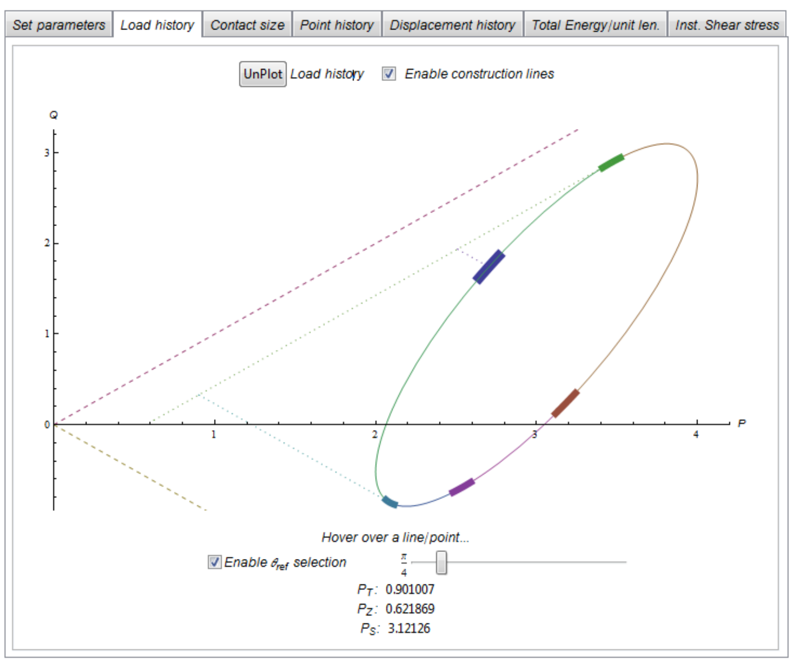

Figure 2 - 'Load history' tab with default values

Contact size history and setting x_{ref}

The third tab shows the contact size history through two cycles. Again, the 'Plot' button must be pressed to display this information. The contact size history is shown by the blue line, and the stick zone size is shown by the red line in the advancing reverse slip phase, and the yellow and green line for the two phases of advancing forward slip. If a timeframe has been selected on the second tab, this is shown as a vertical dashed line on the plot. Additionally, the contact and stick zone half width is shown numerically on the line below the plot.

If the 'Enable x_{ref} selection' option on the bottom row is checked, a slider on the right of the plot allows any position that comes into contact at some point to be selected. This will define the location used in the 'point history' and 'displacement history' tabs. The normalised value of this location is also shown on the bottom row.

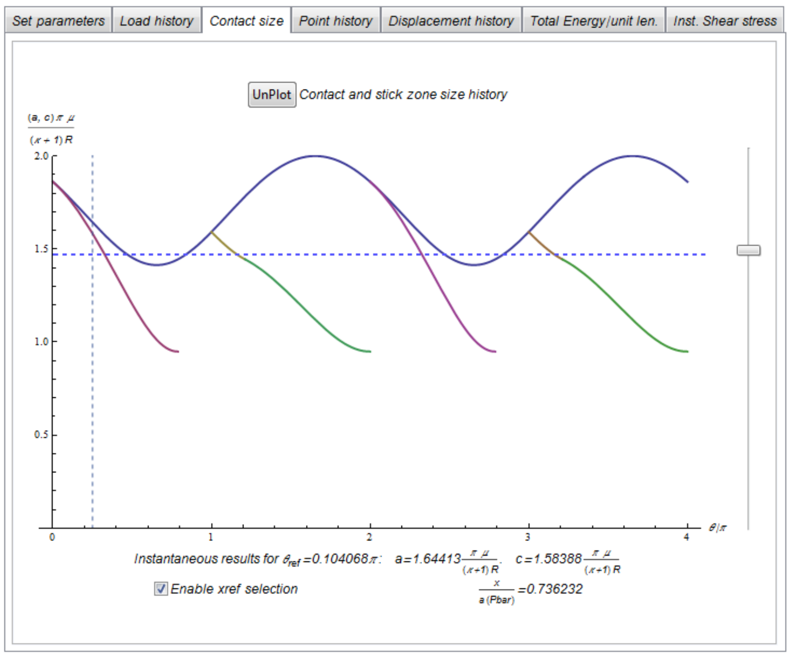

Figure 3 - 'Contact size' tab with default values

Point/Displacement history

The fourth tab gives a simple summary of the behaviour of the point selected on the previous tab. It states whether the point is sticking, slipping or out of contact through the four phases of a single cycle.

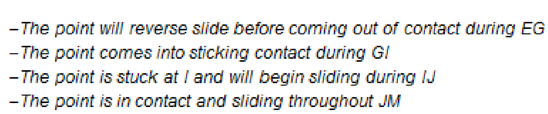

Figure 4 - 'Point history' tab

The fifth tab gives this history in more detail, including the exact point at which contact is made or broken and the displacement history between this and a point initially opposite in the contacting body, again the 'Plot' button must be pressed to display this information.

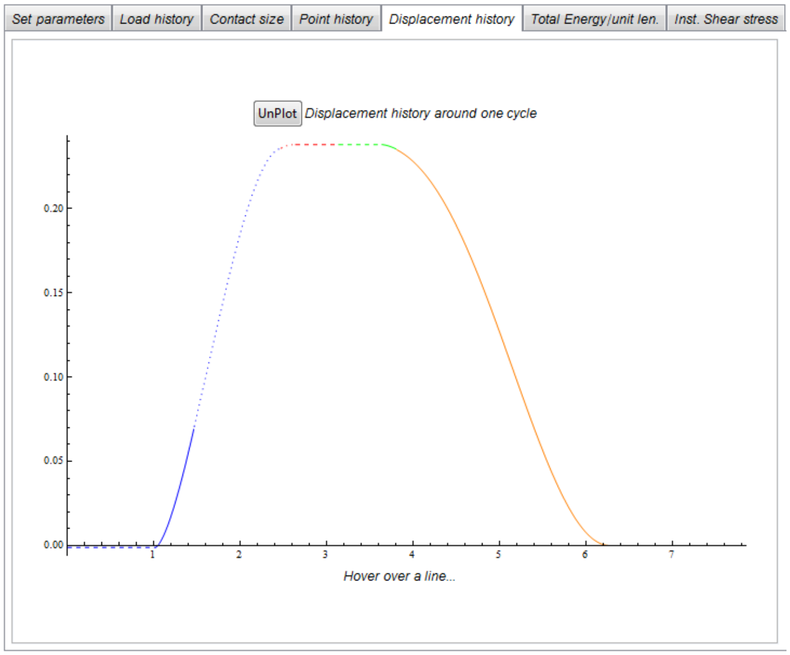

Figure 5 - 'Displacement history' tab

The line style indicates whether the specified point is sliding (solid line), sticking (dashed line) or out of contact (dotted line). Each phase identified in the paper has a particular colour, these are summarised below.

- EG - Blue
- GI – Red
- IJ – Green
- JM – Orange

Hovering over a segment of the line will cause this information to be displayed below the plot.

Note that the default numerical solutions occasionally result in slight errors that cause the relative displacement between the start and end of the cycle.

Energy dissipation during a single cycle

The total energy dissipated during a single cycle, expressed as energy per unit length against position, is shown on the 'Total Energy/unit len.' tab. Pressing the 'Plot' button reveals the plot, which can take a short time to be displayed. The blue, purple and yellow lines represent the three regions in which relative slip occurs (EG, IJ and JM respectively) and the green line represents the total dissipation around a full cycle.

The total energy absorbed by the entire contact around a single cycle is given below the plot.

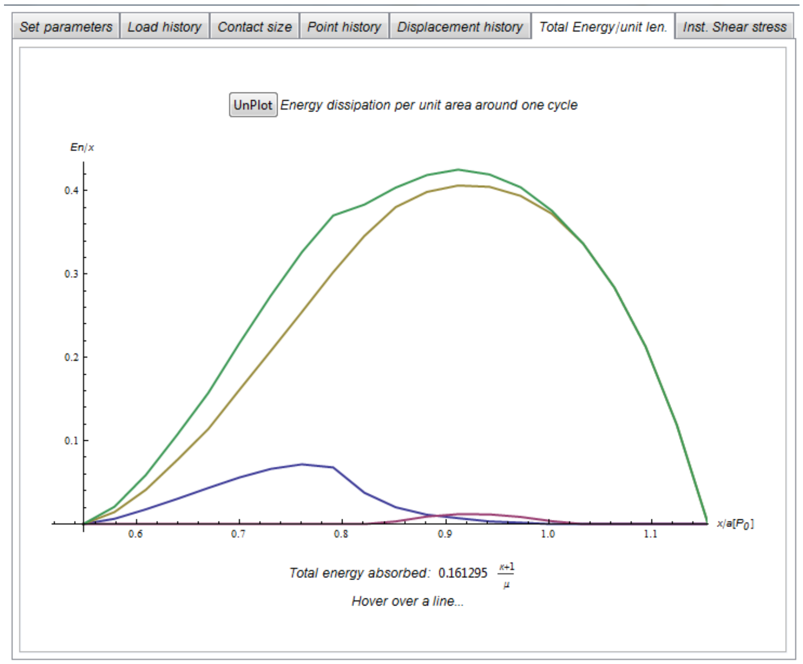

Figure 6 - 'Total Energy/unit len.' tab

Shear stress

The instantaneous shear stress distribution at the time defined on the 'Load history' tab is shown on the 'inst. Shear stress' tab.

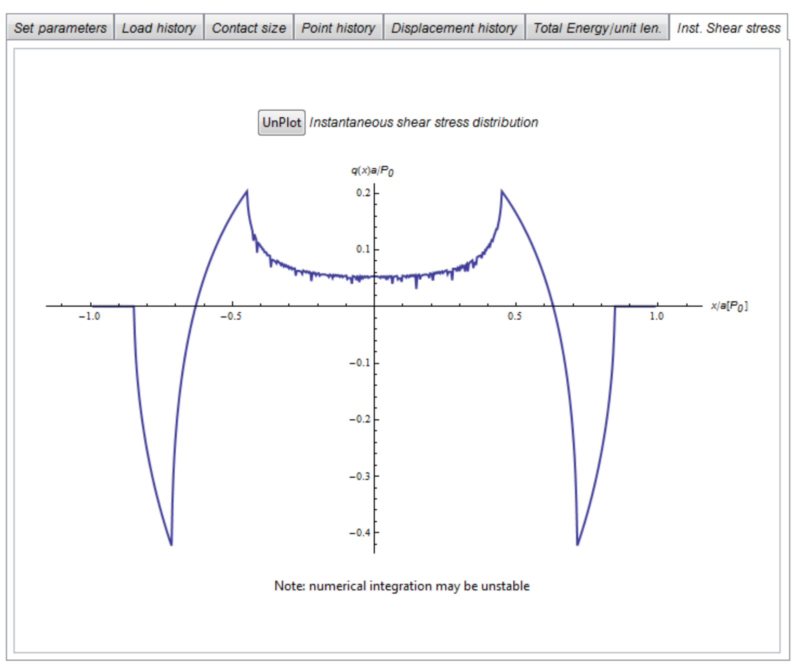

Figure 7 - 'Inst. Shear stress' tab

The numerical integration used can be unstable for the regions in which stuck material is laid down, which can cause some noise in the results. This can be reduced by increasing the number of abscissa which is discussed in the ‘Troubleshooting’ section.

Troubleshooting

There are several parameters associated with the programme that balance the solution time against the accuracy and refinement of the solution. Default values have been set that will provide short execution times so that the program will run smoothly. Slower computers will require fewer elements conversely, obtaining smoother plots will require more. There are two values that control element numbers n(gen) specifies the general number of elements for the plots on all but the shear stress tab, n(shear) controls the number of elements on the shear stress tab. It should be noted that the execution time will approximately follow the square of the number of elements.

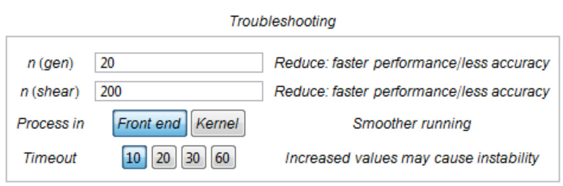

Figure 8 – ‘Troubleshooting’ section on 'Set parameters' tab

If a large number of elements is required, the additional run time may cause the execution to timeout, in which case ‘$Aborted’ will be displayed, as shown in figure 9. This occurs because execution occurs by default in the Mathematica front end (see the Mathematica help for more information), which has a maximum execution time. This value can be changed using the ‘Timeout’ option at the bottom of the panel and will have immediate effect.

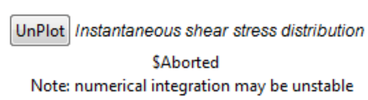

Figure 9 – Example of execution timeout

To take advantage of multiple processing cores, the execution can be sent to the default Mathematica Kernel. To enable this, the ‘Process in’ option should be changed to ‘Kernel’. Once the setting has been changed, plots must be removed and re-plotted. It is recommended that all plots are removed prior to changing tabs.

Defining alternate contact forms

It is possible to change the form of the contacting body from the default (which is a Hertz cylinder) to any incomplete contact. To do this new functions for the contact law should be specified. This is not incorporated into the graphical interface and requires the full version of Mathematica.

To define a new contact law, use the Mathematica 'SetDelayed' function this should accept two arguments, the first is the normal load and the second is used to specify the associated constants. The default settings for Hertzian contact are shown below.

$$aa[P\_,\gamma\_] := \sqrt{P\gamma}$$

$$\gamma = \frac{(\kappa+1)R}{\pi\mu}$$

These should be entered directly into a Mathematica notebook and executed. In order to give dimensionless variables, the application only calls the function with the second argument equal to one. Additional parameters (such as the flat region length) should be defined separately. (see the 'Example problem' section)

Example problem

An example for a flat and rounded contact with the following parameters is given below

Parameter	Value	Parameter	Value
Flat region length, b/R	2.5	Mean normal load, P_0	1.0
Edge radius, R	1.0	Change in normal load, P_1	0.7
Eccentricity, ϕ	0.7π	Mean shear load, Q_0	-0.2
Transient intercept, Q_Z	0.001	Change in shear load, Q_1	0.4
Coefficient of friction, f	0.6		

The following element numbers were used

Parameter	Value	Parameter	Value
Flat region length, b	40	Mean normal load, P_0	

To define the flat and rounded contact, the following functions were defined

$b = 2.5;$

$$aa[P\_,\gamma\_] := a/.\mathrm{FindRoot}\left[P == \frac{2}{\gamma\pi^2}\left(a^2\mathrm{ArcCos}\left[\frac{b}{a}\right] - b\sqrt{a^2-b^2}\right),\{a,10\}\right][[1]]$$

$$\begin{aligned} p[x\_,P\_,a\_] := \mathrm{Re}[&\frac{1}{2\sqrt{(a^2-b^2)(a^2-x^2)}}\Bigg(2\sqrt{a^2-b^2}(a^2-x^2)\mathrm{ArcCos}\left[\frac{b}{a}\right] \\ &+ \sqrt{(a^2-b^2)(a^2-x^2)}\Big(-2x\mathrm{Log}[a] - (b+x)\mathrm{Log}[x^2-b^2] \\ &+ b\mathrm{Log}\left[2a^2-b^2-x^2-2\sqrt{(a^2-b^2)(a^2-x^2)}\right] \\ &+ x\mathrm{Log}\left[a^2(b^2+x^2)+2bx\left(\sqrt{(a^2-b^2)(a^2-x^2)}-bx\right)\right]\Big)\Bigg) \end{aligned}$$

The cycle in PQ space is

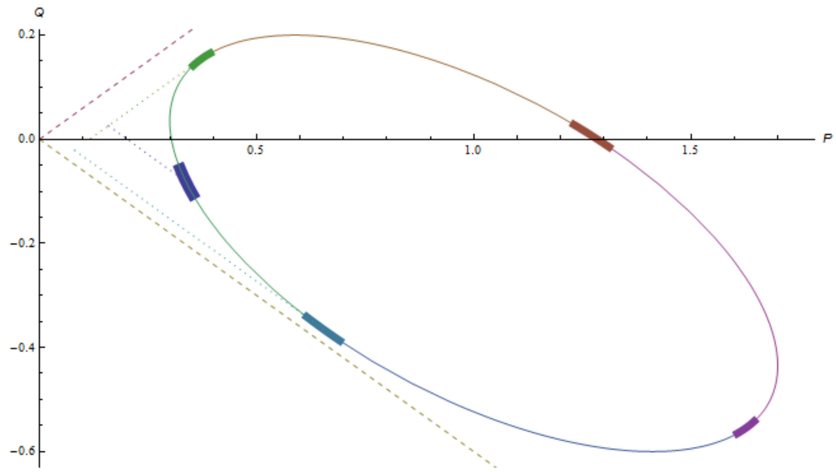

Figure 10 – PQ plot for example problem

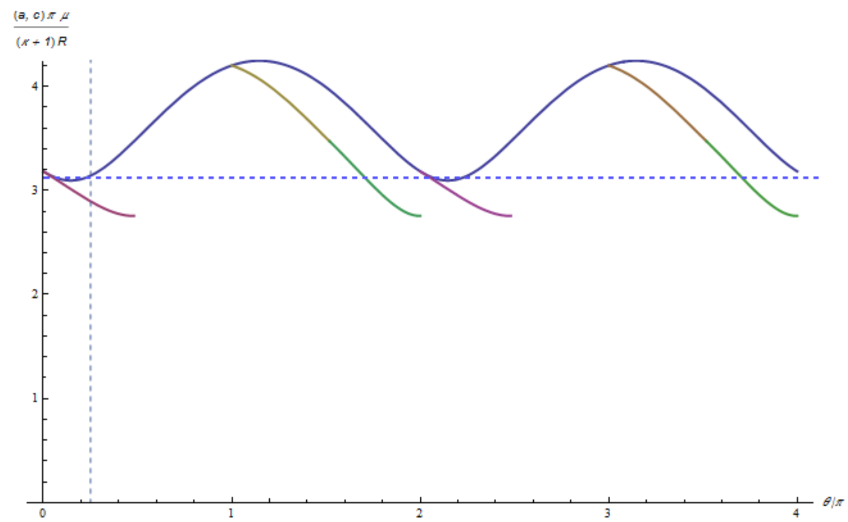

Figure 11 – Contact and stick zone size history

–*The point begins reverse slip then comes out of contact and returns to reverse slip during EG*
–*The point is stuck throughout GI*
–*The point is stuck throughout IJ*
–*The point is stuck at J and will begin sliding during JM*

Figure 12 – Displacement history for the point specified in figure 11

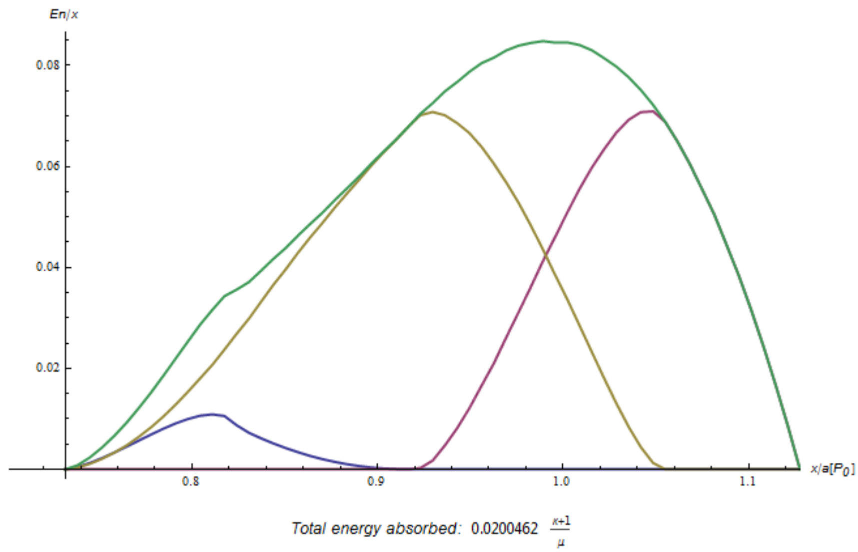

Figure 13 – Total energy dissipation per unit length for the example problem

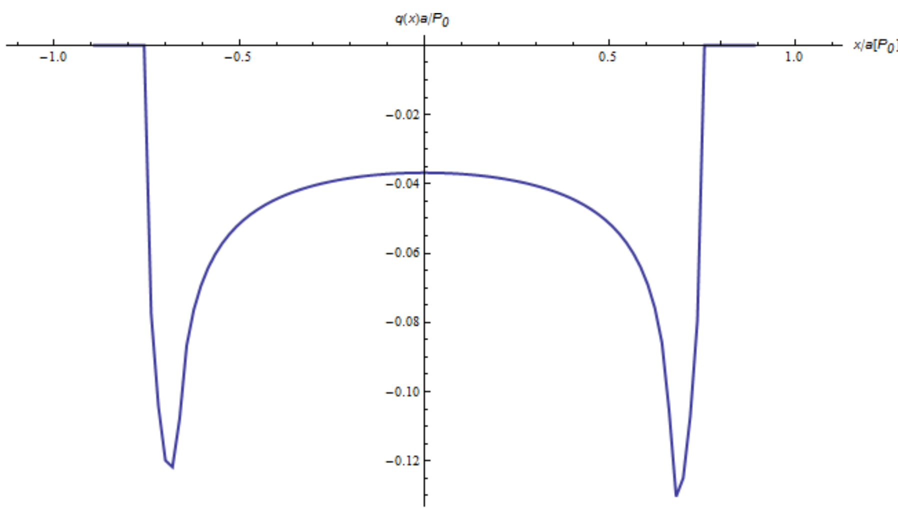

Figure 14 – Instantaneous shear traction distribution for the time specified in figure 10/11

Contact details

The author can be contacted at mat.davies@eng.ox.ac.uk